IMPACTS OF SOIL REDISTRIBUTION PROCESSES ON SOIL ORGANIC CARBON STOCKS AND FLUXES IN A SMALL AGRICULTURAL CATCHMENT

INAUGURAL-DISSERTATION

zur

Erlangung des Doktorgrades

der Mathematisch-Naturwissenschaftlichen Fakultät

der Universität zu Köln

vorgelegt von

Verena Dlugoß

aus Duisburg

2011

Berichterstatter: PD Dr. Peter Fiener

Prof. Dr. Karl Schneider

Tag der mündlichen Prüfung: 05.04.2011

ABSTRACT

Soils play a major role in the global carbon cycle and have a huge potential for either sequestering or releasing carbon (C) to the atmosphere. Globally, large amounts of soil organic carbon (SOC) are laterally redistributed on sloped arable land by soil erosion. Besides the lateral SOC fluxes, soil erosion also indirectly alters the vertical C fluxes between terrestrial and aquatic ecosystems and the atmosphere. Whether this results in a net source or sink of atmospheric CO_2 is unclear. Global estimates range from a source of ~1 Pg C per year to a sink of the same magnitude. Against this background, this study investigates impacts of soil redistribution processes on SOC stocks and fluxes and the corresponding C source or sink function in a small agricultural catchment (4.2 ha) in Germany. Spatial patterns of SOC stocks were studied by analysis of soil samples of the plough layer and two subsoil layers (up to a depth of 0.9 m) taken in a 17 x 17 m raster. Results revealed a substantial accumulation and stabilisation of SOC in the subsoil at depositional sites, stressing the importance of subsoil C for budgets on agricultural land prone to erosion. *In situ* measurements of soil respiration were carried out in the most dynamic area with respect to soil redistribution in three consecutive growing periods (2007-2009). No universal relation to modelled patterns of soil redistribution or to other parameters (soil properties, plant parameters, and terrain attributes) was found for the three measurement periods, underlining the large variability of soil respiration. However in two years, heterotrophic soil respiration was significantly linearly related to total erosion (including water and tillage erosion). Hence, a possible C sink at erosion sites might partly be compensated by enhanced mineralisation at depositional sites. Besides bulk SOC, depth distributions of particle-size SOC fractions at erosional, depositional, and reference (without erosion or deposition) sites were compared to improve the understanding of the involved processes. Results showed that the labile SOC pool was depleted in the topsoil of eroding profiles, indicating that the reduced decomposition not only resulted from a general depletion of SOC but also from a relative higher abundance of more passive SOC pools. As the labile SOC pool was also depleted in the topsoil at the depositional profile, this fraction was either mineralised during transport or rapidly after deposition, or it was exported out of the test site. On the one hand, this supports an enhanced mineralisation at depositional sites, and on the other hand, this suggests an enrichment of the labile pool in the exported soil. For a spatially integrated analysis of the impact of soil redistribution on SOC

dynamics at the catchment scale, the combined soil erosion and SOC model SPEROS-C was modified and applied at the test site. It was applied for the period from 1950 to 2007, covering first a period of conventional tillage followed by a period of conservation tillage. Measured SOC stocks in the three soil layers were satisfactorily reproduced, indicating a good process representation within the model. Deposition was successfully validated by two depth profiles of ^{14}C measured by accelerator mass spectrometry. The erosion induced net vertical C flux showed substantial spatial variation within the test site. Depositional areas acted as a C source due to the mineralisation of buried C while erosional sites acted as a C sink due to (partial) dynamic C replacement. As erosion sites constituted two thirds of the catchment area, the erosion induced mean net vertical C flux was a sink for atmospheric CO_2 at the test site. However, a substantial amount of C was lost laterally due to the export by water erosion. This resulted in an overall negative C balance for the test site. Land management had a profound effect on the lateral and vertical C fluxes. The change from conventional to conservation agriculture reduced the lateral C export and enhanced the vertical C fluxes, leading to a reduced negative C balance. Overall, this study substantially improves the knowledge about the impacts of soil redistribution on SOC stocks and fluxes at the small catchment scale and provides improved and new methods applicable in future research.

KURZZUSAMMENFASSUNG

Böden nehmen eine wichtige Rolle im globalen Kohlenstoffkreislauf ein und haben ein großes Potential zur Bindung und Freisetzung von Kohlenstoff (C). Auf geneigten Ackerflächen werden global große Mengen organischen Bodenkohlenstoffs (C_{org}) durch Bodenerosion verlagert. Neben diesem lateralen C_{org}-Fluss verändert Bodenerosion zudem die vertikalen C-Flüsse zwischen terrestrischen und aquatischen Ökosystemen und der Atmosphäre. Es ist unklar, ob diese Veränderungen eine Quelle oder Senke für atmosphärisches CO_2 darstellen. Globale Schätzungen reichen von einer Quelle von ~1 Pg C pro Jahr bis zu einer Senke derselben Größenordnung. Vor diesem Hintergrund untersucht diese Arbeit die Auswirkungen von Bodenerosionsprozessen auf Speicher und Flüsse des organischen Bodenkohlenstoffs sowie die daraus resultierende C-Senke oder -Quelle in einem kleinen agrarisch genutzten Einzugsgebiet (4.2 ha) in Deutschland. Räumliche Muster des C_{org}-Bestands wurden mit Hilfe von Bodenproben aus dem Pflughorizont und aus zwei Unterbodenschichten (bis 0.9 m Tiefe), entnommen in einem 17 x 17 m Raster, untersucht. Die Ergebnisse zeigen eine deutliche Akkumulation und Stabilisierung von C_{org} im Unterboden von Depositionsstandorten und betonen so die Notwendigkeit der Berücksichtigung von Unterbodenschichten bei der Erstellung von C-Bilanzen in Gebieten mit Bodenerosion. *In situ* Messungen der Bodenatmung wurden in drei aufeinanderfolgenden Vegetationsperioden (2007-2009) im dynamischsten Bereich hinsichtlich der Bodenerosion im Untersuchungsgebiet durchgeführt. Da keine allgemeingültige Beziehung der Messungen zu modellierten Mustern der Bodenerosion und zu weiteren Parametern (Bodeneigenschaften, Pflanzenparameter und topographische Eigenschaften) für alle drei Messperioden gefunden werden konnte, wurde der stark variable Charakter der Bodenatmung hervorgehoben. In zwei Messperioden gab es jedoch einen signifikanten linearen Zusammenhang der heterotrophen Bodenatmung zur Gesamterosion (Wasser- und Bearbeitungserosion). Demzufolge könnte eine mögliche C-Senke an Erosionsstandorten teilweise durch eine verstärkte Mineralisierung an Depositionsstandorten kompensiert werden. Zur Verbesserung des Prozessverständnisses wurden neben der Untersuchung des organischen Gesamtkohlenstoffs Tiefenprofile von korngrößenspezifischen C_{org}-Fraktionen an Erosions-, Depositions- und Referenzstandorten (ohne Erosion und Deposition) verglichen. Der labile C_{org}-Pool war im Oberboden der Erosionsprofile abgereichert. Dies zeigt, dass eine reduzierte Mineralisierung an

Erosionsstandorten nicht nur aus einer generellen Abreicherung von C_{org} stammt, sondern auch durch das relativ höhere Vorhandensein passiver Pools. Da der labile Pool auch im Oberboden der Depositionsprofile abgereichert war, wurde diese Fraktion entweder während des Transports oder direkt nach der Ablagerung mineralisiert, oder sie wurde aus dem Untersuchungsgebiet exportiert. Einerseits unterstützt dieses Ergebnis eine erhöhte Mineralisierung an Depositionsstandorten, andererseits deutet es auf eine Anreicherung von labilem C_{org} in exportiertem Bodenmaterial. Für eine räumlich integrative Analyse des Einflusses der Bodenerosion auf die Dynamik von C_{org} wurde das kombinierte Erosions- und Bodenkohlenstoffmodell SPEROS-C verändert und im Untersuchungsgebiet für den Zeitraum 1950 bis 2007 angewendet. Der Simulationszeitraum umfasste eine Periode konventioneller Bewirtschaftung und eine darauffolgende Periode konservierender Bewirtschaftung. Die zufriedenstellende Reproduktion der gemessenen C_{org}-Bestände in den drei Bodenschichten bestätigte eine gute Prozessdarstellung im Modell. Die kumulative Deposition wurde erfolgreich anhand zweier mit Beschleuniger-Massenspektrometrie gemessener ^{14}C-Profile validiert. Der erosionsbedingte vertikale Netto-C-Fluss zeigte eine ausgeprägte räumliche Variabilität im Untersuchungsgebiet. Depositionsstandorte stellten eine C-Quelle aufgrund der Mineralisierung von begrabenem C_{org} dar, während Erosionsstandorte eine C-Senke aufgrund von (partiellem) dynamischen C-Ersatz waren. Da die Erosionsflächen ca. zwei Drittel der Einzugsgebietsfläche einnehmen, war der erosionsbedingte mittlere vertikale Netto-C-Fluss im Untersuchungsgebiet eine Senke für atmosphärisches CO_2. Allerdings wurde eine große Menge C_{org} lateral durch Wassererosion aus dem Gebiet exportiert, so dass die Gesamtbodenkohlenstoffbilanz des Untersuchungsgebietes negativ war. Die Bewirtschaftung hatte einen großen Einfluss auf die lateralen und vertikalen C-Flüsse. Der Wechsel von konventioneller zu konservierender Bewirtschaftung verringerte den lateralen C-Export und erhöhte die vertikalen C-Flüsse, so dass die negative C-Bilanz verringert wurde. Insgesamt verbessert diese Arbeit erheblich das Prozessverständnis der Einflüsse von Bodenerosion auf C_{org}-Speicher und -flüsse auf der kleinen Einzugsgebietsskala und liefert gleichzeitig neue und verbesserte Methoden für zukünftige Untersuchungen.

ACKNOWLEDGEMENTS

The present thesis was prepared within the framework of the German Research Foundation (DFG) project 'Soil redistribution in agricultural landscapes – source or sink of CO_2?'. I gratefully acknowledge the financial support.

In this context, I thank PD Dr. Peter Fiener for substantially promoting the application of this project. Furthermore, his intensive supervision of this thesis was more than self-evident. I especially acknowledge his many practical tips and the numerous encouraging and inspiring discussions.

I sincerely thank Prof. Dr. Karl Schneider for the opportunity to work in his research group, for providing all essential background conditions that made this thesis possible, and for being the second supervisor of this thesis. Prof. Dr. Susanne Crewell is thanked for acting as commission head.

Furthermore, I gratefully acknowledge the helpful support of Prof. Dr. Kristof Van Oost, who provided the SPEROS-C model code to me. He was always willing to answer my many questions and to discuss results during my visits to Louvain-la-Neuve.

For their help in SOC fractionation and for the determination of black carbon, I thank Prof. Dr. Wulf Amelung, Dr. Gerd Welp and Dr. Ludger Bornemann. Dr. Josef Griese and the Landesamt für Natur, Umwelt und Verbraucherschutz Nordrhein-Westfalen is thanked for the provision of yield and precipitation data.

Special thanks also go to Philip Töllner, the farm owner of the Heiderhof, for his permission to carry out several field campaigns and his patience in answering field management questions. Albert Wolter is acknowledged for his permission to install a runoff monitoring station within the Dissenbach brook.

Without the active support of many student assistants, the intense field and laboratory measurements investigated in this thesis could not have been accomplished. My special thanks go to Sven Bremenfeld, who not only worked very staunchly, but who also showed a great patience with CN analysers, sonificators, etc. Additionally, I am grateful to all my colleagues within the Hydrogeography and Climatology Research Group for a comfortable

working atmosphere and valuable discussions. Especially I thank Dr. Christian Klar for acting as a member of the commission. I am also indebted to Sebastian Dötterl for good times in Louvain-la-Neuve and for reviewing parts of this thesis. Special thanks also go to Matthias Wagner, the English teacher whom I trust.

Last but not least, I deeply thank Robert for encouraging me in hard times and laughing with me in good times. Many thanks also go to my parents, Inge and Erhard, for supporting me throughout my entire life.

CONTENTS

LIST OF FIGURES

LIST OF TABLES

1 INTRODUCTION

The role of soils in the global terrestrial carbon cycle has become an important issue of global climate change research, and carbon sequestration in soils has been suggested as a means of reducing the rate of increase of atmospheric CO_2 (e.g. Janzen, 2006; Kutsch et al., 2009; Lal, 2004a/b; 2009; Schlesinger and Andrews, 2000). The global soil carbon pool up to 1 m depth is estimated at 2500 Pg including about 1550 Pg soil organic carbon (SOC) and 950 Pg soil inorganic carbon (SIC) (Lal, 2004b). SOC constitutes about 58% of soil organic matter, which encompasses plant, animal, and microbial residues in all stages of decay as well as a diversity of heterogeneous organic substances associated with mineral soil components (Christensen, 1992). The global SOC pool corresponds to twice the amount of atmospheric C and triple the amount of C stored in the biosphere (Schlesinger, 2005). As SOC is highly dynamic (Janzen, 2006), it has a huge potential for either sequestering or releasing carbon to the atmosphere. SIC consists of lithogenic (primary) carbonates, derived from the weathering of calcareous soil parent material, and pedogenic (secondary) carbonates, derived from the dissolution of primary carbonates and the re-precipitation of weathering products (Eshel and Fine, 2007). As the reactivity of the SIC pool is generally slow and SIC is predominantly important in arid and semi-arid environments (Eshel and Fine, 2007; Lal, 2003b), the scope of this thesis is limited to SOC.

Human interventions like deforestation and cultivation have decreased - and still are decreasing - the global SOC pool compared to the quantity the pool could achieve under natural vegetation due to enhanced decomposition, reduced C input, and C loss by harvesting and soil erosion (Smith et al., 2009). Following Lal (2008), soils in temperate climate lose 30-50% of their SOC in 50 to 100 years after the conversion to agricultural land. This historic loss constitutes a potential to sequester atmospheric carbon that can be achieved by judicious land management on crop- and grassland. This includes agronomic practices that increase the C input into the soils and/or reduce C losses and CO_2 emissions, like e.g. conservation reserve programs on degraded soils, zero or reduced tillage, integrated management of nutrients and organic manure, improved water management on irrigated and drained land, etc. (Smith et al.,

2007) that need to be adapted site-specifically (Lal, 2004b; Smith et al., 2009). Estimations of the global potential of agricultural soils to sequester C show strong variations due to the choice of assumptions and constraints on these management practices (Smith et al., 2009). Recently, Lal (2004b) made a global estimate of 0.9 ± 0.3 Pg C a^{-1}, including conversion from conventional to conservation or no till systems, and adopting improved systems of crop management like e.g. the inclusion of cover crops in the crop rotation, organic manuring, agroforestry, improved irrigation, and pest management.

The Kyoto protocol (Article 3.4) stresses the relevance of C sequestration in the world's agricultural soils, as it offers the opportunity to offset part of the anthropogenic carbon emissions by removal of C from the atmosphere through improved management (Smith et al., 2009). Additionally, the sequestration of C in the soils of the world's agricultural land constitutes a win-win strategy (e.g. Janzen, 2006; Lal, 2004a; 2010). Besides the mitigation of the greenhouse effect, it has further on- and off-site benefits. Among the most important is the improvement of soil quality including e.g. an increase of water capacity, aggregate stability, and nutrient retention. The subsequent increase in yields helps to assure global food security for a rising global population (Lal, 2010).

However, soil carbon sequestration has a limited duration and cannot be maintained indefinitely (Smith et al., 2009). According to West and Post (2002), the adoption of improved management practices provides a short-term sink of atmospheric C in the order of 15 to 60 years, until a new equilibrium between SOC formation and decomposition is reached. But if atmospheric CO_2 levels are to be stabilised at specific targets by 2100, drastic reductions in emissions are required especially over the next 20 to 30 years (IPCC, 2000; Smith et al., 2009).

Given that global C budgets and estimates of the response of SOC to alternative management strategies mostly do not consider any interaction of the mere biogeochemical processes with geomorphic processes (Van Oost et al., 2009), one of the major challenges in current soil organic matter research is the interplay between SOC and soil erosion (e.g. Berhe et al., 2007; Kuhn et al., 2009; Lal, 2009; Van Oost et al., 2007). Soil erosion is a major thread to the agriculturally used soils of the world (e.g. Lal, 2001; Montgomery, 2007; Oldeman et al., 1991; Pimentel, 2000; 2006), as it implies severe on-and off-site effects. These include e.g. the loss of nutrients and fine soil particles, a reduced water holding capacity, the truncation of soil profiles, and direct damages on cultivated crops, all threatening

the sustainability of agriculture and the insertion of sediments and nutrients into watercourses. Soil erosion is supposed to accelerate under global climate change especially in the mid latitudes (e.g. Nearing et al., 2004; O´Neal et al., 2005; Pruski and Nearing, 2002; Scholz et al., 2008) due to increased precipitation amounts and intensities (IPCC, 2007). Hence, understanding the impact of soil erosion on SOC dynamics and the fate of eroded SOC are crucial to assess the role of soils in the global carbon cycle (Lal, 2004b). Van Oost et al. (2007) estimate that globally 0.47 to 0.61 Pg SOC per year are moved laterally as a result of agricultural soil erosion. But whether soil redistribution on agricultural land constitutes a C sink or source for the atmosphere is discussed controversially.

In general, SOC dynamics in stable landscapes are controlled by the balance of two opposing vertical C fluxes between pedosphere and atmosphere: (i) The SOC formation through C input by plant residues and roots, and (ii) the SOC decomposition by the microbial biomass (heterotrophic soil respiration). These two processes are assumed to be in equilibrium at undisturbed sites so that there is no net C flux between soils and atmosphere. Soil redistribution alters this steady state condition by removing SOC from erosional sites and laterally transporting it to depositional sites. But the indirect consequences for the vertical C fluxes by changing the rate of SOC formation or decomposition are not fully understood. Soil erosion is a multistage process that encompasses the detachment, transport, and deposition of soil particles in terrestrial ecosystems as well as their export into the fluvial system (Van Oost et al., 2009). Accordingly, five key mechanisms were identified that potentially alter the net vertical C flux between terrestrial and aquatic ecosystems and the atmosphere due to soil erosion (Fig. 1.1):

i. A (partial) *dynamic replacement of SOC at eroding sites* (Harden et al., 1999; Stallard, 1998) is induced by the balance between reduced respiration due to the removal of SOC from eroding topsoils and continued SOC formation through C input by plants. Few studies provide direct measurements of dynamic replacement by ^{14}C measurements (Harden et al., 1999) or by measurements of net primary productivity (Berhe et al., 2008) at different landscape positions. However, other studies provide indirect evidence of dynamic replacement by either measurement (Quine and Van Oost, 2007) or modelling (e.g. Billings et al., 2010; Van Oost et al., 2005a).
ii. A *sequestration of SOC at depositional sites* is caused by the burial of SOC rich topsoil below the plough layer (e.g. Berhe et al., 2008; Gregorich et al., 1998; McCarty and Ritchie, 2002; Ritchie et al., 2007; VandenBygaart, 2001) combined with decreased

decomposition. This originates from a combination of physical and chemical processes, like e.g. higher soil moisture, limited aeration, compaction, and physical protection in newly formed soil aggregates (e.g. Gregorich et al., 1998; Smith et al., 2001; 2005).

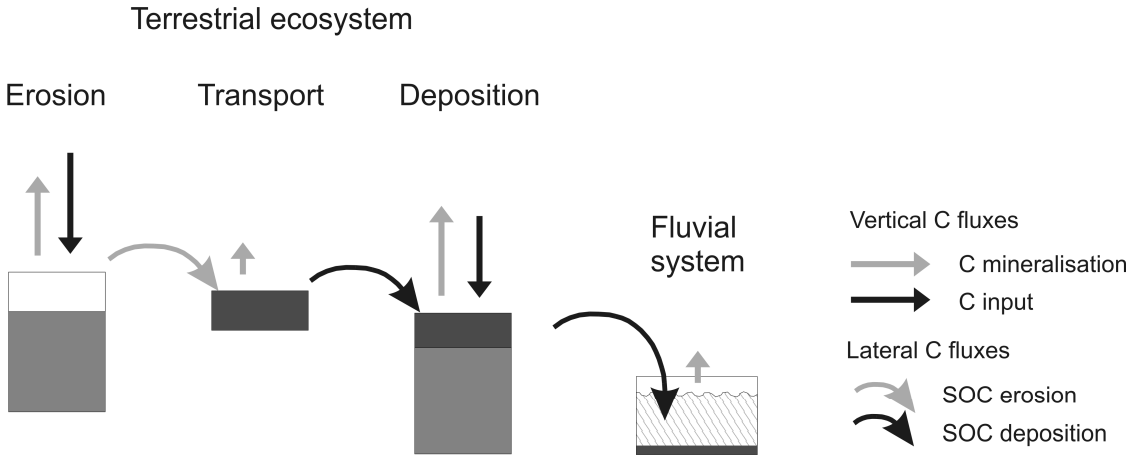

Fig. 1.1: Schematic overview of lateral and vertical C fluxes induced by soil redistribution (Fiener 2010, unpublished).

iii. The *decomposition of SOC during detachment and transport* of soil particles by water induced erosion is enhanced due to the breakdown of stabilising aggregates (Jacinthe and Lal, 2001; Lal, 2003a; Lal et al., 2004). However, direct measurements of this effect have so far not been conducted, but rates of 20 to 40% were estimated indirectly from budgeting of long-term plot data (Jacinthe and Lal, 2001) and from laboratory incubation experiments of delivered sediment (Jacinthe et al., 2004; Polyakov and Lal, 2008).

iv. A mechanism that links SOC dynamics between terrestrial and aquatic ecosystems is the *enrichment of C in eroded and exported sediment* due to preferential detachment and transport of C by water induced erosion (e.g. Quinton et al., 2006; Schiettecatte et al., 2008; Wang et al., 2010). Enrichment might also be a selective process with respect to specific SOC fractions and thus SOC quality (Chaplot et al., 2005; Van Hemelryck et al., 2010b).

v. The least understood mechanism is the *decomposition of eroded C within the aquatic system*. Results of Cole and Caraco (2001) indicate that even relatively passive SOC pools might be rapidly mineralised once they have reached the fluvial system.
(As this thesis is mainly restricted to terrestrial processes, this last mechanism will not be considered further on.)

Current global estimates of the CO_2 sink or source strength caused by anthropogenic soil redistribution range from a source of 0.8 – 1.2 Pg C per year (Lal, 2003a; Lal et al., 2004) to a sink of 0.12 – 1.5 Pg C per year (Renwick et al., 2004; Smith et al., 2001; Stallard, 1998; Van Oost et al., 2007). Some authors (Smith et al., 2001; Stallard, 1998) even attribute soil erosion to the so-called 'missing sink' (Tans et al., 1990) in the global carbon cycle. This large discrepancy is caused by differing assumptions referring to the extent and balance of the involved mechanisms and by differing estimates of global soil erosion rates.

The erosion induced source strength of Lal (2003a) is based on the assumption that 20% of the eroded SOC is emitted into the atmosphere, whereupon erosion rates were derived from estimates of global suspended sediment yield. Schlesinger (1990; 1995) even estimated that almost 100% of eroded C is decomposed during detachment and transport. As this leaves no opportunity for the deposition and burial of SOC, they concluded that soil erosion is a significant C source. The studies suggesting an erosion induced C sink highlight the importance of the mechanisms of dynamic replacement in combination with the preservation of SOC at depositional sites. Based on global sedimentation data, Stallard (1998) found that two thirds of the eroded sediment is sequestered in colluvia, alluvia, reservoirs, or impoundments and floodplains. Smith et al. (2001) showed that accounting for the eroded and deposited C in C budgets for the US increased previous estimates of the soil C sequestration potential by up to 47%. Water erosion rates were calculated using the USLE (Universal Soil Loss Equation; Wischmeier and Smith, 1978). By globally extrapolating their result, they calculated a net global C uptake of ~1 Pg C per year through soil redistribution. A substantially lower global sink of 0.12 Pg C per year was estimated by Van Oost et al. (2007). Their result is based on the derivation of general relationships between lateral and vertical C fluxes using ^{137}Cs as a tracer for soil and SOC redistribution combined with global estimates of lateral SOC movements. Instead of assuming that SOC at erosion sites is at steady state (i.e. 100% replacement of eroded C) as done by Smith et al. (2001), they restricted dynamic replacement to the active SOC pool resulting in a replacement of eroded C of ~26%. Additionally, the authors argue that global soil erosion rates have been overestimated in some studies, because of the reliance on the extrapolation of results on the plot scale or due to the application of erosion models on coarse grids (Van Oost et al., 2007). Hence, they applied scaling functions derived from fine-resolution catchment scale erosion modelling to calibrate their coarse-resolution global erosion estimates.

Recently, some authors (e.g. Berhe et al., 2007; Kuhn, 2010) argued that besides the mere biogeochemical processes, additionally the economic aspects of erosion leading to enhanced CO_2 emissions have to be considered for a complete assessment of the impact of agricultural soil erosion on the global carbon cycle. Accordingly, Kuhn (2010) calculated the CO_2 emissions caused by the production of fertilisers necessary to account for the amount of nitrogen lost by soil erosion in the United States at 0.02 to 0.04 Pg C a^{-1}. This corresponds to 15-30% of the SOC buried by soil erosion in the studies of Van Oost et al. (2007) and Quinton et al. (2010).

The contradicting global estimates highlight the existence of large knowledge gaps of the linkages between soil redistribution processes and soil C dynamics and the relative importance of the involved mechanisms. Following Van Oost et al. (2009) there is a need for spatially comprehensive investigations explicitly considering the spatial variation of SOC stocks and fluxes in horizontal and vertical direction at the catchment scale. Such studies shall, on the one hand, provide comprehensive datasets and, on the other hand, help to calibrate and verify the process representation in model approaches that link C dynamics and erosion at the landscape scale.

Spatial patterns of SOC stocks in sloped agricultural fields were mostly investigated by soil sampling in regular grid schemes or in toposequences, both covering different slope positions and thus erosional conditions. In many studies (e.g. Berhe et al., 2008; Gregorich et al., 1998; McCarty and Ritchie, 2002; Ritchie et al., 2007; VandenBygaart, 2001) a burial of SOC below the plough layer at depositional sites was observed. However, these were mostly based on single soil profiles at different landscape positions. Explicit spatial distributions of SOC stocks at the catchment scale, necessary for an improved understanding of spatial patterns of SOC stocks, can generally be achieved by the spatial interpolation of point measurements. But studies that explicitly deal with the interpolation of SOC were solely performed for the topsoil layer (< 0.3 m; e.g. Mueller and Pierce, 2003; Takata et al., 2007; Terra et al., 2004). As spatial patterns of SOC might differ substantially in subsoil layers due to differing controls on SOC dynamics compared to the topsoil layer (Salomé et al., 2010), further research is needed including subsoil C dynamics under the impact of soil erosion.

To understand the development of spatial SOC patterns, it is obligatory to analyse the processes leading to or altering these patterns. Considering the vertical C fluxes on sloped arable land, there is a lack of studies that measure the *in situ* mineralisation of SOC, i.e.

heterotrophic soil respiration, at the field or catchment scale. Contradictory results were found by studies that investigate differences in SOC decomposition at different landscape positions by laboratory (incubation) experiments (e.g. Berhe et al., 2008) and the few studies that directly measured soil respiration at various landscape positions in the field (Bajracharya et al., 2000; Van Hemelryck et al., 2010b). Berhe et al. (2008) showed that decomposition at depositional sites was hampered, supporting the mechanism of SOC sequestration. In contrast, Bajracharya et al. (2000) did not find any significant differences of soil respiration by *in situ* measurements at different slope positions under continuous corn in the US and Van Hemelryck et al. (2010b) even found an increased mineralisation at depositional sites directly in the field.

In general, the investigation of the role of soils in the global carbon cycle is exacerbated by the complex nature of SOC, being composed of different decomposition and humification products. These components are conceptualised into different SOC pools with differing turnover times in most SOC dynamics models (Trumbore, 1996), and different operational fractionation schemes exist aiming at the explicit separation of specific SOC pools (reviews in Christensen (1992) and von Lützow et al. (2007)). To our knowledge, implications of soil redistribution on SOC fractions were so far considered under a conceptual point of view only, but no detailed investigation on operational SOC fractions in the context of soil redistribution were carried out at the field scale. For example, Jacinthe et al. (2004) and Van Hemelryck et al. (2010b) concluded from their results that the labile SOC pool was preferentially transported by water induced erosion due to aggregate-breakdown. In contrast, Chaplot et al. (2005) found that black carbon, generally considered as an inert carbon pool, was preferentially eroded and deposited within the Mekong catchment in Vietnam. Based on these results, we hypothesise that specific SOC fractions might be preferentially eroded and/or deposited leading to differences in the SOC pool composition at different slope positions. This potentially leads to spatially differing SOC decomposition or stabilisation in catchments prone to soil redistribution. The investigation of the composition of SOC fractions in the parent soil material as well as in the deposited and exported sediment might substantially improve the knowledge about the processes involved in the interaction of soil redistribution and SOC dynamics.

The use of ^{14}C measured by accelerator mass spectrometry (AMS) might be a fruitful addition for the analysis of the effects of soil erosion on specific SOC pools. On undisturbed landscape positions, bomb radiocarbon data measured by AMS has been intensively used to

study SOC dynamics on decadal timescales (Trumbore, 2009). In combination with different SOC fractionation schemes, ^{14}C AMS data were used to calculate turnover rates of various SOC pools (e.g. Brovkin et al., 2008; Bruun et al., 2005; Leifeld et al., 2009) and to analyse stabilisation and destabilisation processes of soil organic matter (e.g. Flessa et al., 2008; Marschner et al., 2008). ^{14}C depth distributions of bulk SOC on arable fields without erosion or deposition (Rethemeyer et al., 2005) reveal a decreasing ^{14}C content with increasing soil depth, indicating a predominance of relatively young plant residues in the topsoil and a relative increase of older SOC pools in the subsoil. As soil redistribution on arable land potentially causes a spatial variation of the SOC pool composition, this might also result in variable depth distributions of ^{14}C in areas prone to erosion. This is indicated by the results of Berhe et al. (2008), who found a more pronounced decrease of bulk ^{14}C on erosional slope positions of their toposequence than on depositional slope positions. But further investigations, concerning the interaction of soil redistribution processes, spatial variation of certain SOC fractions, and ^{14}C need to be performed.

As the depth distribution of ^{14}C contents at different slope positions is potentially influenced by soil redistribution processes, AMS ^{14}C measurements might furthermore exhibit a potential for estimating soil redistribution rates. In many soil erosion studies, radiogenic nuclides, especially ^{137}Cs (e.g. Li et al., 2010; Walling et al., 2003), are used as tracers to analyse time integrating spatially distributed erosion and deposition patterns. As the use of ^{137}Cs is exacerbated or even impossible in areas that besides a contamination by nuclear weapon testing also experienced a ^{137}Cs contamination following the Chernobyl disaster (e.g. Higgitt et al., 1992; Schimmack et al., 2001), there is a general need for further possibilities to derive spatially distributed soil redistribution rates in Europe.

Besides the need for further process understanding with respect to the key mechanisms, spatially integrated approaches that link soil and carbon dynamics at erosional and depositional sites across the landscape are needed (Van Oost et al., 2009). Due to the intrinsic complexity, the application of coupled spatially explicit SOC and soil redistribution models is useful. Several approaches of combined modelling of soil redistribution and soil carbon cycling have been presented in literature (for reviews refer to e.g. Polyakov and Lal (2004) or Van Oost et al. (2009)). First approaches were restricted to single points at different landscape positions and to the simulation of the topsoil layer (e.g. Gregorich et al., 1998; Harden et al., 1999; Pennock and Frick, 2001). In contrast, the models developed by Liu et al. (2003) and Billings et al. (2010) simulate several soil layers with explicit controls on the depth variation

of SOC formation and decomposition. However, these models fail to include spatial integration, as they are also limited to the application on single soil profiles at different landscape positions. In recent advances, models allow for an improved integrated spatial analysis of the impact of soil redistribution on SOC dynamics at the catchment scale by combining spatially explicit geomorphic models, including soil redistribution, with models of SOC dynamics (Rosenbloom et al., 2001; Van Oost et al., 2005a; Yadav and Malanson, 2009; Yoo et al., 2005). These models focus on the catchment-scale C balance adopting a multiple soil layer structure. While the models presented by Rosenbloom et al. (2001) and Yoo et al. (2005) focus on the long-term hillslope response due to diffusive geomorphic processes on grasslands, the SPEROS-C model developed by Van Oost et al. (2005) and the model presented by Yadav and Malanson (2009) focus on contemporary soil redistribution on arable land. SPEROS-C is the only model that besides water induced soil redistribution also considers soil redistribution by tillage operations (e.g. Govers et al., 1994; Lindstrom et al., 1992). Tillage erosion can be more important than water erosion on sloped arable fields and substantially changes soil redistribution patterns (Govers et al., 1994).

Against this background, this thesis analyses impacts of soil redistribution processes on SOC stocks and fluxes in a small agricultural catchment (4.2 ha) in Germany. Therefore, detailed field measurements of SOC stocks, particle-size SOC fractions, ^{14}C, and further soil properties in three dimensions as well as *in situ* measurements of soil respiration are explored (chapters 3-5). In a modelling approach using an adapted version of SPEROS-C, these measurements are synthesised and the spatially integrated effects of soil redistribution processes on SOC stocks and fluxes are investigated at the catchment scale (chapter 6).

The main research questions of this thesis are:

- Does soil redistribution constitute a C sink or source in a small agricultural catchment in Germany?
- Which mechanisms contribute to the C sink or source in the test site?
- Does agricultural management alter the erosion induced C sink or source in the test site?

To address the general questions, the specific objectives of this study can be summarised as:

(i) To evaluate measured spatial patterns of SOC stocks in the plough layer (0-0.25 m) and two subsoil layers (0.25-0.5 and 0.5-0.9 m) with respect to terrain attributes and patterns

of soil redistribution and to produce accurate and precise SOC maps serving as validation data for modelling (chapter 3),

(ii) to investigate the effect of soil redistribution on *in situ* measured heterotrophic and combined heterotrophic and autotrophic soil respiration at different slope positions and to define parameters (soil and plant properties, terrain attributes) that affect the spatial variability of soil respiration and thus alter SOC stocks (chapter 4),

(iii) to analyse the preferential erosion and/or deposition of particle-size SOC fractions and to investigate differences in ^{14}C depth distributions in relation to these SOC fractions at different slope positions (chapter 5), and

(iv) to quantify the lateral and vertical soil C fluxes induced by soil redistribution by applying the model SPEROS-C as well as their sensitivity to uncertainties in model inputs and changes in land management (chapter 6).

2 TEST SITE

The Heiderhof test site (4.2 ha; 125-154 m a.s.l.; 50°43'N, 7°12'E) is a representative sub-catchment within the Dissenbach catchment (~150 ha; 104-186 m a.s.l), situated in the Pleiser Hills (Pleiser Hügelland) (Fig. 2.1) about 8 km east of Bonn in North Rhine-Westphalia, Germany.

Climate in the test site region is moderate maritime with warm summers and mild winters. The mean annual air temperature in the Cologne-Bonn area is ~10°C with a significant variation throughout the year. The mean air temperature in January is 2.3°C and in July it is 18.3°C, respectively [data from the meteorological stations Bonn-Friesdorf (1949-1998; 62 m a.s.l.) and Köln-Wahn (1961-2009; 92 m a.s.l) provided by the Deutsche Wetterdienst]. Precipitation is equally distributed throughout the year with an average of 790 mm per year (1975-2007) [data from the precipitation station Bockeroth, situated about 2.5 km east of the test site (151 m a.s.l.) (Fig. 2.1) provided by the Landesamt für Natur, Umwelt und Verbraucherschutz Nordrhein-Westfalen]. Highest rainfall intensities occur from May to October (Bartels et al., 1997).

The Pleiser Hills are formed on a complex geology comprising a Palaeozoic sedimentary basement, marine sediments and volcanic material of Tertiary age, as well as Quaternary sediments. They are located in the transitional zone between the Lower Rhine Embayment (Niederrheinische Bucht) in the North and the Rhenish Slate Mountains (Rheinisches Schiefergebirge) in the South, whose twofold tectonic subsidence and uplift had a profound formative effect on the development of the Pleiser Hills in geologic history (Henningsen and Katzung, 1998). Today, the topography of the Pleiser Hills is undulating with a high drainage density. Drainage direction is towards the river Sieg in the North (Fig. 2.1).

The bedrock material in the upper part of the Dissenbach catchment consists of Tertiary loam, developed from marine and estuarine sediments deposited in congruence with the Alpine orogenesis, and Quaternary sediments (mainly gravel and sand) from the main terrace of the Rhine. Approximately two thirds of the Dissenbach catchment is covered with loess,

blown in from the west and north-west during the Pleistocene glaciations, when the test site region was a periglacial environment (Geologisches Landesamt Nordrhein-Westfalen, 1975). The oldest loesses on which contemporary soils are formed are dated back to the Pommersche stadial (~18.000 BP) (Grunert, 1988).

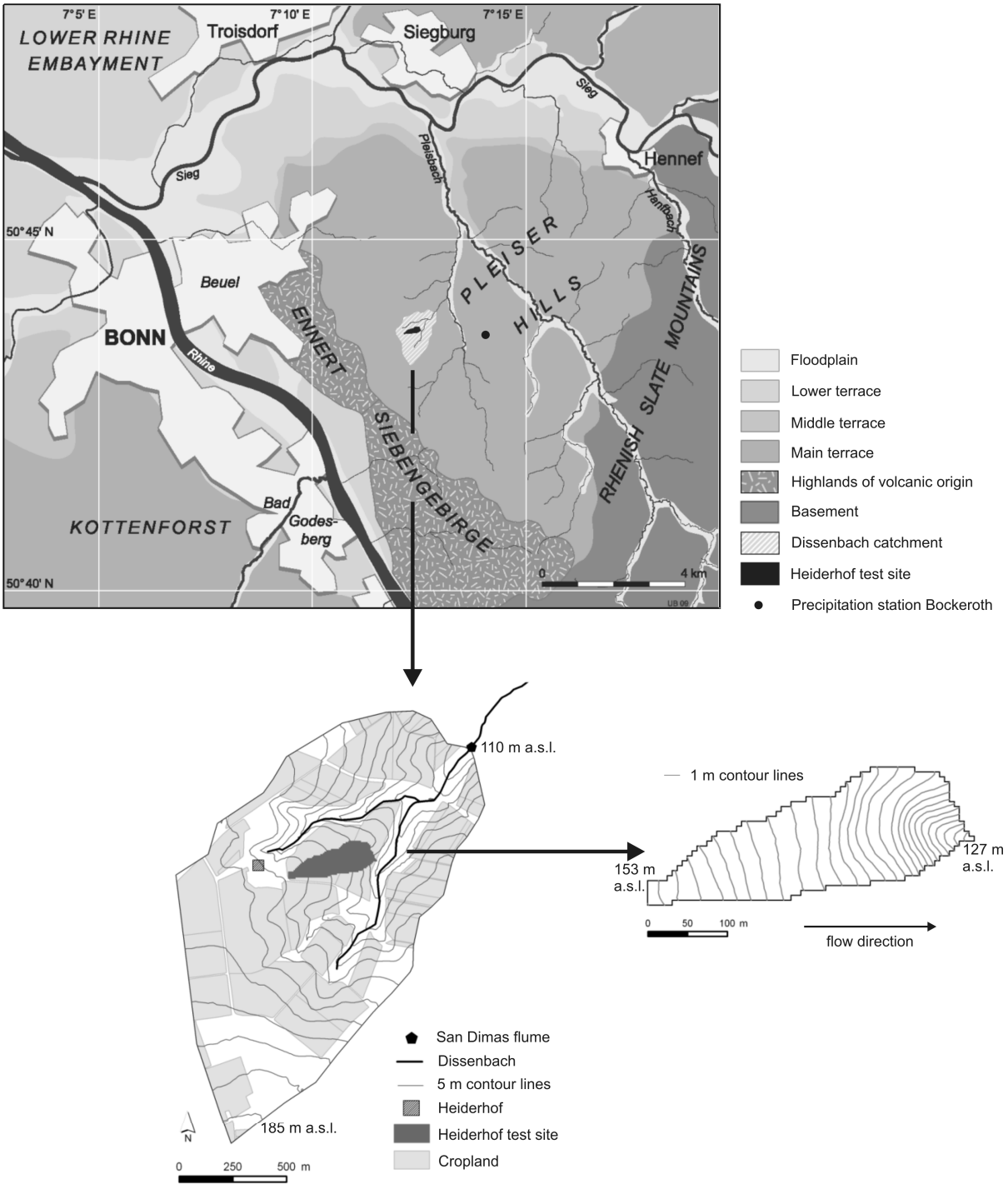

Fig. 2.1 Location and topography of the Dissenbach catchment and the Heiderhof test site (Cartography: overview map by Udo Beha).

Being the climax soil on loess sites, two thirds of the Dissenbach catchment is covered with Luvisols (FAO, 1998). Additionally, Stagnosols that evolved from the Luvisols can be found on sites where drainage is impeded. In the alluvial area of the Dissenbach, Colluvisols as well as Gleysols have emerged under the impact of groundwater. On highly eroded sites Calcaric Regosols have again developed (Geologischer Dienst NRW, 2001).

Due to its fertile soils and its climatic favour, the Pleiser Hills have a long history of arable land use, dating back to early Neolithic (5000-1500 BC) and being pursued by the Celtic and Germanic populations. Two phases of Frankish expansion followed, from the middle of the third century BC onwards, associated with intense settling and agriculture (Preston, 2001). Since its first agricultural use, the test site region was prone to enhanced soil erosion due to its undulating topography and the high silt content of the soils. Historical soil erosion studies in the region (e.g. Lessmann-Schoch et al., 1991) suggest that anthropogenic colluviation can be dated back to the 14th century BC.

Today, the Dissenbach catchment is used intensively as arable land. Approximately 70% of its area, especially the moderate slopes (0-10°), is used for arable agriculture (Fig. 2.1), while the flat and wetter areas along the Dissenbach are used as grassland (~20% of the catchment area). The steep slopes (up to 29°) along the Heidersiefen (northern tributary of the Dissenbach; Fig. 2.1) are used as forest. Residential and traffic areas encompass ~4% of the Dissenbach catchment.

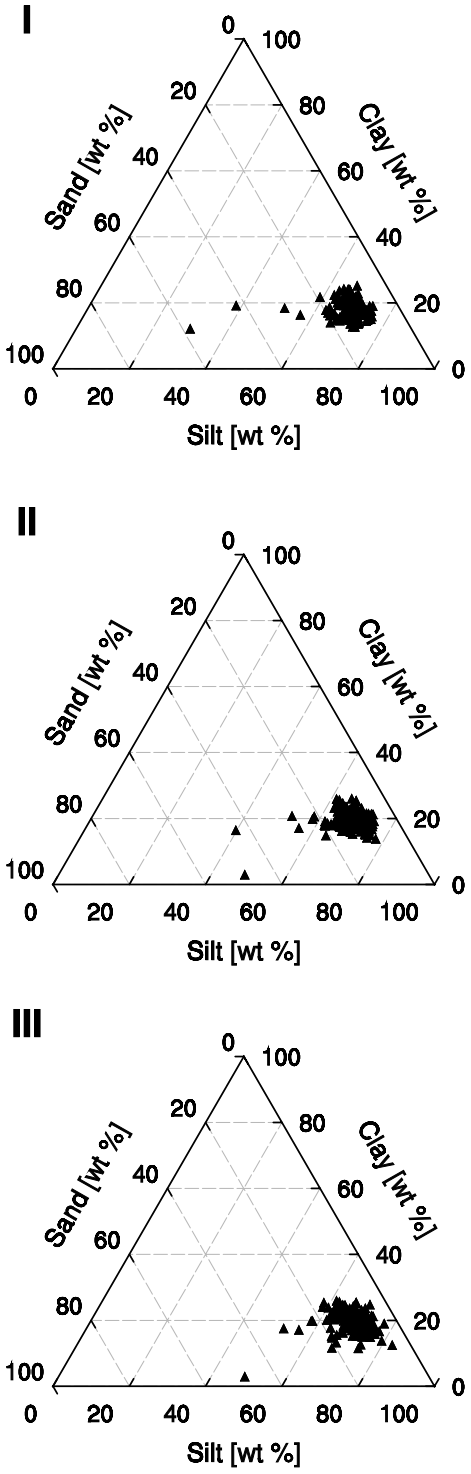

Fig. 2.2: Soil texture diagrams (sand: 63-2000 µm, silt: 2-63 µm, clay: < 2 µm) for three soil layers (I: 0-0.25 m; II: 0.25-0.5 m; III: 0.5-0.9 m) derived from sampling points situated in a 17x17 m raster in the test site (n = 144).

The Heiderhof test site is representative within the loess-burden and fertile Dissenbach catchment with respect to its slopes, its soil type and texture as well as its arable use. It is a small catchment (4.2 ha) within a larger agricultural field (~12 ha). Almost two-thirds of the test site (middle to western part) is relatively flat, with slopes ranging between 1 and 2°. Steep slopes (up to approximately 9.5°) exist in the eastern part, where a small thalweg area with still relatively high slopes (3-5°) is incorporated that is heading to the outlet (Fig. 2.1).

An intense soil sampling campaign carried out in 2006 and 2007 on the test site (for a further description of soil sampling and sample analysis refer to chapter 3.2.1) confirmed that the Heiderhof test site is also dominated by Luvisols with a silty and silty-loamy texture (Fig. 2.2) developed on loess. The mean sand, silt, and clay content up to 0.9 m depth are 13 wt%, 68 wt%, and 19 wt%, respectively (n = 144). Towards the outlet of the test site the texture gets sandier (up to 35-40 wt% sand content) due to depositional processes. There, also gleyic horizons are visible in the subsoil due to the influence of groundwater.

The Heiderhof settlement (Fig. 2.1) is attributed to the first Frankish expansion phase (~500-550 AD) (Preston, 2001), so that the potential first agricultural use of the test site can be dated back to that period. The present crop rotation of the Heiderhof test site consists of sugar beet (*Beta vulgaris* L.), winter wheat (*Triticum aestivum* L.), and winter barley (*Hordeum vulgare* L.). Until 1980, the test site was conventionally tilled by mouldboard ploughing with a tillage depth of 0.25 m. Since 1980, a conservation tillage system has been established with chisel instead of mouldboard ploughing (tillage depth 0.15 m) and the cultivation of mustard (*Sinapis arvensis* L.) as cover crop after winter barley.

3 LAYER-SPECIFIC ANALYSIS AND SPATIAL PREDICTION OF SOIL ORGANIC CARBON USING TERRAIN ATTRIBUTES AND EROSION MODELLING*

3.1 INTRODUCTION

Detailed and precise maps of the distribution of soil organic carbon (SOC) are an essential prerequisite for analysing the possibilities of soils to sequester atmospheric CO_2, as well as for other environmental issues, like e.g. the analysis of soil quality and the adaptation of management practices. Especially in agricultural regions the complex arrangement and combination of topography, soil, and management practices as well as the biological processes controlled by these parameters lead to a high spatial variability of SOC. A rolling topography also affects the spatial heterogeneity of SOC in agricultural fields by soil redistribution processes.

To produce accurate SOC maps, in general, different kinds of interpolation schemes are applied based on point measurements. As field measurements are costly and time-consuming, the improvement of interpolation methods to derive spatial SOC patterns using secondary information is important and was intensively tested. Terrain attributes of various complexities were used as proxies for relief driven processes of pedogenesis. In most studies primary terrain parameters, which can be easily derived from digital elevation models (DEMs), such as (relative) elevation (Mueller and Pierce, 2003; Ping and Dobermann, 2006; Sumfleth and Duttmann, 2008), slope (Mueller and Pierce, 2003; Ping and Dobermann, 2006; Sumfleth and Duttmann, 2008; Takata et al., 2007), aspect (Odeh et al., 1994; 1995), and curvature (Takata et al., 2007; Terra et al., 2004) were used as secondary information. These primary terrain parameters can also be combined, resulting in more complex secondary terrain parameters or

* Based on: Dlugoß, V., P. Fiener and K. Schneider. 2010. Layer-specific analysis and spatial prediction of soil organic carbon using terrain attributes and erosion modelling. Soil Science Society of America Journal 74 (3): 922-935.

indices comprising landscape processes more explicitly. Often the wetness (or topographic) index (Beven and Kirkby, 1979) was tested for its capability to improve the interpolation of SOC and other soil properties (e.g. Herbst et al., 2006; Sumfleth and Duttmann, 2008; Takata et al., 2007). In addition to these terrain parameters also other parameters were used in literature as covariables for interpolation schemes. Takata et al. (2007), for example, used the enhanced vegetation index, whereas Chen et al. (2000) used soil colour to successfully predict the spatial distribution of SOC. Both parameters were derived from remote sensing data. Another covariable utilised effectively to improve the interpolation of SOC is the electrical conductivity of the topsoil layer (Ping and Dobermann, 2006; Simbahan et al., 2006; Terra et al., 2004).

A variety of statistical and geostatistical methods exist to interpolate point data with and without consideration of secondary information (e.g. Isaaks and Srivastava, 1989; Webster and Oliver, 2001). While simple statistical approaches, such as a (multiple) linear regression performed well to interpolate SOC under certain circumstances (e.g. Mueller and Pierce, 2003), often geostatistical kriging approaches which account for the spatial structure of SOC as well as that of covariables performed better. Whereas ordinary kriging utilises only the spatial autocorrelation of the target variable, there are several geostatistical techniques that allow incorporating a spatial trend caused by spatial patterns of secondary parameters in the kriging approach. Most often regression kriging (RK) or kriging with external drift (KED) is applied. In contrast to KED, which is a one-algorithm system, RK is a stepwise approach combining a regression between target and covariable with simple or ordinary kriging of the regression residuals. While the target and the covariable have to be linearly related in KED, RK also allows integrating more complex regression models (i.e. multiple linear or non-linear functions). KED and linear RK only differ in the computational steps used, but the resulting predictions are the same given the same input data (target and covariable) and the same regression fitting method (Hengl et al., 2007).

Odeh et al. (1994; 1995) defined three types of regression kriging, of which regression kriging model C, where the trend function is calculated using ordinary least squares, and the residuals are interpolated using ordinary kriging, was successfully used to improve the interpolation of soil organic carbon as well as that of other soil properties in many studies (e.g. Herbst et al., 2006; Sumfleth and Duttmann, 2008; Takata et al., 2007; Terra et al., 2004).

A geostatistically more sophisticated approach, which overcomes some statistical deficiencies of KED and RK, is REML-EBLUP (Lark et al., 2006). In this method the trend model is estimated using residual maximum likelihood (REML), and subsequently the estimated parameters are used for the empirical best linear unbiased prediction (EBLUP). However, Minasny and McBratney (2007a/b) who compared RK model C with REML-EBLUP for interpolating four different soil properties concluded, that although statistically somewhat inappropriate, RK has proven to be a robust technique for practical applications. In concordance to these results, Chai et al. (2008), who analysed the effect of different covariables on the spatial interpolation of soil organic matter, concluded that REML-EBLUP performed more stable, but that the improvement was not significant compared to RK.

To our knowledge all studies which explicitly deal with the interpolation of SOC and its possible improvement by incorporating covariables in the interpolation process focus on the topsoil layer (< 0.3 m; e.g. Mueller and Pierce, 2003; Ping and Dobermann, 2006; Simbahan et al., 2006; Sumfleth and Duttmann, 2008; Takata et al., 2007; Terra et al., 2004). However, the spatial patterns of SOC in sloped agricultural catchments might differ substantially in different soil depths. This aspect should be taken into account for studies addressing the soil carbon balance as well as for simulations of soil carbon dynamics.

Against this background, the objectives of this chapter are:

(i) To evaluate the spatial patterns of SOC in different soil layers in a small agricultural catchment and to analyse their relation to spatial patterns of terrain parameters and results from soil redistribution modelling, and
(ii) to evaluate if these (easily available) parameters can serve as improving covariables in a layer-specific interpolation of SOC data by regression kriging, and hence potentially allow for a reduction of SOC sampling density without a loss of mapping quality.

3.2 Materials and Methods

3.2.1 Soil sampling and SOC measurement

In order to investigate the vertical and horizontal distribution of SOC in the test site, a first set of soil samples was taken in April 2006. It consisted of 92 soil cores of which 71 cores were positioned on a regular 25 x 25 m raster. To account for small scale spatial variability of SOC, additionally a north-south transect in the eastern part of the test site with point distances

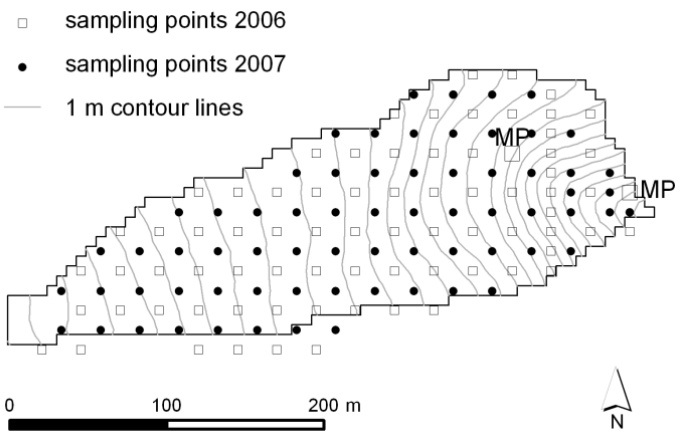

Fig. 3.1: Test site with location of soil sampling points; each of the two micro-plots (MP) consists of nine sample points arranged in a 1 x 1 m grid; flow direction is from west to east.

of 12.5 m and two micro-plots consisting of nine sample points each in a 1 x 1 m raster were augered. In each of the micro-plots the central sampling point belongs to the regular 25 x 25 m raster. Micro-plots were selected to cover different slope positions. To increase the density of the first sampling grid, a second set of soil cores (n = 65) was taken in March 2007 using a 25 x 25 m raster which was offset by 12.5 m to the north and west in relation to the 2006 raster. Additionally, three samples were taken near the outlet of the test site to account for a small colluvial area. Thus, soil samples are available in a regular 17.7 x 17.7 m raster with a density of 38 samples per ha (Fig. 3.1), with additional samples along the transect and in the micro-plots. Within each sampling campaign soil cores were extracted with a Pyrckhauer soil auger (approximately 2 cm diameter) and soil samples were taken in three depths (I: 0-0.25 m, II: 0.25-0.50 m, and III: 0.50-0.90 m). All sampling points were surveyed with a dGPS (differential Global Positioning System) with a horizontal accuracy between 0.5 and 2.0 m.

After oven drying at 105°C for 24 hours the samples were ground and coarse particles were separated by 2 mm-sieving. Roots and other recognisable undecomposed organic matter particles were removed. Total C content was determined by dry combustion using a CNS elemental analyser (vario EL, Elementar, Germany). Although loess soils in the area are in most cases deeply decalcified, all soil samples were checked for lime ($CaCO_3$) with hydrochloric acid (10 %). If any inorganic C content was recognised, its amount was determined according to the Scheibler method (Deutsches Institut für Normung, 1996). Combining both methods, if necessary, SOC was calculated from total minus inorganic carbon.

3.2.2 Terrain analysis

A set of primary terrain attributes and secondary terrain indices which may affect the spatial distribution of SOC was calculated. The indices combine different primary terrain

attributes and thus represent landscape processes more explicitly. The derivation of these parameters was based on a digital elevation model (DEM) with a 6.25 x 6.25 m grid. The DEM was interpolated from Lidar data (2–3 m point distance) provided by the Landesvermessungsamt North Rhine-Westphalia using ordinary kriging (spherical model; nugget: 0.6; sill: 46.2; range: 237 m) within the Geostatistical Analyst of the Geographical Information System ArcGis 9.2 (ESRI Inc., USA). The grid size of 6.25 x 6.25 m was chosen to assure that each sampling point is located in the centre of a grid cell.

The following primary terrain attributes were calculated using ArcGis 9.2: The relative elevation (*RE*), which is the vertical distance of every grid cell to the outlet of the catchment, the slope *s*, the aspect *A*, and the curvature. The curvature is the second derivative of the surface and is separated into profile curvature (*C-prof*; curvature in the direction of maximum slope) and plan curvature (*C-plan*; curvature perpendicular to the direction of maximum slope). Another primary terrain attribute used in this study is the catchment area *CA* calculated for each grid cell using the extension HydroTools 1.0 for ArcView 3.x (Schäuble, 2004). The multiple flow algorithm of Quinn et al. (1991) was applied, in which the flow is distributed among three down slope grid cells weighted by slope gradient. The catchment area takes into consideration the amount of surface water that is distributed towards each grid cell. The parameter thus is related to soil moisture and infiltration as well as erosion and deposition. The two combined indices, wetness index (*WI*) and stream power index (*SPI*), differentiate between these two process groups more explicitly through the incorporation of the local slope gradient. The wetness index (*WI*) characterises the distribution of zones of surface saturation and soil water content in landscapes (Beven and Kirkby, 1979) and is calculated as:

$$WI = \ln \frac{SCA}{\tan s} \tag{3.1}$$

where *SCA* is the specific catchment or contributing area ($m^2\ m^{-1}$) orthogonal to the flow direction and is calculated as the catchment area *CA* divided by the grid length (6.25 m) and *s* is the slope (°).

The stream power index (*SPI*) is the product of the specific catchment area *SCA* ($m^2\ m^{-1}$) and the slope *s* (°) (Moore et al., 1993).

$$SPI = SCA \cdot \tan s \tag{3.2}$$

It is directly proportional to stream power and can thus be interpreted as the erosion disposition of overland flow.

3.2.3 Erosion modelling

In order to more explicitly consider different soil redistribution processes due to water (E_{wat}), tillage (E_{til}) and total (E_{tot}) erosion and deposition, corresponding patterns were calculated applying the long-term soil erosion and sediment delivery model WaTEM/SEDEM version 2.1.0 (Van Oost et al., 2000; Van Rompaey et al., 2001; Verstraeten et al., 2002).

WaTEM/SEDEM is a spatially distributed model combining WaTEM (Water and Tillage Erosion Model) (Van Oost et al., 2000) and SEDEM (Sediment Delivery Model) (Van Rompaey et al., 2001). WaTEM consists of a water and a tillage erosion component which can be run separately. The water erosion component uses an adapted version of the revised Universal Soil Loss Equation (RUSLE, Renard et al., 1996). Adaptations consist of the substitution of slope length with the unit contributing area calculated following Desmet and Govers (1996a) and the integration of sedimentation following an approach of Govers et al. (1993). Tillage erosion is caused by variations in tillage translocations over a landscape and always results in a net soil displacement in the down slope direction. The net down slope flux Q_{til} (kg m^{-1} a^{-1}) due to tillage implementations on a hill slope of infinitesimal length and unit width is calculated with a diffusion-type equation adopted from Govers et al. (1994) and is proportional to the local slope gradient:

$$Q_{til} = k_{til} \cdot s = -k_{til} \cdot \frac{\Delta H}{\Delta x} \tag{3.3}$$

where k_{til} is the tillage transport coefficient (kg m^{-1} a^{-1}), s is the local slope gradient (%), H is the height at a given point of the hill slope (m) and x the distance in horizontal direction (m). The local erosion or deposition rate E_{til} (kg m^{-2} a^{-1}) is then calculated as:

$$E_{til} = -\frac{\Delta Q_{til}}{\Delta x} = \frac{\Delta^2 H}{\Delta^2 x} \tag{3.4}$$

As tillage erosion is controlled by the change of the slope gradient and not by the slope gradient itself, erosion takes place on convexities and soil is accumulated in concavities. The intensity of the process is determined by the constant k_{til} that ranges between 500 and 1000 kg m^{-1} a^{-1} in western Europe (Van Oost et al., 2000).

A second module of WaTEM/SEDEM is the calculation of sediment transport and sedimentation. The sediment flow pattern is calculated with a multiple flow algorithm. The sediment is routed along this flow pattern towards the river taking into account its possible

deposition. Deposition is controlled by the transport capacity computed for each grid cell. The transport capacity is the maximal amount of sediment that can pass through a grid cell and is assumed to be proportional to the potential rill (and ephemeral gully) erosion (Van Rompaey et al., 2001). If the local transport capacity is lower than the sediment flux, deposition is modelled.

WaTEM/SEDEM requires the input of several GIS maps as well as various constants and was implemented as follows: The 6.25 x 6.25 m DEM served as the basis for the calculations. Additionally, a land use map containing field boundaries and a map containing the tillage direction of the test site were derived from digital aerial photographs provided by the Landesvermessungsamt North Rhine-Westphalia. The K factor of the RUSLE was also given as a map with values ranging from 0.058 to 0.061 kg h m^{-2} N^{-1}. This map was derived from a digital soil map (scaled 1:50000) provided by the Geological Survey of North Rhine-Westphalia. Accounting for the crop rotation and the implemented soil conservation practice in the test site, the C factor was set to 0.05 (Deutsches Institut für Normung, 2005). The R factor of the USLE was calculated with a regression equation between R factor and mean summer precipitation developed for North Rhine-Westphalia (Deutsches Institut für Normung, 2005). Therefore precipitation data (1975-2007) of the precipitation station Bockeroth situated about 2.5 km east of the test site (151 m a.s.l.) (Fig. 2.1) were used, resulting in an R factor of 67 N h^{-1} a^{-1}. Since no sediment yield data for model calibration were available, modelling was first performed on a 20 x 20 m grid, which is equal to the grid size in earlier, calibrated simulations under similar environmental conditions in the Belgium Loess Belt (Verstraeten et al., 2006). The results of this first simulation were used to recalibrate the transport capacity coefficients to run the model on a 6.25 x 6.25 m grid. All other constants necessary for running WaTEM/SEDEM were set to default, since no absolute but only relative erosion and deposition values were needed.

3.2.4 Statistical and geostatistical analysis

Statistical analysis

For statistical and geostatistical analysis three SOC input grids with different sampling densities were created. To achieve a dense 17.7 x 17.7 m sample raster (R_{17}), SOC data of the 2006 and 2007 sampling campaign were combined in each soil layer. For the topsoil layer, it was assumed that inter-annual differences of sampling date and thus of planted crops, soil management, and climate could have resulted in differences of SOC concentrations as

measured during the two sampling campaigns. Thus, after assessing normal distribution by analysing skewness coefficients, a Student's T-test (although not optimal when used with spatially auto-correlated data) was applied to estimate the equality of means of the SOC data of the two sampling years. In the two deeper soil layers these influences were considered negligible. Here the SOC contents of the two sampling dates were simply combined to one data set. The 2006 sampling points (n = 92) arranged in a 25 m raster (R_{25}) served as input data set with a medium density of 17 samples per hectare for each soil layer. To produce a low density 50 m input raster (R_{50}; n = 44) every second data point of R_{25} was eliminated resulting in a density of approximately 6 samples per hectare. Each raster contained the transect and the two micro-plots to include short distances in geostatistics.

The relationship between the spatial patterns of SOC and the spatial patterns of potential covariables was tested using Pearson correlation coefficients calculated between all parameters and the SOC data for each soil layer and each raster width, respectively. In this correlation analysis the eight additional points of the micro-plots were excluded, since all nine sampling points of a micro-plot are located in one grid cell with one value for the relevant parameter. Parameters which were significantly ($p < 0.05$) related to SOC in a soil layer were tested for their potential to improve interpolation results when used as a linear trend in regression kriging.

Geostatistical analysis

Geostatistical methods are based on the theory of regionalised variables (Matheron, 1963). For further information concerning the theoretical background of geostatistics we refer to Isaaks and Srivastava (1989) or Webster and Oliver (2001). The basic assumption is that sample points located close to each other are more similar than sample points far apart. This spatial autocorrelation is quantified in an empirical semivariogram of the sampled data, where the semivariance is plotted as a function of lag distance. For a data set $z(x_i)$, $i = 1, 2,...$, the semivariance γ of a certain lag distance h is calculated as

$$\gamma(h) = \frac{1}{2n(h)} \sum_{i=1}^{n(h)} (z(x_i) - z(x_i + h))^2 \qquad (3.5)$$

with $n(h)$ being the number of pairs of data points separated by lag h. To apply this semivariogram in the following interpolation process, known as kriging in geostatistics, a theoretical model has to be fit to the sample variogram.

Ordinary kriging (OK) which only uses the spatial autocorrelation of the target variable can be considered as a basic geostatistical interpolation method. It can be described as a weighted spatial mean, where sample point values x_j are weighted according to the semivariance as a function of distance to the prediction location x_0. The weights λ_i are chosen by solving the ordinary kriging system in order to minimise the kriging variance:

$$\sum_{i=1}^{n} \lambda_i \gamma(x_i, x_j) + \varphi = \gamma(x_i, x_0)$$
$$\sum_{i=1}^{n} \lambda_i = 1 \qquad (3.6)$$

where $\gamma(x_i,x_j)$ is the semivariance between the sampling points x_i and x_j and $\gamma(x_i,x_0)$ is the semivariance between the sampling point x_i and the target point x_0 and φ is a Lagrange-multiplier necessary for the minimisation process (Ahmed and DeMarsily, 1987).

The regression kriging used in this study follows regression kriging model C described in Odeh et al. (1995) and accounts for a possible trend in the data combining linear regression with ordinary kriging of the residuals. In a first step a linear regression function of the target variable with the covariables is used to create a spatial prediction of the target variable at the new locations. In a second step ordinary kriging is applied to the residuals of the regression resulting in a spatial prediction of the residuals. Finally, the spatially distributed regression results and the kriged residuals are added to calculate the target variable at all new locations.

As a prerequisite of geostatistics, SOC data in each soil layer and in each raster width should be normally distributed. Following Kerry and Oliver (2007a) this prerequisite can be met in geostatistical analysis if the absolute skewness coefficient (SC) is < 1. Moreover, data with an asymmetry caused by aggregated outliers need not to be transformed if the absolute SC is < 2 (Kerry and Oliver, 2007b). If this was true, SOC data were not transformed. For use in regression kriging the residuals resulting from linear regression with the significantly correlated parameters in each soil layer and in each raster width should also be normally distributed. Skewness coefficients as well as normal Q-Q plots of residuals were analysed. If residuals showed strong deviations from normal distribution, the corresponding parameters were log-transformed and a linear regression analysis was applied (subsequently these transformed covariables are indicated by the subscript tr).

For each raster width and for each of the three soil layers SOC was interpolated using OK and RK with the selected parameters as covariables to target points spanning a 6.25 x 6.25 m

raster within the test site. For the construction of omnidirectional empirical semivariograms of the original SOC data as well as of the residuals the maximum distance up to which point pairs are included was set to 200 m which is half of the maximum extent of the test site in east-west-direction. Lag increments were set to 10 m. In each approach two theoretical variogram models (exponential and spherical) and three methods for fitting the variogram model to the empirical variogram including ordinary least squares (i.e. equal weights to all semivariances) and two weighted least square methods (weighting by n_p = number of pairs and weighting by $n_p h^{-2}$ with h = lag distance) were applied. To evaluate the various theoretical variograms against the original data and to choose the best model, a cross-validation procedure was implemented. In the cross-validation procedure one measurement is omitted in the variogram construction, this value is subsequently estimated by the kriging (OK and RK) method and the estimate is finally compared to the measurement. This procedure is applied to all measurements one at a time.

As a measure of spatial dependence the ratio of nugget to sill (%) was calculated reflecting the influence of the random component to the spatial variability. Following Cambardella et al. (1994) nugget-to-sill ratios between 0 and 25 % show that data are highly spatially structured with low nugget variances, whereas ratios between 25 and 75 % indicate moderate spatial dependence. Data with ratios > 75 % are weakly spatially structured with a high proportion of unexplained variability.

3.2.5 Validation

The previously described cross-validation procedure was also used to validate the kriging results of the high-density input grid (R_{17}) and to compare the performance of the different geostatistical approaches in this raster width, although it systematically underestimates the quality of predictions when using a regular input grid (Isaaks and Srivastava, 1989; Mueller et al., 2001; 2004). Nevertheless, we used this procedure to avoid a loss of information in the input data. When using the reduced sampling grids R_{25} or R_{50} as input data, the 2007 sampling points (n = 67) were used for validation and for comparing the different kriging approaches within each raster width. Analogously to the cross-validation procedure, this procedure also underestimates the prediction quality, since the tested prediction distance is much larger than the requested prediction distance of the resulting SOC maps. Hence, the measures of goodness-of-fit can be regarded as somewhat conservative. However, since the main objective of this study was to analyse, if the prediction precision can be improved within one raster

width when incorporating secondary parameters in the kriging process, this validation method can be accepted as a suitable approach.

Since different validation schemes had to be applied for the three input data sets due to the lack of an independent and randomised validation data set, a direct quantitative comparison of the interpolation results obtained for R_{17} and the two reduced input data sets is not possible. Comparisons of the different raster widths can only be done in qualitative terms.

To evaluate the goodness-of-fit of the various kriging results, a set of indices was used. To account for the bias and the precision of the prediction, the mean error *ME* and the root mean square error *RMSE* were calculated:

$$ME = \frac{1}{n}\sum_{i=1}^{n} z(x_i) - \hat{z}(x_i) \tag{3.7}$$

$$RMSE = \sqrt{\frac{1}{n}\sum_{i=1}^{n}(z(x_i) - \hat{z}(x_i))^2} \tag{3.8}$$

where *n* constitutes the number of points in the validation sample or the number of points used for cross-validation, $z(x_i)$ the observed and $\hat{z}(x_i)$ the predicted values. The *ME* should be close to zero for unbiased predictions, and the *RMSE* should be as small as possible. Additionally, the model-efficiency coefficient (*MEF*) by Nash and Sutcliffe (1970) was calculated.

$$MEF = 1 - \frac{\sum_{i=1}^{n}(z(x_i) - \hat{z}(x_i))^2}{\sum_{i=1}^{n}(z(x_i) - \bar{x})^2} \tag{3.9}$$

The *MEF* is a measure of the mean squared error to the observed variance and ranges between $-\infty$ and 1. If the value of $MEF = 1$, the model or interpolation represents a perfect fit. If the error is in the same order of magnitude as the observed variance ($MEF = 0$), the arithmetic mean $\bar{x}$ of the observed values can represent the data as good as the interpolation.

The relative improvement *RI* (%) of prediction precision of RK with the selected covariables compared to OK was derived as:

$$RI = \frac{RMSE_{OK} - RMSE_{RK}}{RMSE_{OK}} \cdot 100 \tag{3.10}$$

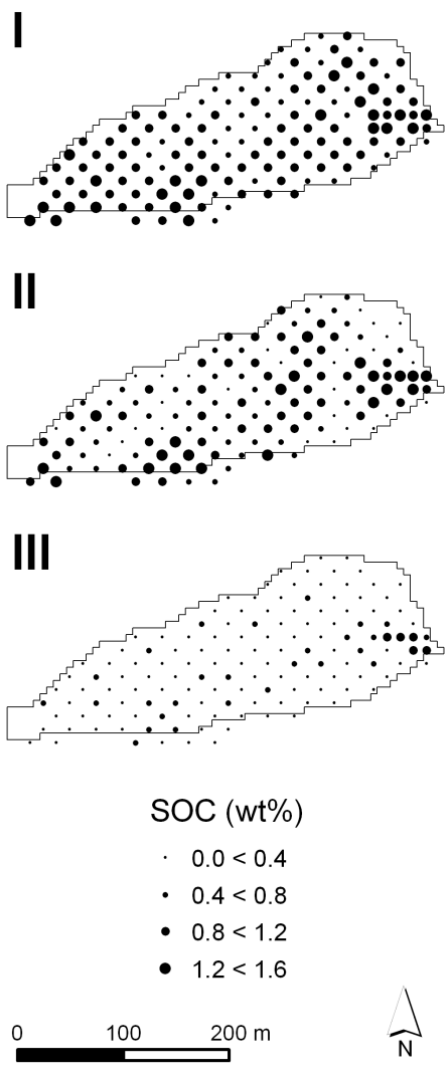

Fig. 3.2: Measured SOC contents [wt%] at the 17.7 x 17.7 m raster sampling points for three soil layers (I: 0-0.25 m, II: 0.25-0.50 m, III: 0.50-0.90 m).

where $RMSE_{RK}$ and $RMSE_{OK}$ are root mean square errors for a certain regression kriging approach and for ordinary kriging, respectively.

Additionally, prediction quality was assessed by visual examination of plots of predicted vs. measured SOC contents of different kriging approaches. High quality is given when the scatter of data and/or its linear regression fit adheres closely to the 1:1 line (Mueller et al., 2004).

The statistical and geostatistical analysis was carried out with GNU R version 2.6 (R Development Core Team, 2007) and the supplementary geostatistical package gstat (Pebesma, 2004).

3.3 Results and Discussion

3.3.1 Measured horizontal and vertical SOC distribution

Since Student's T test clearly shows that the SOC contents of the two sampling dates in soil layer I belong to the same population, SOC contents in each soil layer were combined to one data set. After merging the data sets SOC values in soil layer I range from 0.68 to 1.67 wt %, in soil layer II from 0.13 to 1.19 wt %, and in soil layer III from 0.04 to 1.18 wt % (Tab. 3.1). Maximum values in all soil layers were found in the flat area near the outlet of the test site (Fig. 3.2) indicating accumulation of SOC by depositional processes. This phenomenon is more pronounced with increasing soil depth. Another small area of relatively high SOC concentrations primarily in the two upper soil layers is located in the upper part near the southern boundary of the test site. We assume that this was caused by areas formerly used for dung or sugar beet storage, but no detailed data to verify or falsify this assumption regarding its location exist. Remarkably, the SOC distribution of the mid soil layer shows more small scale variability than that of the other two soil layers. This indicates a small scale change of the depth of the boundary between topsoil with high SOC concentrations and subsoil with

lower SOC concentrations relative to the surface, which can be ascribed to soil redistribution processes. The results show that the majority of these transitions take place in this medium soil layer.

The maps of the measured SOC content (Fig. 3.2) show a decrease of SOC content and an increase of spatial variability with increasing soil depth, also indicated by increasing coefficients of variation (CV) (Tab. 3.1). The low spatial variability in soil layer I can be attributed to homogenisation caused by management practices as well as to high turnover rates of soil organic matter in this soil layer. In the deepest soil layer high SOC contents in the depositional area near the outlet of the test site are most pronounced resulting in a skewness coefficient of 1.5 indicating a non-normal distribution. Since this non-normality was caused by outliers aggregated in the depositional area (Fig. 3.2), the data were not transformed before further geostatistical analysis.

Tab. 3.1: Statistics of SOC content for the 2006, 2007 and the merged (merg.) dataset in three soil depths (I: 0-0.25 m; II: 0.25-0.50 m; III: 0.50-0.90 m).

Soil layer	Data set	n†	SOC [wt%] Mean	Median	SD	CV	Min	Max	SC
I	2006	92	1.16	1.14	0.18	15.13	0.68	1.68	0.75
II	2006	92	0.67	0.67	0.22	32.62	0.13	1.19	0.24
III	2006	92	0.32	0.24	0.18	62.13	0.05	0.90	1.51
I	2007	67	1.11	1.08	0.16	12.23	0.85	1.43	0.30
II	2007	68	0.75	0.77	0.23	30.44	0.18	1.18	-0.32
III	2007	68	0.36	0.33	0.22	62.55	0.04	1.18	1.57
I	merg.	159	1.14	1.12	0.17	14.91	0.68	1.68	0.74
II	merg.	160	0.71	0.71	0.22	30.99	0.13	1.19	0.01
III	merg	160	0.34	0.27	0.21	62.61	0.04	1.18	1.50

† n:sample size; SD: standard deviation; CV: coefficient of variation; SC: skewness coefficient

In general, the results show that the spatial patterns of SOC contents in the three soil layers differ substantially. This suggests that an evaluation of total SOC pools in a hilly agriculturally used terrain may fail, if SOC analysis is restricted to the topsoil layer.

3.3.2 Terrain parameters and patterns of soil redistribution

Statistics and spatial patterns of the calculated terrain and soil redistribution parameters are shown in Tab. 3.2 and Fig. 3.3. All possible covariables own a considerable spatial variability within the test site, indicating their appropriateness for use in RK. The relative elevation *RE* has a clear tendency from west to east with a maximum value of 27.4 m at the western boundary of the test site and a minimum of 0 m at the outlet. The slope *s* shows a

more complex pattern: almost two thirds of the test site (mid to western part) is relatively flat with slopes ranging between 1 and 2°. Steep slopes (up to approximately 9.5°) exist in the eastern part. Incorporated into this easterly part is a very small thalweg area with still higher slopes (3-5°) than the flat westerly part. The spatial distribution of the aspect *A* indicates the differentiation between a south facing (values > 135°) and a north facing slope (values < 45°) in the east. The flat westerly part is orientated to the east with aspects ranging from approximately 60 to 120°. Profile and plan curvature show a diffuse behaviour in the flat west, whereas the pattern of convexities and concavities in the east corresponds well to the derived slope pattern. The catchment area *CA* and the two indices *WI* and *SPI* are distributed in similar patterns with a concentrated area of high values near the outlet of the test site. Compared to *SPI,* this area is smaller in north-south-direction and more elongated in east-west-direction in the patterns of *CA* and *WI*.

Tab. 3.2: Statistics of terrain attributes and soil redistribution parameters within the test site (n = 1030); considered are: relative elevation RE, slope s, aspect A, profile and plan curvature (C-prof and C-plan), catchment area CA, wetness index WI, stream power index SPI, and patterns of tillage (E_{til}), water (E_{wat}) and total (E_{tot}) erosion.

Parameter	Mean	Median	SD	CV†	Min	Max	SC‡
RE [m]	15.82	16.44	5.97	---	0.00	27.42	-0.31
s [°]	3.93	3.21	1.87	47.58	1.56	9.46	1.05
A [°]	87.33	78.82	28.17	32.26	40.37	166.38	1.23
C-prof [0.01 m]	-0.03	-0.02	0.20	---	-1.08	0.95	-0.10
C-plan [0.01 m]	-0.04	-0.01	0.26	---	-1.27	0.72	-1.05
CA [m²]	1568.91	868.15	2634.86	167.94	105.17	25612.13	5.45
WI [-]	7.79	7.90	0.90	---	5.73	11.00	-0.03
SPI [-]	20.67	7.15	41.19	199.27	0.68	325.99	4.28
E_{til} [mm a^{-1}]	0.02	-0.16	1.49	---	-5.28	15.00	2.96
E_{wat} [mm a^{-1}]	-0.50	-0.23	0.66	---	-5.81	-0.02	-3.58
E_{tot} [mm a^{-1}]	-0.47	-0.44	1.30	---	-5.39	13.19	1.82

† CV: coefficient of variation. The CV cannot be calculated for variables containing negative values or possessing a negative skewness coefficient (Isaaks and Srivastava, 1989).
‡ SC: skewness coefficient

Comparing the distributions of tillage and water erosion (E_{til} and E_{wat}) derived from WaTEM/SEDEM clearly shows different spatial patterns of erosion and deposition resulting from these two processes, which agrees well with other studies (Govers et al., 1994; Van Oost et al., 2000). Areas with the steepest slopes have the highest water induced erosion rates resulting in an aggregated area of high erosion rates with values between –1.5 and –5.8 mm a^{-1} in the test site. This aggregated area corresponds well to the areas of high values of *SPI* indicating that these parameters represent similar processes. The rest of the test site is dominated by only slight water induced erosion rates with values between –1 and 0 mm a^{-1}. No water induced deposition was calculated inside the test site, since WaTEM/SEDEM is not

capable to model the backwater effect induced by land use change at the outlet of the test site. Tillage induced erosion generally occurs on convexities and on the down slope side of field boundaries, whereas deposition occurs on concavities and on the upslope side of field boundaries (Govers et al., 1994; Van Oost et al., 2000). High tillage induced deposition rates with values ranging from 2 up to 15 mm a^{-1} were simulated in the thalweg area near the outlet of the test site, whereas highest erosion rates (-0.5 – -3 mm a^{-1}) were simulated on the shoulders of the north-south-facing slope in the easterly part. The most pronounced difference between water and tillage erosion patterns were modelled along the thalweg: Here deposition by tillage counteracts with water induced erosion. The pattern of total erosion (E_{tot}) adds the two soil redistribution patterns. Most grid cells experiencing tillage induced deposition in the thalweg area are still depositing sites in the total erosion pattern.

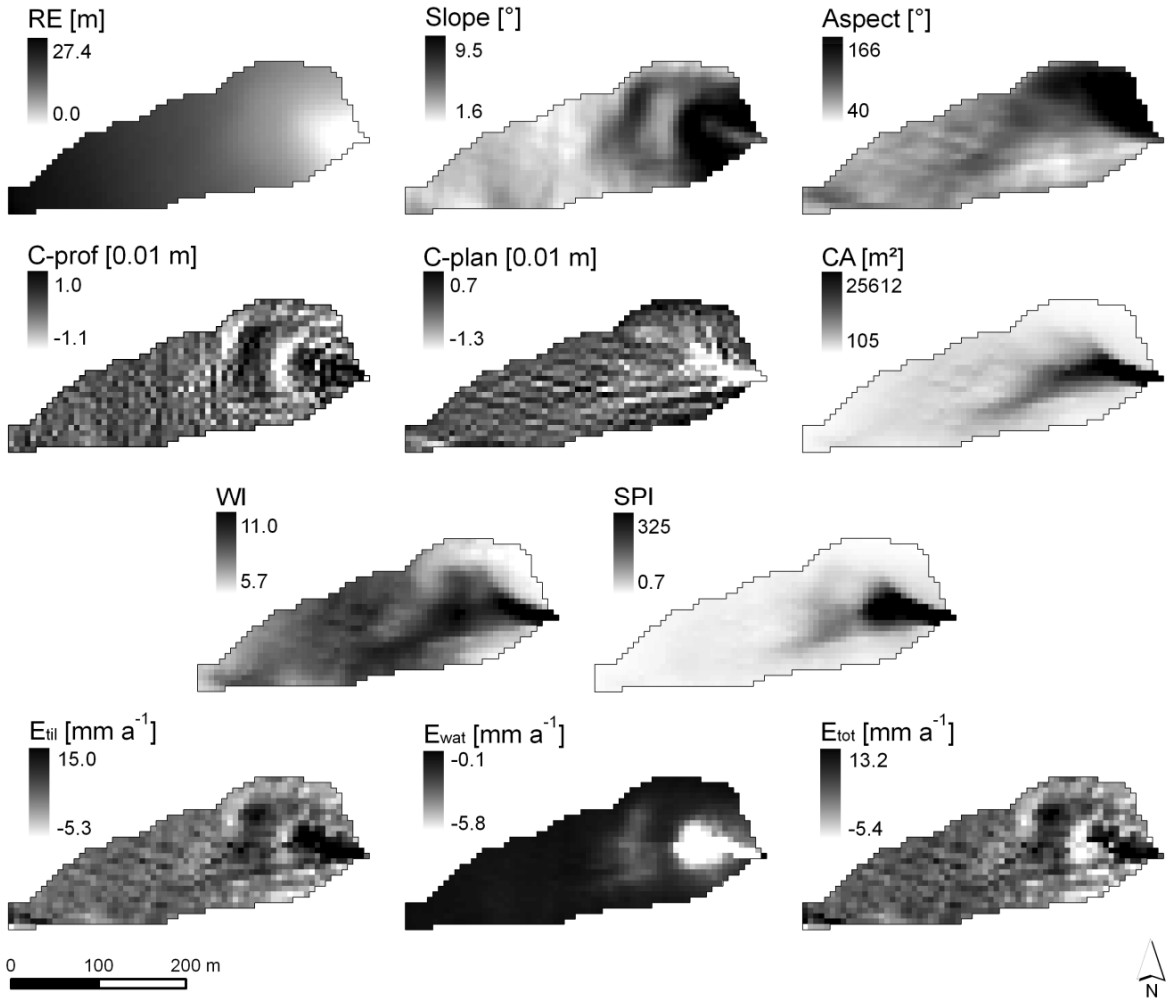

Fig. 3.3: Maps of terrain attributes and patterns of soil redistribution derived from WaTEM/SEDEM; for abbreviations of parameters refer to Tab. 3.2; a positive curvature (C-prof and C-plan) indicates that the surface is upwardly convex, and a negative value indicates that the surface is upwardly concave; regarding the erosion patterns (E_{til}, E_{wat}, and E_{tot}) negative values represent erosion, while positive values represent deposition.

3.3.3 Relation between soil organic carbon and secondary parameters

Among the primary terrain attributes, *C-prof*, *C-plan* and *CA* show significant linear relationships to SOC in all soil layers and in all input raster widths (Tab. 3.3). Correlation coefficients with *C-prof* and *CA* are always positive, whereas correlations with *C-plan* are always negative. Additionally, *RE* shows a negative correlation with SOC in soil layer III for all raster widths. The *SPI* and the soil redistribution patterns based on water and tillage erosion modelling all significantly correlate with SOC in all soil layers and in all raster widths, whereas the *WI* is only significantly correlated with SOC in the two subsoil layers. Correlations between SOC and E_{til} and E_{tot}, respectively, are positive in each soil layer and in each raster width indicating an accumulation of SOC on depositional sites and a loss of SOC on eroding sites. In contrast, the water induced erosion pattern expressed by E_{wat} and *SPI* result in a different picture: Here high erosion rates correspond to high SOC concentrations in each soil layer. This results from the counterbalancing effect of water and tillage erosion which in most cases leads to a net deposition considering both processes (see E_{tot}), while water erosion alone leads to net erosion. Hence, it is misleading to use water erosion or corresponding indices alone as a covariable for any SOC interpolation scheme in agriculturally used landscapes.

Tab. 3.3: Quality of correlation between SOC content [wt%] and all calculated parameters in the three soil layers (I: 0-0.25 m; II: 0.25-0.50 m; III: 0.50-0.90 m) expressed as Pearson correlation coefficients; results are given for the three different raster widths (R_{17}, R_{25}, R_{50}) used as input for geostatistics; for abbreviations and units of parameters refer to Tab. 3.2.

	SOC R_{17} (n_I = 143 , $n_{II,III}$ = 144)			SOC R_{25} (n = 76)			SOC R_{50} (n = 28)		
	I	II	III	I	II	III	I	II	III
RE	- 0.04	- 0.03	- 0.28 **	- 0.16	- 0.15	- 0.31 **	- 0.37	- 0.23	- 0.45 *
S	0.13	0.03	0.14	0.22	0.15	0.28 *	0.26	0.15	0.37
A	0.12	- 0.01	0.08	0.28 *	0.05	0.10	0.37	- 0.12	0.04
C-prof	0.37 **	0.44 **	0.39 **	0.49 **	0.47 **	0.44 **	0.53 **	0.70 **	0.55 **
C-plan	- 0.28 **	- 0.36 **	- 0.56 **	- 0.38 **	- 0.34 **	- 0.44 **	- 0.46 *	- 0.45 *	- 0.52 **
CA	0.19 *	0.27 **	0.67 **	0.36 **	0.46 **	0.66 **	0.48 **	0.51 **	0.65 **
WI	0.14	0.35 **	0.53 **	0.08	0.37 **	0.41 **	0.24	0.48 **	0.46 *
SPI	0.25 **	0.29 **	0.67 **	0.38 **	0.43 **	0.67 **	0.53 **	0.52 **	0.71 **
E_{til}	0.36 **	0.45 **	0.67 **	0.48 **	0.51 **	0.57 **	0.59 **	0.59 **	0.61 **
E_{wat}	- 0.22 **	- 0.25 **	- 0.53 **	- 0.25 *	- 0.32 **	- 0.50 **	- 0.51 **	- 0.45 **	- 0.68 **
E_{tot}	0.33 **	0.42 **	0.55 **	0.41 **	0.41 **	0.35 **	0.47 **	0.50 **	0.40 **

* Significant at 95 %, ** significant at 99 %.

In general, the linear relationship between SOC and the two indices as well as between SOC and the erosion/deposition patterns increases with increasing soil depth within each

raster width. The same is true for the relationship between SOC and *CA*. This indicates (i) that relief driven processes play a less significant role in the topsoil layer where periodic management practices homogenise soil properties in agricultural areas and (ii) that more process-related terrain attributes such as *CA*, the two indices *WI* and *SPI*, and the patterns of soil redistribution play a more important role in the spatial distribution of soil organic carbon in the deeper soil layers. The correlation between SOC and water erosion (*SPI* and E_{wat}) as well as between SOC and tillage erosion (E_{til}) indicates the importance of erosion and deposition in the deeper soil layers. The increasing correlations of SOC with CA and *WI* with increasing soil depth points out that also processes affecting soil moisture and infiltration influence the SOC patterns in these soil layers. The *WI* represents areas where water accumulates, and zones with higher *WI* values tend to have higher biomass production, lower SOC mineralisation, and higher sediment deposition compared to zones of low *WI* (Terra et al., 2004).

In some respect our results disagree with other results where correlations between SOC and various primary terrain attributes were found. Mueller and Pierce (2003) for example derived the highest correlation coefficients between SOC and elevation in three different raster widths for the topsoil layer. They and other authors (e.g. Takata et al., 2007; Terra et al., 2004) also found significant correlations with slope. The positive correlations to *CA* and *WI* correspond with findings of other authors (e.g. Sumfleth and Duttmann, 2007; Terra et al., 2004).

3.3.4 Soil organic carbon kriging results

For the high density SOC input data different combinations of theoretical variogram models and weighting methods performed best for the original SOC data in the three soil layers. Theoretical variogram parameters (Tab. 3.4) show that the original SOC data of R_{17} are moderately to highly spatially structured for all three soil layers with low nugget-to-sill ratios. Ranges are much larger than the raster width with a maximum value of 216 m for the SOC data in soil layer I, indicating that the sampling scheme used here accounts for most of the spatial variation of SOC in the three soil layers. The nugget variances comprising small scale variability as well as measurement errors are close to zero in all soil layers. Mean errors calculated from cross-validation for OK in each soil layer are close to zero indicating unbiased predictions (Tab. 3.4). Root mean square errors resulting from OK are 0.12, 0.20 and 0.15 wt % SOC for soil layers I, II, and III, respectively, corresponding to approximately

10, 28 and 44 % of the mean SOC values in the different soil layers (Tab. 3.1). This indicates a loss of precision with increasing soil depth. In contrast, model efficiency (MEF) is highest in soil layer III (MEF = 0.53) and lowest in soil layer II (MEF = 0.23). Plots of predicted versus measured SOC contents (Fig. 3.4) show highest deviations from the 1:1-line in case of soil layer II. The SOC maps derived from OK (Fig. 3.5) represent well the spatial distributions of SOC in each soil layer which are already visible in the patterns of the measured SOC values at the sampling points (Fig. 3.2).

Tab. 3.4: Theoretical semivariogram parameters of original SOC data and residuals resulting from linear regression with different covariables as well as cross-validation results from ordinary (OK) and regression kriging (RK) of SOC content [wt%] in three soil layers (I: 0-0.25 m; II: 0.25-0.50 m; III: 0.50-0.90 m) using the 17.7 x 17.7 m raster data set (R_{17}) (n_I = 159; $n_{II,III}$ = 160); RK results are included only when improving the prediction compared to OK; no covariable indicates OK; for exponential models the practical range is given; goodness-of-fit was tested using mean error (ME), root mean square error (RMSE), model efficiency (MEF), and relative improvement (RI); the transcript tr means that covariables were transformed to logarithms so that linear regression residuals meet normal distribution.

		Theoretical semivariogram parameters						Kriging results			
Soil layer	Covariable†	Model	Weights‡	Nugget	Sill	Range [m]	Nugget/ Sill [%]	ME	RMSE	MEF	RI [%]
I	---	exponential	equal	0.013	0.034	216	40	-0.001	0.123	0.45	---
	C-prof	exponential	equal	0.008	0.023	113	33	-0.002	0.115	0.53	6.50
II	---	exponential	$n_p h^{-2}$	0.000	0.054	40	0	-0.002	0.196	0.23	---
	C-prof	exponential	$n_p h^{-2}$	0.000	0.038	28	0	-0.001	0.192	0.26	2.04
	C-plan	exponential	$n_p h^{-2}$	0.000	0.047	35	0	-0.001	0.192	0.25	2.04
	CA	exponential	$n_p h^{-2}$	0.000	0.051	35	0	-0.002	0.194	0.24	1.02
	WI	exponential	$n_p h^{-2}$	0.000	0.050	36	0	-0.002	0.190	0.28	3.06
	E_{til}	exponential	$n_p h^{-2}$	0.000	0.039	28	0	-0.002	0.187	0.29	4.59
	E_{wat}	exponential	$n_p h^{-2}$	0.000	0.050	37	0	-0.002	0.195	0.24	0.51
	E_{tot}	exponential	$n_p h^{-2}$	0.000	0.040	29	0	-0.002	0.187	0.29	4.59
III	---	spherical	n_p	0.013	0.044	64	30	-0.002	0.145	0.53	---
	C-plan	spherical	n_p	0.011	0.030	64	37	-0.001	0.139	0.57	4.14
	CA_{tr}	spherical	n_p	0.008	0.037	79	23	-0.001	0.131	0.62	9.66
	WI_{tr}	spherical	n_p	0.010	0.041	87	24	-0.002	0.130	0.62	10.35
	SPI_{tr}	spherical	n_p	0.009	0.037	73	25	-0.000	0.136	0.59	6.21
	E_{til}	exponential	equal	0.000	0.024	22	0	-0.003	0.134	0.60	7.59
	E_{tot}	spherical	n_p	0.012	0.030	53	40	-0.002	0.134	0.60	7.59

† For abbreviations and units of covariables refer to Tab. 3.2.

‡ Weighting of the semivariogram model is done by ordinary least squares (i.e. equal weigths to all semivariances) and two weigthed least square methods (weigthing by n_p = number of pairs and weigthing by $n_p h^{-2}$ with h = lag distance [m]).

Regarding the theoretical variogram parameters of the residuals resulting from linear regression with the different significantly related covariables in the three soil layers (Tab. 3.4), the same conclusions as for the original SOC data in each soil layer can be drawn. The residuals are moderately or even highly spatially structured, and ranges are larger than the raster width. The sill of the different residual variograms is reduced compared to the sill of the raw data in all soil layers reflecting the success of regression fitting (Hengl et al., 2004; Terra et al., 2004). Nugget variances are all close to zero.

In all three soil layers the geostatistical interpolation of SOC could be improved incorporating covariables in RK (Tab. 3.4). For soil layer I there is only one covariable, namely *C-prof*. For soil layer II *C-prof*, *C-plan*, *CA*, *WI*, and the three soil redistribution patterns derived from modelling are able to ameliorate interpolation results, and in soil layer III improvements are achieved by using *C-plan*, CA_{tr}, SPI_{tr}, WI_{tr}, E_{til} and E_{tot} as covariables in RK. Mean errors are still close to zero for all kriging approaches in all soil layers indicating unbiased predictions. Due to the high spatial density of the original SOC data, relative improvements of the described RK approaches compared to OK are only low to moderate in all three soil layers. In soil layer II and III the integration of the more complex covariables outperformed that of the primary terrain parameters (Tab. 3.4). The improvement in soil layer III especially results from the more definite representation of high SOC contents situated in the depositional area at the down slope end of the test site (Fig. 3.4). In general, spatial distributions resulting from the best RK approach in each soil layer (Fig. 3.5) are similar to those derived from OK but show more small scale variability.

Although a minimum number of at least 50 better 100-150 sampling points is recommended for geostatistical analysis (Webster and Oliver, 2001), the theoretical semivariogram parameters of the SOC data and the values describing the goodness-of-fit for OK of the two reduced input raster widths R_{25} (n = 92) and R_{50} (n = 44) still show reasonable results in each soil layer (Tab. 3.5 and Tab. 3.6). As for the high density sampling grid (R_{17}) different combinations of theoretical variogram models and weighting methods performed best for the original SOC data. Nugget-to-sill ratios show that the primary SOC data in the two subsoil layers are highly spatially structured in both raster widths, and SOC data in the topsoil are moderately spatially dependent. This indicates that the low density sampling schemes are still suitable to resolve the spatial continuity of the original SOC data. For R_{25} the ranges are larger than the raster width, only in soil layer II in R_{50} this is not the case. Nevertheless, the results of the R_{50} interpolation are still reasonable, since the short distances formed by the transect and the two micro-plots were kept in each input raster. Nugget and sill variances of the original SOC data tend to be in the same order of magnitude than in R_{17} for each soil layer. Mean errors resulting from OK are still relatively low indicating unbiasedness, and relations of the root mean square errors to the mean values of the original SOC data also remain similar compared with the relations in R_{17} for each soil layer. Model efficiency through OK is 0.23 (R_{25}) and 0.14 (R_{50}) in soil layer I and 0.01 (R_{25}) and 0.15 (R_{50}) in soil layer II. Higher values for OK are again reached in the deepest soil layer where a MEF of 0.34 (R_{25}) and 0.39 (R_{50}) is found. Deviations between measured and predicted SOC contents

from the 1:1 line (Fig. 3.4) are similar for the two reduced raster widths as compared to the high density input grid, although a direct comparison between the different raster widths is not possible due to the use of different validation schemes.

The interpolated SOC distributions resulting from OK with the medium and low input data sets (Fig. 3.5) are smoothed compared to those using the high density input data set in each soil layer. But even with coarse sampling (R_{50}), there is still a pronounced area with high SOC concentrations in the east in all soil layers. The second region with high SOC values (southern edge and centre), however, is no longer detectable in the R_{50}-interpolation results for the deepest soil layer. As it is the case in R_{17}, nugget-to-sill ratios and the ranges of the various residuals for the different soil layers show a moderate to high spatial structure. Sills are also lower than for the original SOC data, and nuggets are close to zero.

Tab. 3.5: Theoretical semivariogram parameters of original SOC data and residuals resulting from linear regression with different covariables as well as results from ordinary (OK) and regression kriging (RK) of SOC content [wt %] in three soil layers (I: 0-0.25 m; II: 0.25-0.50 m; III: 0.50-0.90 m) using the 25 x 25 m raster data set (R_{25}) (n = 92); the values describing the goodness-of-fit result from the comparison with a validation data set (n = 67); RK results are included only when improving the prediction compared to OK; no covariable indicates OK; for exponential models the practical range is given; goodness-of-fit was tested using mean error (ME), root mean square error (RMSE), model efficiency (MEF), and relative improvement (RI); the transcript tr means that covariables were transformed to logarithms so that linear regression residuals meet normal distribution.

		Theoretical semivariogram parameters						Kriging results			
Soil layer	Covariable†	Model	Weights‡	Nugget	Sill	Range [m]	Nugget/ Sill [%]	ME	RMSE	MEF	RI [%]
I	---	exponential	equal	0.003	0.035	41	9	-0.033	0.118	0.23	---
II	---	exponential	$n_p h^{-2}$	0.000	0.052	40	0	0.058	0.226	0.01	---
	WI	exponential	$n_p h^{-2}$	0.000	0.050	37	0	0.049	0.217	0.09	3.98
	E_{til}	spherical	n_p	0.006	0.029	34	20	0.055	0.221	0.06	2.21
	E_{wat}	exponential	$n_p h^{-2}$	0.000	0.047	31	0	0.058	0.223	0.04	1.33
	E_{tot}	exponential	$n_p h^{-2}$	0.000	0.031	25	0	0.053	0.207	0.17	8.40
III	---	spherical	equal	0.010	0.044	56	23	0.053	0.181	0.34	---
	C-plan	spherical	$n_p h^{-2}$	0.001	0.032	57	3	0.053	0.171	0.41	5.55
	CA_{tr}	spherical	equal	0.006	0.040	65	16	0.048	0.159	0.50	12.15
	WI_{tr}	spherical	equal	0.016	0.044	67	26	0.047	0.159	0.48	12.15
	SPI_{tr}	spherical	equal	0.006	0.037	57	17	0.051	0.167	0.43	7.73
	E_{til}	exponential	$n_p h^{-2}$	0.000	0.027	53	0	0.054	0.158	0.50	12.71
	E_{wat}	spherical	equal	0.013	0.037	66	35	0.053	0.172	0.40	4.97
	E_{tot}	spherical	equal	0.015	0.034	70	44	0.050	0.159	0.49	12.15

† For abbreviations and units of covariables refer to Tab. 3.2

‡ Weighting of the semivariogram model is done by ordinary least squares (i.e. equal weigths to all semivariances) and two weigthed least square methods (weigthing by n_p = number of pairs and weigthing by $n_p h^{-2}$ with h = lag distance [m]).

In contrast to the use of the high resolution sampling grid R_{17} as input data, no improvements compared to OK were achieved in soil layer I by RK when using R_{25} and R_{50} (Tab. 3.5 and Tab. 3.6). In soil layer II RK including total erosion improves predictions best with R_{25} and R_{50} (RI = 8.4 and 6.2%, respectively). Relative improvements in soil layer III are

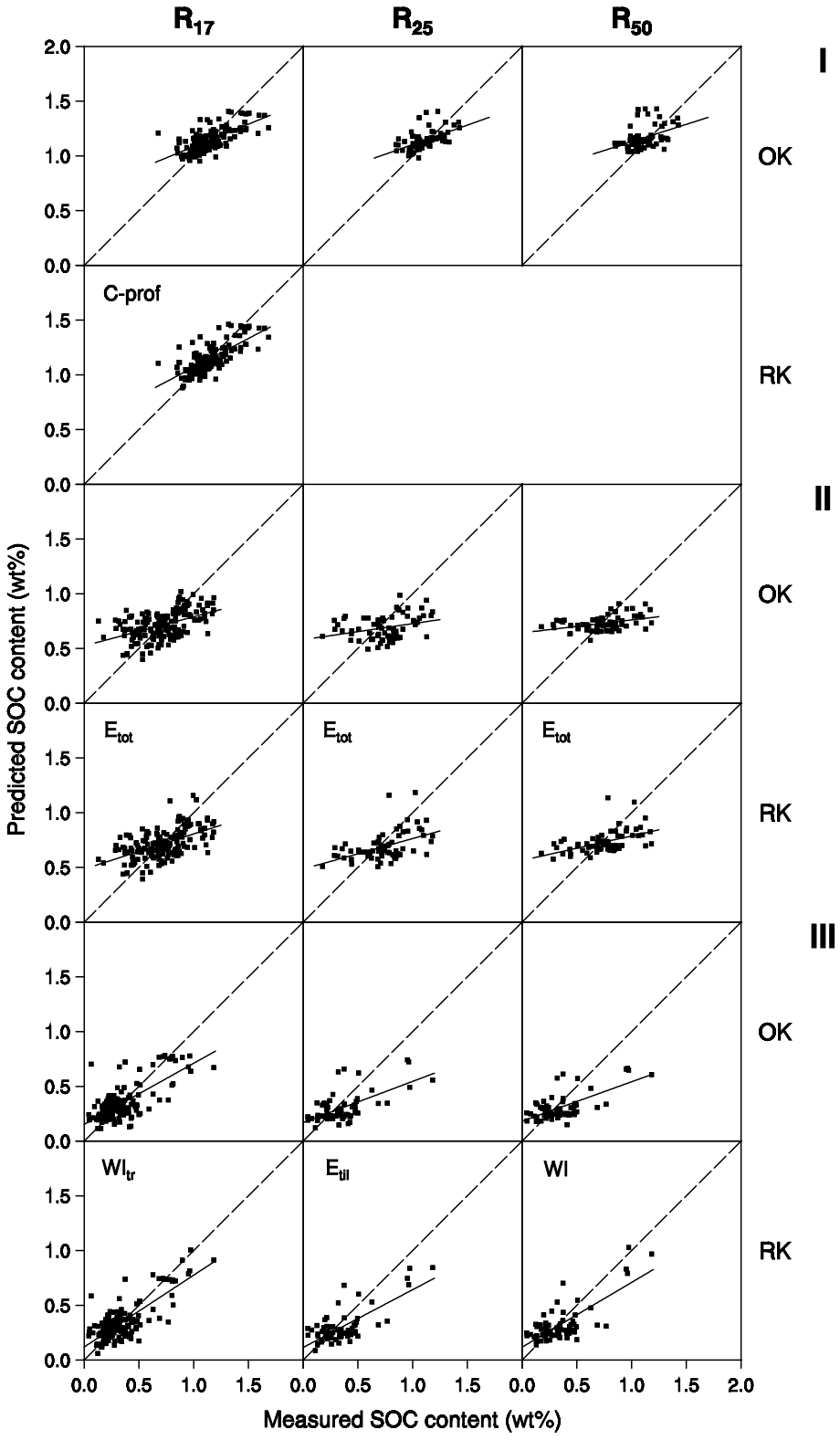

Fig. 3.4: Plots of predicted versus measured SOC contents for three soil layers (I: 0-0.25 m; II: 0.25-0.50 m; III: 0.50-0.90 m) resulting from ordinary (OK) and the best regression kriging (RK) approach using three different raster widths R_{17} (17.7 x 17.7 m), R_{25} (25 x 25 m) and R_{50} (50 x 50 m) as input; covariables of the RK approaches are given in each plot; for abbreviations and units of covariables refer to Tab. 3.2; the transcript tr means that covariables were transformed to logarithms so that linear regression residuals meet normal distribution; the 1:1 line is dashed, linear regression fit is indicated by solid line.

even higher in the medium and low density raster than for soil layer II. In R_{25} the spatial pattern of tillage erosion and in R_{50} the wetness index *WI* performed best in improving RK results (Tab. 3.5 and Tab. 3.6, Fig. 3.4).

In general, relative improvements in soil layer II and III referring to RK vs. OK are more pronounced in case of medium and low density compared to the high density input data. Moreover, SOC maps produced by RK in soil layer II and III with R_{25} and R_{50} (Fig. 3.5) show considerably more detail and compare more favourably to the spatial patterns produced with R_{17} input data. Although a direct comparison of the interpolation results with the different input raster widths is not possible due to a missing independent data set, it has to be recognised that a reduction of input data density seems to slightly decrease MEF and increase RMSE with decreasing data density.

Tab. 3.6: Theoretical semivariogram parameters of original SOC data and residuals resulting from linear regression with different covariables as well as results from ordinary (OK) and regression kriging (RK) of SOC content [wt %] in three soil layers (I: 0-0.25 m; II: 0.25-0.50 m; III: 0.50-0.90 m) using the 50 x 50 m raster data set (R_{50}) (n = 44); the values describing the goodness-of-fit result from the comparison with a validation data set (n = 67); RK results are included only when improving the prediction compared to OK; no covariable indicates OK; for exponential models the practical range is given; goodness-of-fit was tested using mean error (ME), root mean square error (RMSE), model efficiency (MEF), and relative improvement (RI); the transcript tr means that covariables were transformed to logarithms so that linear regression residuals meet normal distribution.

		Theoretical semivariogram parameters						Kriging results			
Soil layer	Covariable†	Model	Weights‡	Nugget	Sill	Range [m]	Nugget/ Sill [%]	ME	RMSE	MEF	RI [%]
I	---	spherical	n_p	0.014	0.047	75	30	-0.055	0.139	0.14	---
II	---	exponential	n_ph^{-2}	0.000	0.060	48	0	0.015	0.210	0.15	---
	C-prof	exponential	n_ph^{-2}	0.000	0.019	15	0	0.015	0.206	0.18	1.90
	E_{til}	spherical	n_p	0.011	0.029	48	41	0.019	0.202	0.20	3.81
	E_{tot}	spherical	n_p	0.012	0.029	50	40	0.015	0.197	0.25	6.19
III	---	spherical	n_p	0.007	0.071	79	10	0.046	0.174	0.39	---
	WI	spherical	n_p	0.010	0.070	75	14	0.028	0.149	0.55	14.37
	E_{til}	spherical	n_p	0.012	0.045	76	27	0.041	0.158	0.49	9.20
	E_{tot}	spherical	equal	0.018	0.050	84	36	0.040	0.162	0.47	6.90

† For abbreviations and units of covariables refer to Tab. 2

‡ Weighting of the semivariogram model is done by ordinary least squares (i.e. equal weigths to all semivariances) and two weigthed least square methods (weigthing by n_p = number of pairs and weigthing by n_ph^{-2} with h = lag distance [m]).

Except for the high density input data, our results for the topsoil layer are in correspondence with Terra et al. (2004) who found that OK predicted SOC best compared to cokriging, regression kriging and multiple regression for the uppermost 30 cm and for three different densities of input data (8, 32 and 64 samples ha^{-1}). In contrast, other authors (e.g. Mueller and Pierce, 2003; Simbahan et al., 2006; Sumfleth and Duttmann, 2008) could improve the prediction of SOC in the topsoil layer by using (relative) elevation and electrical conductivity, respectively, as covariables in

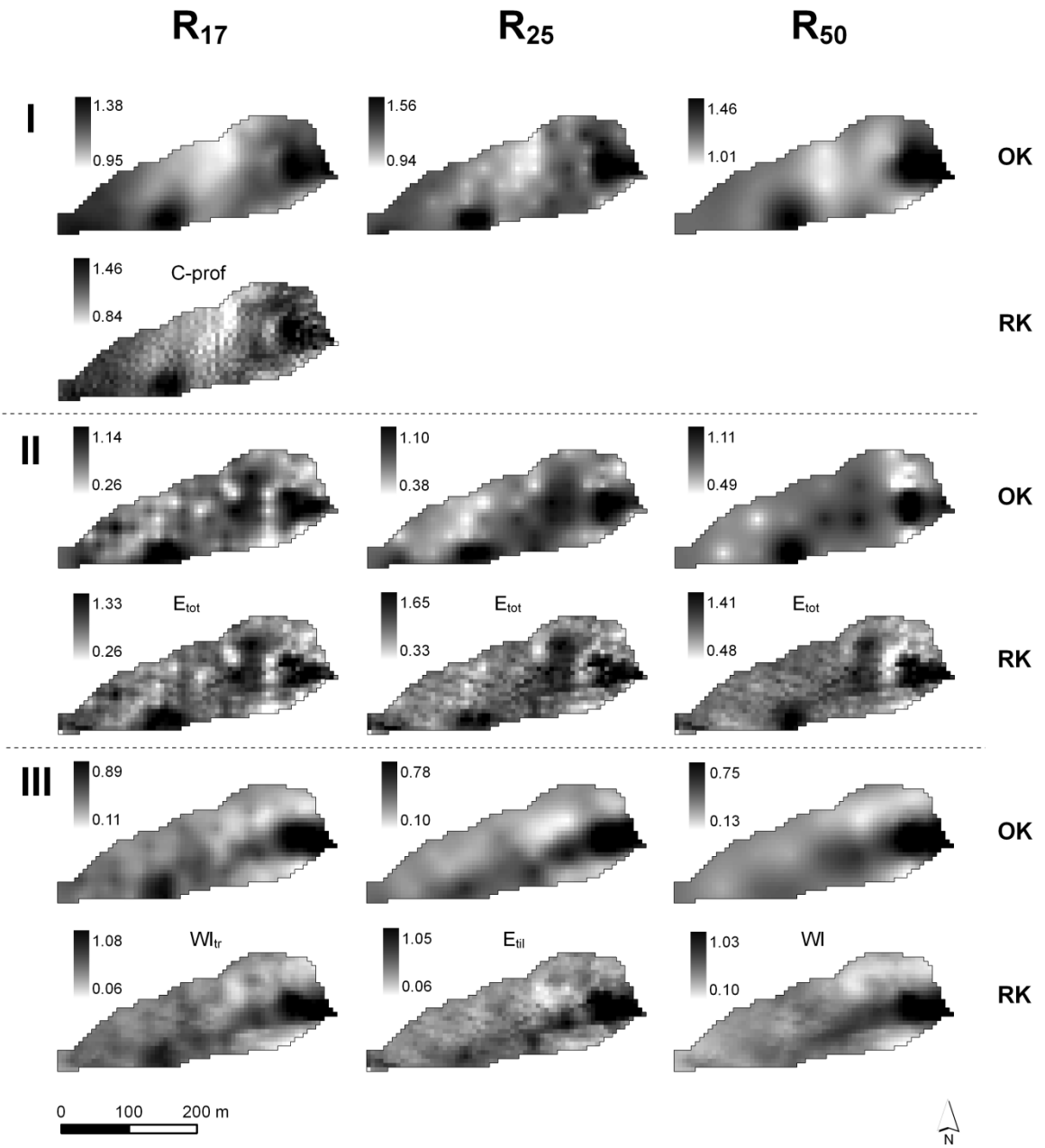

Fig. 3.5: Maps of SOC content [wt %] for three soil layers (I: 0-0.25 m; II: 0.25-0.50 m; III: 0.50-0.90 m) resulting from ordinary (OK) and the best regression kriging (RK) approach using three different raster widths R_{17} (17.7 x 17.7 m), R_{25} (25 x 25 m) and R_{50} (50 x 50 m) as input; covariables of the RK approaches are given above each map; for abbreviations and units of covariables refer to Tab. 3.2; the transcript tr means that covariables were transformed to logarithms so that linear regression residuals meet normal distribution.

regression kriging and / or kriging with external drift. Their studies show that the sampling density played an important role for improving the performance of geostatistics when incorporating covariables. E.g. Mueller and Pierce (2003) also used three different input raster widths in their test site. For their high resolution input raster (10.7 samples ha^{-1}) they also found only modest differences between the applied interpolation techniques, but for their two reduced raster widths (2.7 and 1 samples ha^{-1}) different interpolation methods incorporating covariables could outperform OK. This was also true for the three test sites of Simbahan et al.

(2006) with sampling densities of 2.5 to 4.2 samples ha^{-1}. Our result of no or only slight improvements in the first soil layer might be caused by (i) our high sampling densities (38, 17, and 6 samples ha^{-1}), (ii) homogenisation effects of management and the corresponding low spatial variability, and (iii) the area of high SOC concentrations at the southern boundary of the test site which is most pronounced in the topsoil. The existence of this area cannot be ascribed to relief driven processes, and in combination with homogenisation it is thus leading to relatively low correlations between SOC and the various parameters in the topsoil layer.

In contrast, considerable improvements of RK over OK in our study were achieved in the two subsoil layers. In soil layer II this improvement is highest when using the patterns of tillage or total erosion as covariable in RK. This indicates that especially tillage induced erosion and deposition processes affect the SOC distribution in this layer. This makes it necessary to not only consider water induced soil redistribution processes, which are already represented in other primary and secondary terrain attributes (*CA* and *SPI*) used here and in other studies. Relative patterns of tillage erosion and deposition can easily be derived with well tested erosion and sediment delivery models such as the WaTEM/SEDEM model. To implement the tillage erosion component only a DEM and an estimation of the tillage transport coefficient are required (Van Oost et al., 2000).

Although the tillage and total erosion patterns significantly improved SOC prediction in the deepest soil layer in all three raster widths, comparable and in some instances even better results were produced by RK with *CA* and *WI*. This indicates that not only soil redistribution processes affect the spatial distribution of SOC in the deepest soil layer but also processes concerning the spatial distribution of infiltration and soil moisture. Both processes may increase SOC contents in the thalweg area due to (i) infiltration and absorption of dissolved organic carbon (DOC) and (ii) limited mineralisation of SOC in case of high soil moisture contents.

In contrast to the topsoil layer, in the two subsoil layers improved SOC interpolations were actually obtained when using a high density of input data for RK. This was possibly caused by higher spatial variations of SOC in these soil layers, expressed as coefficient of variation (Tab. 3.1).

3.4 CONCLUSION

Our results show that the spatial SOC patterns in a sloped arable test site differ significantly between three soil layers. Whereas the topsoil SOC pattern was homogenised by tillage operations, the patterns of the two subsoil layers show an increasing spatial variability primarily caused by high SOC contents in the depositional area at the down slope end of the test site. In the mid soil layer (0.25-0.50 m) the best RK result was produced with the patterns of tillage and total erosion, indicating the importance of soil redistribution (especially the inclusion of tillage erosion) for the spatial distribution of SOC in agricultural areas. In the third soil layer (0.50-0.90 m) tillage and total erosion as well as the wetness index and partly the catchment area performed best. This indicates that besides soil redistribution also processes concerning the distribution of soil moisture affect the spatial pattern of SOC in the deepest soil layer. Here SOC contents in the depositional area are as high as topsoil SOC contents indicating the importance of including deeper soil layers when assessing soil carbon balances especially in hilly agriculturally used areas.

Since patterns of topsoil SOC distribution might be dissimilar to subsoil patterns particularly in agriculturally used areas prone to soil erosion and deposition, estimating total SOC stocks from topsoil SOC, for instance by applying remote sensing techniques (e.g. Stevens et al., 2008), might not be appropriate.

In general, it was shown that (especially) integrating patterns of soil redistribution (which must include tillage erosion) in kriging approaches, can substantially improve SOC interpolation of subsoil data in hilly arable landscapes. This is an important finding insofar as high resolution subsoil SOC data are rare and that the promising approach to improve spatial estimates of SOC by applying remote sensing techniques is limited to topsoil SOC.

4 SPATIAL VARIABILITY OF SOIL RESPIRATION– ARE PATTERNS OF SOIL REDISTRIBUTION IMPORTANT?*

4.1 INTRODUCTION

In terrestrial ecosystems soil respiration is the key pathway of C to the atmosphere (Trumbore, 2006) estimated at 75 Pg C per year globally (Schlesinger and Andrews, 2000). As soils contain roughly twice the amount of C stored in the atmosphere (Schlesinger, 2005), a small change in soil respiration rates can cause a significant alteration in atmospheric CO_2 levels. Soil respiration is highly variable in time and space (e.g. Borken et al., 2002; Davidson et al., 2006; Fang et al., 1998). The temporal variability at a single location can be determined relatively easily with a series of automated measurements over a certain time period (e.g. Liu et al., 2010). This is possible with different kinds of open- or closed-chamber systems. In contrast, capturing spatial patterns of soil respiration, e.g. within a single arable field, is much more difficult, because small scale variability requires a large number of spatially distributed measurements (Herbst et al., 2008; Rodeghiero and Cescatti, 2008). Hence, this small scale spatial variability of soil respiration is often ignored in C balances at the field scale, but the integrative signal of CO_2 efflux is determined by eddy-covariance methods (e.g. Reth et al., 2005a). Corresponding single point soil respiration measurements are then used to separate between heterotrophic and autotrophic respiration as well as to fill gaps (especially at night) in the eddy-covariance measurements. However, there is also a number of studies dealing with temporal and spatial variability of soil respiration and its controls using automated or campaign measurements at spatially distributed locations (e.g. Epron et al., 2006; Herbst et al., 2009; Martin and Bolstad, 2009; Moyano, 2008; Pacific et al., 2008). Most of these studies focus on the variability of soil temperature as first order control and soil moisture as second order control of soil respiration. Considering spatial variability, soil temperature can be important on large spatial scales or in steep terrain, where soil temperature is variable due to differences in incoming radiation (e.g. Kang et al., 2000; 2003). However, on the field scale

* Based on: Fiener, P., V. Dlugoß, W. Korres and K. Schneider. Spatial variability of soil respiration in a small agricultural watershed – are patterns of soil redistribution important? Submitted to Catena.

in relatively flat terrain typical for agricultural areas, soil moisture is commonly more variable in space compared to soil temperature. Therefore soil moisture is identified in many studies as the most important driver for spatial variability of soil respiration (e.g. Herbst et al., 2009).

Several studies also analyse the spatial variability of soil respiration in relation to patterns of further soil properties, like e.g. root biomass (Fang et al., 1998; Han et al., 2007; Reth et al., 2005b; Xu and Qi, 2001), quantity and quality of soil organic matter (Saiz et al., 2006; Schwendenmann et al., 2003; Scott-Denton et al., 2003; Soe and Buchmann, 2005), soil total porosity (Fang et al., 1998), pH value (Reth et al., 2005b), and microbial biomass (Xu and Qi, 2001). However, these studies were mostly carried out in woodlands and on flat terrain. On sloped land, some rare studies also investigated topographic position as influencing factor of soil respiration (Epron et al., 2006; Hanson et al., 1993; Parkin et al., 2005).

To our knowledge, the only studies that focus on the relation between in situ measured spatial patterns of soil respiration and soil redistribution in arable landscapes were recently conducted by Bajracharya et al. (2000) and Van Hemelryck et al. (2010b). However, processes of soil redistribution were found to have large effects on the spatial variability of soil properties, e.g. SOC content (e.g. Berhe et al., 2007; Dlugoß et al., 2010; Harden et al., 1999; Mabit et al., 2008; Quine and Van Oost, 2007; Van Oost et al., 2007), nutrient content (e.g. De Gryze et al., 2008; Quinton et al., 2010) and soil texture (Heckrath et al., 2005; Papiernik et al., 2007), which potentially affect the spatial variability of soil respiration. But differences in SOC decomposition at different landscape positions in areas prone to soil redistribution were investigated by laboratory (incubation) experiments. For example, Berhe et al. (2008) analysed the decomposition of soil organic matter by litterbag and incubation experiments at different landform positions. The long-term decomposition rate was significantly lower at depositional compared to erosional sites, contributing to the stabilisation of SOC at depositional sites. Contrary results were found by the few studies that directly measured the CO_2 efflux in the field. For example, Van Hemelryck et al. (2010b) measured soil respiration shortly after an important erosion event on erosional, depositional, and comparable sites without sedimentation on an arable field in the Belgian Loess Belt. The authors found an increased mineralisation of SOC at depositional sites. But this effect was only important at the short term, as it vanished when the transported labile SOC fraction was completely mineralised. The results correspond to the findings of a laboratory study (Van Hemelryck et al., 2010a), where a similar but more pronounced increase in soil respiration after soil deposition was observed. In contrast, Bajracharya et al. (2000) did not find any

significant differences of CO_2 effluxes at different slope positions with different erosional stages (slightly to severely eroded and deposition) during a two-year field measurement campaign under continuous corn cultivation in the US.

Due to these contradictory results, there is a general need for further investigations of *in situ* measured soil respiration to gain further insights into the impact of soil redistribution on the CO_2 efflux from soil to atmosphere and the role of soil erosion as C source or sink on agricultural land. Laboratory experiments might not represent real landscape conditions.

Against this background, the objectives of this chapter are:

(i) To evaluate the effects of erosion and deposition on *in situ* measured heterotrophic and combined heterotrophic and autotrophic soil respiration in a small agriculturally used catchment, and
(ii) to define further parameters (soil and plant properties as well as terrain attributes) that affect the spatial variability of soil respiration and potentially modify spatial patterns of SOC stocks.

4.2 Materials and Methods

4.2.1 Soil respiration, soil moisture, and soil temperature

Soil respiration, soil moisture and soil temperature were measured during three vegetation periods in 2007, 2008, and 2009. During the first measuring period sugar beet was cultivated, followed by two years of winter wheat (as exception off the overall crop rotation with winter barley following winter wheat). Bi-weekly to weekly measurements were carried out between 23rd of May and 18th of August in 2007, in 2008 between 8th of January and 28th of July, and in 2009 between 25th of February and 13th of July, respectively. In each vegetation period, measurements were carried out at 20-22 locations arranged in two transects, one in west-east direction and one in north-south direction, in the eastern part of the Heiderhof test site (Fig. 4.1), to cover different erosional as well as depositional sites.

An automated closed dynamic chamber designed for survey measurements (LICOR 8100-103, Lincoln, USA) was used in combination with an infrared gas analyser (LI-8100) to measure soil respiration. The chamber was closed for 120 s, and CO_2 and water vapour concentration as well as chamber headspace temperature were measured every second. The CO_2 concentration was corrected for changes in air density and water vapour dilution. Soil

respiration was calculated by fitting a linear regression to the corrected CO_2 concentrations from 20 s after closing until reopening. Other non-linear analysis methods have been proposed to correct for a possible bias introduced by the effect of the increasing CO_2 concentration in the chamber headspace on the vertical CO_2 gradient and the associated flux (Liu and Si, 2009; Luo and Zhou, 2006). However, these non-linear analysis methods have been found to be less robust and more sensitive to the analysis start time than linear regression (Venterea et al., 2009). In concordance to Graf et al. (2010), we thus preferred to use the linear analysis method in this study.

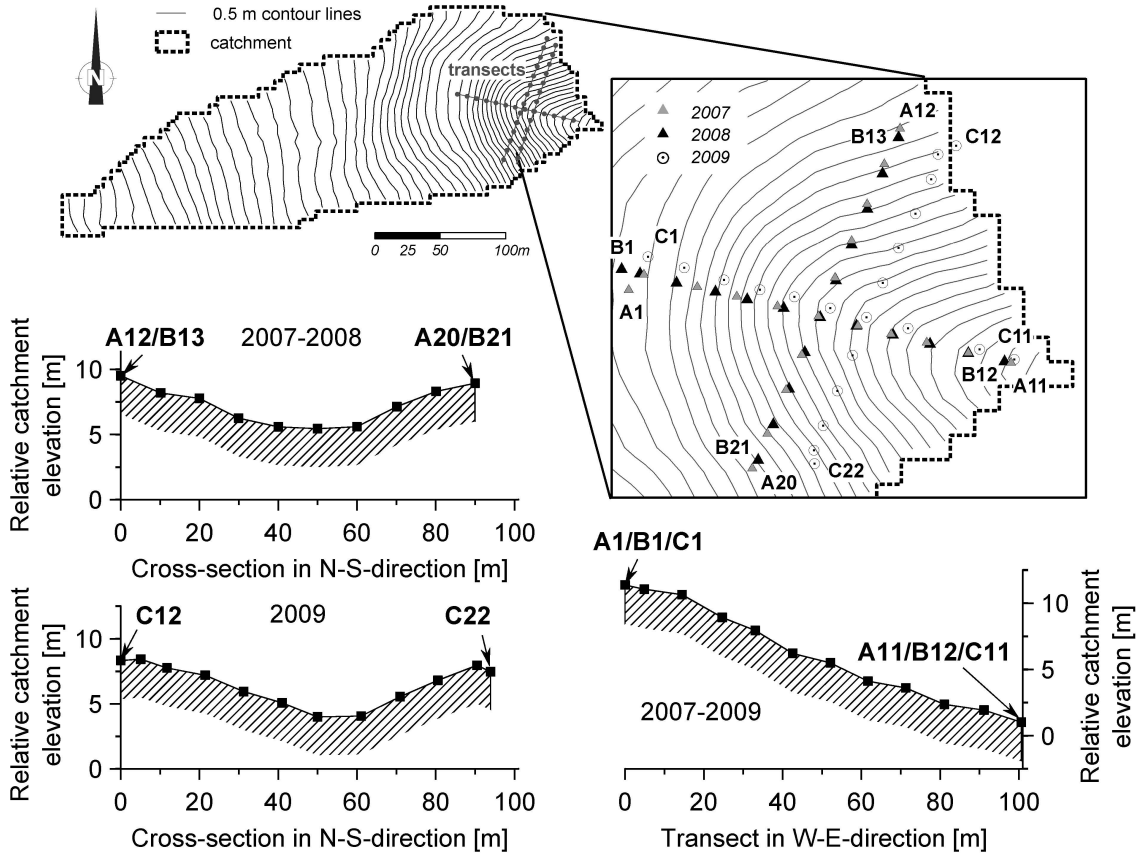

Fig. 4.1: Location of the measuring collars along cross-sections and transects within the test site; measurement locations in 2007, 2008, and 2009 are indicated by A, B, and C, respectively; note that the Y-axis is four-times inflated.

Measurements were carried out on polyvinyl chloride collars (∅ 20 cm) which were inserted 1-2 cm into the soil protruding about 2 cm above the soil surface (= chamber offset) one week before the first measurement. To guarantee the spatial continuity of measurements they were left on site for the entire measurement period in each year. The offset of the soil collars necessary for the calculation of the CO_2 efflux in the chamber was determined at each measuring date. Under sugar beet (2007) the collars were placed between the plant rows, while for winter wheat (2008 and 2009) the seedlings were carefully hand-picked inside the

collars one week before the first measurement date. The location of the collars was determined using a dGPS with a horizontal accuracy of 0.5-1 m. Since the locations of crop rows as well as of wheel tracks slightly differed between the different years, soil collars could not be placed in exactly the same positions in the three measurement periods. At each measuring point soil respiration was determined one to four times a day. Measurement campaigns always started at approximately 10 a.m. and ended between 11:30 a.m. and 16 p.m. depending on the number of measurements per collar. Measurements were carried out in a predefined order starting at collar 1 up to collars 11 or 12 and then back along the transect in east-west direction (Fig. 4.1), followed by the transect in north-south direction starting in the north at collar 12 or 13 up to 20, 21, or 22 and back.

A thermocouple soil temperature probe was connected to the Licor LI-8100 system. Soil temperature was simultaneously measured at a depth of 3 cm for each measurement. Topsoil moisture (< 6 cm) was measured by frequency domain reflectrometry (FDR) (Theta Probe ML2x, Delta-T Devices, UK). Five measurements around each soil collar were taken at each measuring day, and the arithmetic mean of these five measurements was taken as the corresponding soil moisture.

4.2.2 Sampling and analysis

At the end of each measurement period soil samples were taken inside of each soil collar. Two cores were extracted with a 5 cm diameter soil auger (Eijkelkamp, NL) and were separated into two depths (I_a: 0-0.10 m; I_b: 0.10-0.25 m). One core was used for the determination of soil bulk density by weighing the soil samples after oven drying at 105°C (volumetric core method). The other one was used to determine SOC and N contents, pH value, and soil texture. Roots as well as recognisable undecomposed plant residues were hand-picked. Soil samples were then dried at 105°C for 24 hours, ground, and coarse particles were separated by 2 mm-sieving. Although loess soils in the area are in most cases deeply decalcified all soil samples were checked for lime ($CaCO_3$) with hydrochloric acid (10 %). If any inorganic C content was recognised, it was destroyed by means of hydrochloric acid. SOC and N content were then determined by dry combustion using a CNS elemental analyser (vario EL, Elementar, Germany). Soil texture was determined by the combined sieve and pipette method (Deutsches Institut für Normung, 2002) differing the following classes: Coarse sand (630-2000 µm), medium sand (200-630 µm), fine sand (63-200 µm), coarse silt (20-63 µm), medium silt (6.3-20 µm), fine silt (2-6.3 µm), and clay (<2 µm). The median grain

size diameter was calculated following Shirazi et al. (1988) using these seven particle-size classes. The pH value was determined in a 0.01 M $CaCl_2$ solution (Deutsches Institut für Normung, 2006). Besides the soil parameters measured for the topsoil (0-0.25 m) in the collars, geostatistically interpolated SOC data for two subsoil layers (II: 0.25-0.50 m and III: 0.50-0.90 m) were taken from an earlier study (Dlugoß et al., 2010; chapter 3).

To estimate differences in the potential carbon inputs by plants, plant heights were measured in concordance with the respiration measurements near each soil collar. This proxy variable for biomass was used to prevent destructive biomass measurements during the growing period as well as to gain some information concerning the possibility of roots growing under the collars. Moreover, total dry biomass before harvest was determined. Therefore, in 2007 three sugar beet plants were sampled, and in 2009 half a square meter of winter wheat was harvested close to each soil collar. Aliquots of the plants were dried at 70°C and then weighed.

4.2.3 Data analysis

For data preparation, all soil respiration measurements were at first adjusted for the simultaneously measured offset of the soil collar. As a second preparation step predefined start and stop times for calculating the CO_2 efflux were adjusted for single measurements. A change of start time was necessary, when the predefined dead band (i.e. time after the closure of the chamber that is not used for further flux calculations (LI-COR, 2006)) of 20 s was too short for stabilisation inside the chamber; and a change in stop time was necessary, when the CO_2 concentration inside the chamber reached saturation during the measurement time (120 s). Additionally, measurements with an unusual behaviour, i.e. measurements being an outlier or having a coefficient of variation of the linear fit of less than 0.95, and measurements with a difference greater than 0.5 µmol m^{-2} s^{-1} between the fitted linear and exponential flux were examined in detail within the file viewer FV8100 2.0 (Licor, USA). Individual adjustments of the start and stop times of these measurements were carried out as to assure that (i) the exponential flux equalled the linear one, (ii) the coefficient of determination was more than 0.95, and (iii) the total time for flux calculation was not shorter than 60 s. Single measurements that could not be adjusted following these criteria were excluded from further analysis. Outliers were determined using Box-Whisker-plots derived with GNU R version 2.6 (R Development Core Team, 2007).

Since it took about 1.5 h to perform all measurements of one survey at all collars (up to four surveys were carried out per day), potential temporal trends in soil respiration may result from an air temperature change during each measuring survey. To remove unwanted trends and to standardise measured CO_2 effluxes to a single temperature, a linear regression between all respiration measure-ments made at one location and the corresponding soil temperature was carried out. Due to the relatively small number of measurement dates and the restriction to one measurement per collar and day, the correlations in 2007 were mostly only significant on a $p < 0.1$ level. For the following winter wheat years with more measuring dates and multiple measurements per collar and day, all correlations were highly significant ($p < 0.001$). Based on these relations the single respiration measurements were all standardised to a temperature of 15°C (subsequently these measurements are referred as standardised CO_2 efflux). This procedure has several advantages: (i) it allows to calculate average CO_2 effluxes at each location without the dominance of high CO_2 effluxes during warm days; (ii) differences in CO_2 effluxes solely due to heterotrophic respiration at the beginning of the growing period, where no roots from the neighbouring plants are growing into the collars, and combined autotrophic and

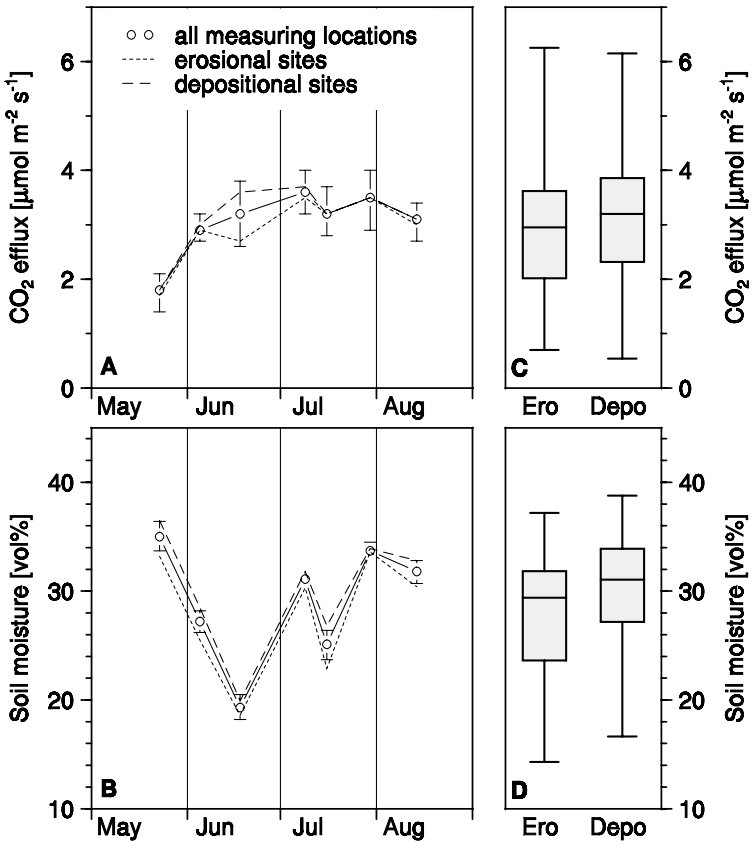

Fig. 4.2: Temporal variability of mean (over all measurement locations) standardised CO_2 efflux (A) and mean soil moisture (B) of all measuring locations (n=20), the erosional sites (n=9) and the depositional sites (n=11) in 2007; error bars give 95%-confidence intervals; box-whiskers show variability in overall CO_2 efflux (C) and soil moisture (D) during the measuring period for erosional (Ero) and depositional (Depo) sites, resp.; boxes give median, 1. and 3. quartile, and whiskers indicate minimum and maximum values; number of individual measurements for erosional sites n=63, for depositional sites n=77.

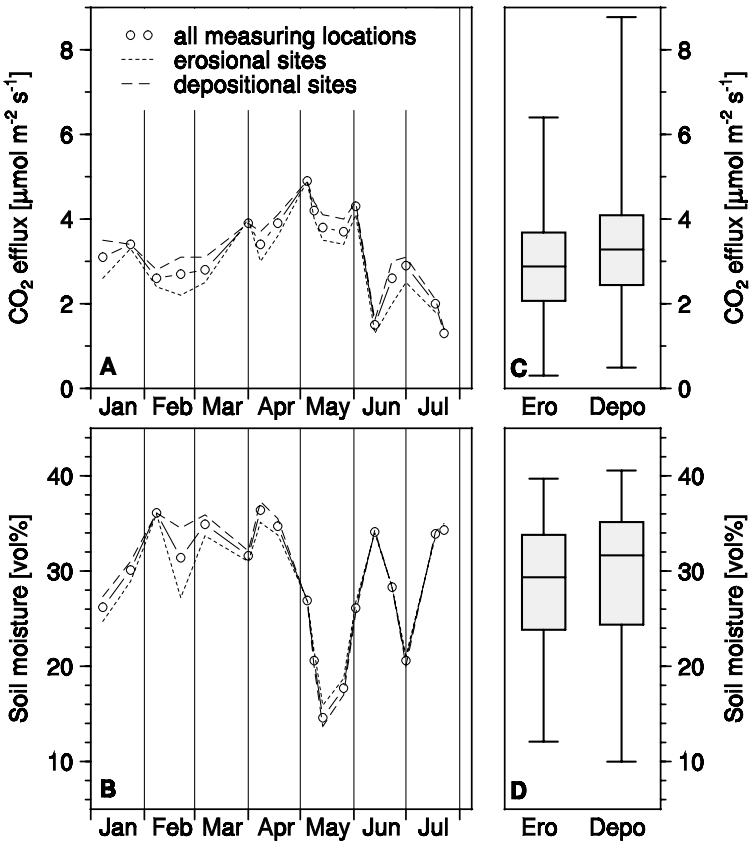

Fig. 4.3: Temporal variability of mean (over all measurement locations) standardised CO_2 efflux (A) and mean soil moisture (B) of all measuring locations (n=20), the erosional sites (n=8) and the depositional sites (n=12) in 2008; error bars give 95%-confidence intervals; box-whiskers show variability in overall CO_2 efflux (C) and soil moisture (D) during the measuring period for erosional (Ero) and depositional (Depo) sites, resp.; boxes give median, 1. and 3. quartile, and whiskers indicate minimum and maximum values; number of individual measurements for erosional sites n=144, for depositional sites n=216.

heterotrophic respiration during the rest of the growing period can be compared without being affected by the seasonality of temperature; and (iii) effects of timing of the measuring campaigns (always starting at 10 a.m.), which might result in an artificial pattern of soil temperature due to the aspect of measuring locations, can be removed. However, this procedure also eliminates potential *in situ* differences in soil temperature between the different locations, which are not analysed in the presented study.

To analyse the temporal variability of soil respiration these standardised values were averaged over all soil collars for each measuring date, whereas the standardised CO_2 effluxes of all measurement days of each soil collar were averaged for investigating spatial variability. Linear regressions between these temporally averaged standardised CO_2 effluxes and soil properties as well as plant growth were analysed. To relate the mean CO_2 effluxes of each soil collar to topography as well as to soil redistribution, linear regressions were calculated with the terrain parameters and the modelled soil redistribution patterns described in chapters 3.2.2 and 3.2.3. All parameters were tested for normality using Q-Q-plots and Shapiro-Wilk tests. Not normally distributed parameters were log-transformed. Significance levels of the

regressions were calculated using two-sided Student's T-tests. All statistical analysis were carried out using the GNU R version 2.6 (R Development Core Team, 2007).

4.3 RESULTS

4.3.1 Soil respiration and soil redistribution

During the three year study soil respiration, moisture and temperature were determined on 42 days at 20-22 locations resulting in an overall number of 2467 measurements. All standardised CO_2 effluxes (Fig. 4.2A-Fig. 4.4A) show a typical seasonality of soil respiration with relatively low values at the beginning of the growing period, when soil respiration in the collars is limited to heterotrophic respiration (subsequently referred as phase one), and an increase with increasing plant growth. Then roots of sugar beet and winter wheat start to grow under the collars and introduce autotrophic respiration (subsequently referred as phase two). In case of winter wheat this additional autotrophic respiration declines at the end of the growing period with plant senescence. It can be recognised that the increase in respiration with fully grown crops was more pronounced under winter wheat compared to sugar beet.

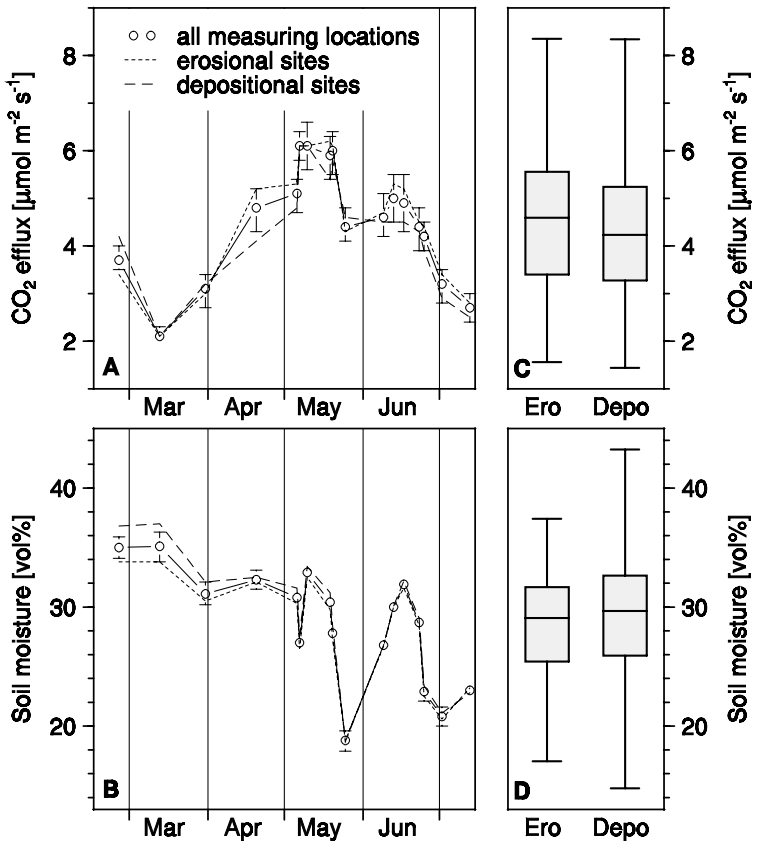

Fig. 4.4: Temporal variability of mean (over all measurement locations) standardised CO_2 efflux (A) and mean soil moisture (B) of all measuring locations (n=22), the erosional sites (n=13) and the depositional sites (n=9) in 2009; error bars give 95%-confidence intervals; box-whiskers show variability in overall CO_2 efflux (C) and soil moisture (D) during the measuring period for erosional (Ero) and depositional (Depo) sites, resp.; boxes give median, 1. and 3. quartile, and whiskers indicate minimum and maximum values; number of individual measurements for erosional sites n=221, for depositional sites n=153.

This probably results from a less dense root network growing under the collars in case of sugar beet, when the collars were placed between plant rows. Moreover, maximum CO_2 effluxes under winter wheat in 2009 were significantly higher, especially in May, than CO_2 effluxes in the same period under winter wheat in 2008.

Comparing temporal variability of standardised CO_2 effluxes with temporal variability of soil moisture at the collars (Fig. 4.2-Fig. 4.4, A and B), there is no obvious relation during sugar beet cultivation, when average soil moisture is in a mid-range on all measuring days (between 19.3 and 35.0 vol %). Under winter wheat, especially in May, some dry days seem to limit soil respiration (minimal average soil moisture in May is 14.6 and 18.8 vol % in 2008 and 2009, respectively). This was more pronounced in 2008 and was probably the reason for the overall smaller respiration in phase two in 2008 compared to phase two in 2009.

Tab. 4.1: Arithmetic mean and standard deviation (SD) of total (E_{tot}), tillage (E_{til}) and water erosion (E_{wat}) [mm a^{-1}] for the erosional (Ero) and depositional (Depo) sites in 2007, 2008 and 2009; note that areas of erosion and deposition are defined referring to total erosion.

		E_{tot}		E_{til}		E_{wat}	
	n	Mean	SD	Mean	SD	Mean	SD
				2007			
Ero	9	-1.60	1.18	-0.36	1.62	-1.24	0.95
Depo	11	1.99	1.06	4.29	1.95	-2.30	1.21
				2008			
Ero	9	-1.52	1.18	-0.24	1.68	-1.28	0.91
Depo	12	2.06	1.33	4.25	2.16	-2.19	1.16
				2009			
Ero	13	-1.98	1.14	-0.99	0.95	-0.99	0.58
Depo	9	2.06	1.49	4.57	2.28	-2.51	1.08

According to modelled total erosion (comprising soil redistribution by water and by tillage operations; Tab. 4.1), nine of the measuring collars were located at erosional sites and eleven and twelve at depositional sites in 2007 and 2008, respectively. Due to the shift of the location of the north-south cross-section of collars (Fig. 4.1) in 2009, which was necessary due to a change of wheel track position, 13 collars were modelled as erosional sites while nine represent depositional sites in this year (Tab. 4.1). Total erosion and deposition at the 2007, 2008 and 2009 collars range between a soil loss of 3.9, 3.1, and 4.1 mm a^{-1} and a soil gain of 3.4, 4.7, and 4.8 mm a^{-1}, respectively. This shows that the measuring locations are representative for the most dynamic area in the catchment referred to soil redistribution. In general, the catchment is dominated by tillage erosion (~80% of total erosion). Soil loss due

to water erosion is modelled at all collars, which is partly overcompensated by deposition caused by tillage erosion.

Mean CO_2 effluxes at the erosional sites are slightly smaller than mean CO_2 effluxes at depositional sites for the years 2007 and 2008 (Fig. 4.2-Fig. 4.3, A and C). Under winter wheat in 2009 this was also true for the first measuring phase in February and March. From mid April onwards CO_2 effluxes from erosional sites slightly exceed those from depositional sites (Fig. 4.4A). Comparing average moisture contents at the erosional and depositional sites (Fig. 4.2-Fig. 4.4, B and D) shows slightly higher average soil moisture at the depositional sites for most of the observed days. The differences in average soil moisture calculated for the total observation periods (Fig. 4.2 - Fig. 4.4 D) are, however, relatively small (2.2, 1.0, 0.9 vol % in 2007, 2008 and 2009, respectively).

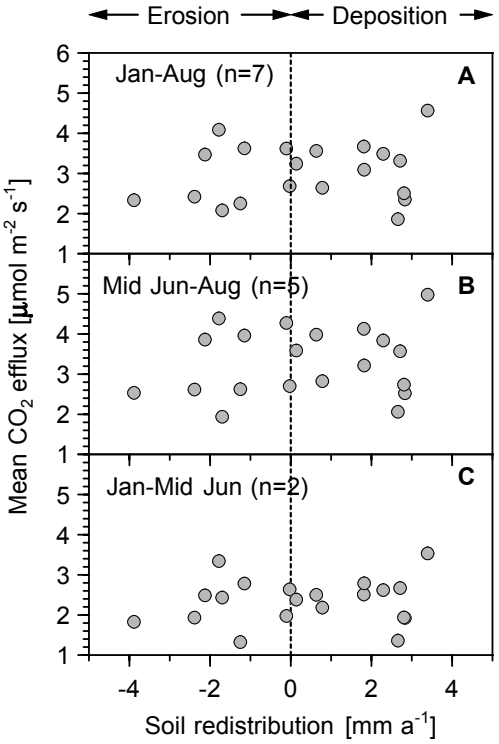

Fig. 4.5: Relation between mean (over all measurements made at one collar) CO_2 efflux and soil redistribution at all collars installed in 2007 for all campaigns (A), campaigns with sugar beet potentially introducing autotrophic respiration (B), and campaigns where sugar beet plants are small and therefore only heterotrophic respiration was measured (C).

Focusing on the spatial variability of standardised CO_2 effluxes in relation to total soil redistribution in more detail, results in a diverse picture. In 2007, under sugar beet cultivation, there was a tendency of decreasing CO_2 efflux with increasing erosion and increasing CO_2 efflux with increasing deposition for the whole measurement period. This tendency (not significant on a $p < 0.1$ level) was also obvious for the first phase of heterotrophic respiration and the second phase of combined heterotrophic and autotrophic respiration (Fig. 4.5). In 2008 under winter wheat standardised CO_2 effluxes significantly decreased with increasing erosion and increased with increasing deposition. This was also true for the phase of exclusive heterotrophic respiration from January to April (winter wheat height < 0.1 m), as well as for the phase of mixed heterotrophic and autotrophic respiration from April to July (Fig. 4.6). As the slopes of both regressions are similar (0.16 and 0.13, respectively), there is neither an indication that root respiration at erosional sites was reduced due to soil degradation processes nor that root respiration increased at depositional sites. The missing spatial difference in plant

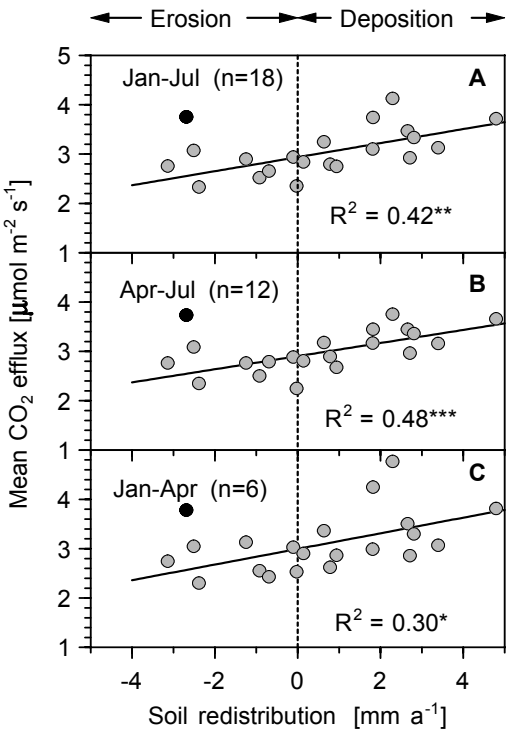

Fig. 4.6: Relation between mean (over all measurements made at one collar) CO_2 efflux and soil redistribution at all collars installed in 2008 for all campaigns (A), campaigns with winter wheat potentially introducing autotrophic respiration (B), campaigns where winter wheat plants are small (plant height < 0.1 m) and therefore only heterotrophic respiration was measured (C); black signature indicates an outlier not taken into account for regressions, where CO_2 effluxes were more than three standard deviations larger during all measuring phases than average effluxes at all erosional sites; significance levels: * is p<0.05; ** is p<0.01; * is p<0.001.**

activity and growth is also indicated by the measured plant heights (as somewhat weak proxy for biomass production and hence root respiration).

In 2009 CO_2 effluxes had a similar behaviour as observed in 2008 in phase one (February-March), with a highly significant decrease with increasing erosion and an increase with increasing deposition (Fig. 4.7C). From April to June no correlation between CO_2 effluxes and soil redistribution was found, which is already indicated in Fig. 4.4A. This probably results from the more dominant root respiration, especially in May, which seems to be not related to patterns in soil redistribution at our test site. This independency of root respiration from soil redistribution patterns is also indicated by the only small but not significant differences between the erosional and the depositional sites referring to average plant height (0.68±0.0 and 0.66±0.0 m) as well as above ground dry biomass determined before harvest (1.58±0.30 and 1.54±0.31 kg m^{-2}).

4.3.2 Soil respiration and soil, plant, and terrain parameters

Besides evaluating the importance of soil redistribution patterns for patterns of soil respiration, we also analysed their correlation with a number of soil, plant and terrain parameters (Tab. 4.2). Under sugar beet cultivation in 2007, CO_2 effluxes had no significant correlation to any of the soil parameters (Tab. 4.3). In the winter wheat years soil properties, especially texture (sand and median grain size diameter D_{50}), had some importance in the first measuring phases governed by heterotrophic respiration (Tab. 4.4 and Tab. 4.5).

Soil texture was of minor importance during the second phases of measurements under winter wheat, indicating that patterns in plant growth and hence autotrophic respiration were not affected by the relatively small spatial differences in texture (Tab. 4.2). Unexpectedly, only in 2009 a significant correlation was found with SOC in the topsoil (0-0.25 m). This might result from the overall small spatial variability of topsoil SOC contents which was most pronounced in 2009 (Tab. 4.2). Additionally, in 2008 and 2009 some correlation with subsoil SOC (0.25-0.50 m and 0.50-0.90 m) was determined. This probably results from a slight respiration increase in case of higher SOC availability in the subsoil, but is also a result of the highly significant correlation between subsoil SOC and soil redistribution (Tab. 4.4 and Tab. 4.5). In both winter wheat years soil nitrogen in the topsoil (0-0.25 m), which potentially affects plant growth, was significantly correlated with soil respiration in the second phase of measurement. However, plant height was only significantly correlated with measured soil respiration under winter wheat in 2008, while no significant correlation existed between plant parameters and soil respiration in 2009.

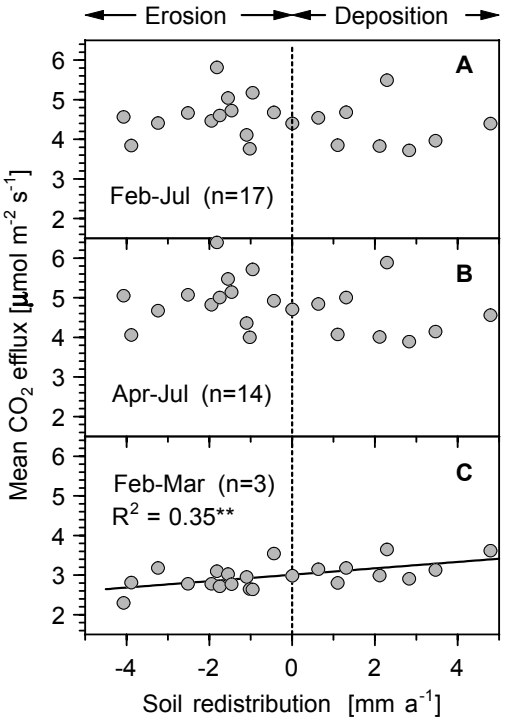

Fig. 4.7: Relation between mean (over all measurements made at one collar) CO_2 efflux and soil redistribution at all collars installed in 2009 for all campaigns (A), campaigns with winter wheat potentially introducing autotrophic respiration (B), campaigns where winter wheat plants are small (plant height < 10 cm) and therefore only heterotrophic respiration was measured (C); significance level: ** is p<0.01.

Among the analysed terrain parameters only curvature (perpendicular to maximum slope in 2007 and in maximum slope direction in 2008 and 2009, respectively) correlated significantly with CO_2 effluxes in all years (Tab. 4.5). The wetness index (*WI*) also had some significance in 2008 and 2009. The importance of soil moisture represented by the *WI* is also supported by the measurements in 2008, when a significant correlation existed between soil moisture and respiration. In general, the positive correlation with *WI* indicates that soil moisture only limited respiration during dry conditions. Therefore, this correlation might be somewhat biased by the timing of the measuring campaigns, which were not carried out during or shortly after rainfall events. In 2008 spatial variability of soil respiration during the two measuring phases was explained to 46% and 50% by the stream power index *SPI* (Tab.

4.4). In the first phase in 2009 the *SPI* explained 23% of the variability (Tab. 4.5). *SPI* represents potential water erosion and is therefore highly significantly correlated with modelled water erosion E_{wat} (R^2 between *SPI* and E_{wat} is 0.67 (2007), 0.71 (2008) and 0.75 (2009), respectively). As indicated in Tab. 4.4 and Tab. 4.5 soil respiration increases with increasing *SPI*, suggesting that more water erosion would lead to more soil respiration. This is somewhat counterintuitive but traces back to the fact that deposition resulting from tillage operations, which is the dominant erosion process at the measuring locations, overcompensates water erosion. Hence, locations of highest water erosion are mostly locations of highest total deposition (Fig. 4.8).

As already shown before, total soil redistribution was only significantly correlated with CO_2 effluxes in 2008 ($p < 0.05$ in first phase, $p < 0.001$ in second phase) and 2009 ($p < 0.01$ in first phase). However, it is worth noting, that soil redistribution patterns correlated with some of the topsoil properties (Tab. 4.5), especially SOC_I and soil moisture (also *WI*) which potentially govern spatial differences in soil respiration. Hence, under more extreme conditions, when soil erosion leads to substantial soil degradation, a more pronounced variability of soil properties (texture, SOC, water holding capacity etc.) associated with soil redistribution can be expected, which may interfere with respiration processes.

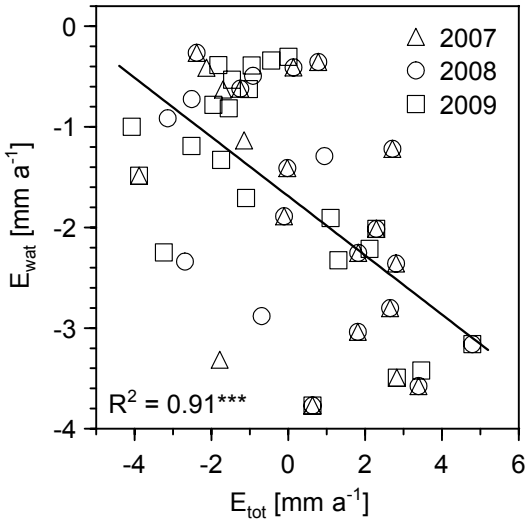

Fig. 4.8: Water erosion (E_{wat}) versus total erosion (E_{tot}) (comprising water and tillage erosion) for all measuring locations in 2007, 2008, and 2009, respectively; regression line and R^2 are calculated over all years.

Tab. 4.2: Statistics of parameters used for correlation analysis with measured CO_2 effluxes, soil moisture and results of erosion modelling; soil parameters measured in the collars are given in two depths (I_a: 0-0.10 m and I_b: 0.01-0.25 m) as well as the weighted mean of both (I: 0-0.25 m); this is indicated with subscripts; soil organic carbon SOC is also given in two subsoil layers (SOC_{gs_II}: 0.25-0.50 m; SOC_{gs_III}: 0.50-0.90 m); N is soil nitrogen; C/N is the ratio of SOC and N; BD is the bulk density; D50 gives the median grain size diameter, C-plan and C-prof are plan and profile curvature perpendicular and in direction of maximum slope, WI is wetness index, SPI is stream power index.

		2007			2008			2009		
Parameter	Unit	Mean	SD‡	CV (%)	Mean	SD	CV (%)	Mean	SD	CV (%)
Plant height	m				0.42	0.02	4.31	0.67	0.03	4.18
Dry biomass†	kg m^{-2}	2.80	0.915	32.50				1.57	0.30	19.11
SOC_{Ia}	wt%	1.24	0.14	11.48	1.42	0.14	9.86	1.37	0.26	18.76
SOC_{Ib}	wt%	1.11	0.17	15.66	1.16	0.14	11.71	1.12	0.24	21.27
SOC_{I}	wt%	1.16	0.15	13.15	1.27	0.10	7.77	1.22	0.21	17.47
$SOC_{gs\ II}$	wt%	0.81	0.23	28.40	0.83	0.23	27.71	0.78	0.22	28.21
$SOC_{gs\ III}$	wt%	0.52	0.32	61.54	0.54	0.31	57.41	0.48	0.30	62.50
N_{Ia}	wt%	0.11	0.02	14.17	0.15	0.02	9.98	0.16	0.02	15.53
N_{Ib}	wt%	0.12	0.02	18.33	0.13	0.02	17.93	0.13	0.02	16.26
N_{I}	wt%	0.12	0.02	15.07	0.14	0.02	11.23	0.14	0.02	13.58
C/N_{Ia}	-	10.9	1.49	13.65	9.33	1.00	10.75	8.69	0.40	4.62
C/N_{Ib}	-	9.37	1.80	19.26	9.27	2.03	21.90	8.51	0.51	6.00
C/N_{I}	-	9.97	1.57	15.74	9.29	1.47	15.81	8.60	0.41	4.83
pH_{Ia}	-	6.88	0.29	4.24	6.98	0.27	3.89	6.77	0.25	3.70
pH_{Ib}	-	6.80	0.38	5.57	7.01	0.27	3.79	6.85	0.31	4.46
pH_{I}	-	6.83	0.34	4.96	6.98	0.24	3.41	6.81	0.27	3.97
BD_{Ia}	10^3 kg m^3	1.37	0.06	4.14	1.22	0.07	5.87	1.20	0.13	10.59
BD_{Ib}	10^3 kg m^3	1.49	0.06	3.76	1.36	0.05	3.32	1.50	0.10	7.01
BD_{I}	10^3 kg m^3	1.44	0.05	3.39	1.30	0.04	3.16	1.38	0.10	6.93
$Sand_{Ia}$	wt%	13.8	3.04	22.10	12.8	5.30	41.26	11.3	5.01	44.34
$Sand_{Ib}$	wt%	12.7	3.98	31.25	12.9	9.09	70.40	10.5	6.18	58.77
$Sand_{I}$	wt%	13.1	3.15	23.99	12.0	5.64	47.01	10.8	5.67	52.38
$Silt_{Ia}$	wt%	71.8	3.56	4.96	71.3	5.76	8.07	73.0	5.65	7.74
$Silt_{Ib}$	wt%	70.3	4.56	6.48	70.3	8.78	12.49	73.7	7.28	9.89
$Silt_{I}$	wt%	70.9	3.72	5.24	71.5	5.83	8.15	73.4	6.52	8.88
$Clay_{Ia}$	wt%	14.5	2.99	20.64	15.8	2.20	13.88	15.7	2.09	13.35
$Clay_{Ib}$	wt%	17.0	3.22	18.92	16.8	1.65	9.81	15.8	2.33	14.74
$Clay_{I}$	wt%	16.0	2.71	16.94	16.5	1.57	9.54	15.8	1.97	12.52
$D50_{Ia}$	µm	12.4	2.20	17.73	11.7	2.44	20.78	11.2	1.86	16.67
$D50_{Ib}$	µm	10.4	2.13	20.42	11.1	3.24	29.24	10.8	1.74	16.12
$D50_{I}$	µm	11.2	1.75	15.57	11.0	2.11	19.12	10.9	1.64	15.03
Slope	°	6.34	1.54	24.28	6.35	1.60	25.26	6.84	1.60	23.36
Aspect	°	112	35.1	31.36	111	34.3	30.85	116	36.8	31.78
C-plan	0.01 m	-0.46	0.45	---	-0.51	0.44	---	-0.26	0.51	---
C-prof	0.01 m	0.01	0.33	---	0.07	0.32	---	-0.04	0.34	---
WI	-	8.45	1.48	17.51	8.54	1.40	16.36	8.02	1.55	19.36
SPI	-	106	94.6	89.14	107	92.2	85.89	88.5	90.3	102.10

† only parameter log-transformed for correlation analysis in case of sugar beet; but given here not transformed.

‡ SD: standard deviation; CV: coefficient of variatio

Tab. 4.3: Correlation matrix of all parameters significantly ($p < 0.05$) correlating either with average CO_2 effluxes without (w/o) and/or with (w) root respiration and/or with total erosion E_{tot} at the 20 locations observed under sugar beet cultivation in 2007 (bold and gray shaded); the data give Pearson correlation coefficients, while the asterisks give significant levels (* is $p < 0.001$; ** is $p < 0.01$, and * is $p < 0.05$); if a significant correlation with one of the soil parameters measured at the collars is found for all measuring depths (I_a: 0-0.1 m; I_b: 0.1-0.25 m) only the correlation with the total depth (I: 0-0.25 m) is given for simplicity; soil organic carbon (wt%) from deeper soil layers (SOC_{gs_II}: 0.25-0.50 m; SOC_{gs_III}: 0.50-0.90 m) were taken from Dlugoß et al. (2010); for units see Tab. 4.2.**

	CO_2 efflux w/o roots	CO_2 efflux w roots	SM w/o roots	SM w roots	SOC_I	N_I	C/N_{Ia}	BD_I	SOC_{gs_II}	SOC_{gs_III}	C-plan	C-prof	WI	SPI	E_{tot}
CO_2 efflux w/o roots		0.71										**0.49**			
CO_2 efflux w roots	***											**0.51**			
SM w/o roots				0.76		0.61	-0.58	-0.45	0.67	0.65	-0.58	0.66	0.78	0.68	**0.63**
SM w roots			***			0.66	-0.67		0.78	0.62	-0.65	0.76	0.69	0.63	**0.60**
SOC_I						0.56				0.59		0.45		0.53	**0.50**
N_I			**	**	*		-0.49		0.83	0.82	-0.66	0.70	0.78	0.77	**0.75**
C/N_{Ia}			**	**		*			-0.64				-0.63		
BD_I			*							-0.49			-0.47	-0.49	
SOC_{gs_II}			***	***		***	**			0.72	-0.73	0.79	0.75	0.69	**0.86**
SOC_{gs_III}			***		**	***		*	***		-0.79	0.69	0.87	0.95	**0.73**
C-plan			**	**		**			***	***		-0.71	-0.77	-0.78	**-0.71**
C-prof	*	*	**	***	*	***			***	***	***		0.66	0.66	**0.73**
WI			***	***		***	**	*	***	***	***	**		0.89	**0.72**
SPI			**	**	*	***		*	***	***	***	**	***		**0.67**
E_{tot}			**	**	*	***			***	***	***	***	***	**	

Tab. 4.4: Correlation matrix of all parameters significantly ($p < 0.05$) correlated either with average CO_2 effluxes without (w/o) and/or with (w) root respiration and/or with total erosion E_{tot} at the 20 locations observed under winter wheat in 2008 (bold and gray shaded); data give Pearson correlation coefficients, while asterisks give significant levels (* is $p < 0.001$; ** is $p < 0.01$, and * is $p < 0.05$); if a significant correlation with one of the soil parameters is found for all measuring depths (I_a: 0-0.1 m; I_b: 0.1-0.25 m) only the correlation with the total depth (I: 0-0.25 m) is given for simplicity; soil organic carbon (wt%) from deeper soil layers (SOC_{gs_II}: 0.25-0.50 m; SOC_{gs_III}: 0.50-0.90 m) were taken from Dlugoß et al.(2010); for units see Tab. 4.2.**

	CO_2 efflux w/o roots	CO_2 efflux w roots	SM w/o roots	SM w roots	Plant height	N_I	$Sand_I$	$Silt_I$	$D50_I$	SOC_{gs_II}	SOC_{gs_III}	C-plan	C-prof	WI	SPI	E_{tot}
CO_2 efflux w/o roots		0.87	**0.55**	-0.60	**-0.50**		**0.77**	**-0.73**	**0.61**		**0.74**	**-0.51**		**0.64**	**0.70**	**0.55**
CO_2 efflux w roots	***		0.70	**-0.49**	**-0.57**	**0.48**	**0.52**	**-0.46**	**0.50**	**0.54**	**0.77**	**-0.59**		**0.80**	**0.79**	**0.69**
SM w/o roots	*	***				0.54				0.63	0.56	-0.54		0.76	0.66	**0.61**
SM w roots	**	*					-0.62	0.56	-0.63							
Plant height	*	**	**								-0.56			-0.62	-0.71	
N_I		*	*							0.50	0.49	-0.64		0.77	0.58	**0.51**
$Sand_I$	***	*		**				-0.96	0.82							
$Silt_I$	***	*		*			***		-0.66		-0.51					
$D50_I$	**	*		**			***	**								
SOC_{gs_II}		**	**			*					0.71	-0.81	0.77	0.68	0.67	**0.83**
SOC_{gs_III}	***	***	*		*	*		*		***		-0.78	0.61	0.85	0.95	**0.69**
C-plan	*	**	*			**				***	***		-0.78	-0.74	-0.76	**-0.79**
C-prof										***	**	***		0.51	0.55	**0.72**
WI	**	***	***		**	***				**	***	***	*		0.88	**0.68**
SPI	***	***	**		***	**				**	***	***	*	***		**0.66**
E_{tot}	*	***	**			*				***	***	***	***	***	**	

Tab. 4.5: Correlation matrix of all parameters significantly ($p < 0.05$) correlated either with average CO_2 effluxes without (w/o) and/or with (w) root respiration and/or with total erosion E_{tot} at the 22 locations observed under winter wheat in 2009 (bold and gray shaded); data give Pearson correlation coefficients, while asterisks give significant levels (* is $p < 0.001$; ** is $p < 0.01$, and * is $p < 0.05$); if a significant correlation with one of the soil parameters is found for all measuring depths (I_a: 0-0.1 m; I_b: 0.1-0.25 m) only the correlation with the total depth (I: 0-0.25 m) is given for simplicity; soil organic carbon (wt%) from deeper soil layers (SOC_{gs_II}: 0.25-0.50 m; SOC_{gs_III}: 0.50-0.90 m) were taken from Dlugoß et al.(2010) for units see Tab. 4.2.**

	CO_2 efflux w/o roots	CO_2 efflux w roots	SM w roots	SOC_I	N_I	C/N_I	pH_I	$Sand_I$	$D50_I$	SOC_{gs_II}	SOC_{gs_III}	Slope	C-plan	C-prof	WI	SPI	E_{tot}
CO_2 flux w/o roots				**0.46**	**0.46**			**0.52**	**0.61**		**0.44**	**-0.50**	**-0.49**	**0.48**	**0.57**	**0.48**	**0.59**
CO_2 flux w roots			**-0.42**	**-0.43**	**-0.43**		**0.49**										
SM w roots		*						-0.50									
SOC_I	*	*			0.99	0.87	-0.45			0.80	0.76		-0.75	0.62	0.90	0.80	**0.73**
N_I	*	*		***		0.77	-0.45			0.78	0.73		-0.71	0.58	0.86	0.76	**0.70**
C/N_I				***	***			0.49		0.70	0.69		-0.73	0.63	0.85	0.75	**0.65**
pH_I		*		*	*										-0.48		
$Sand_I$	*		*			*			0.64		0.54				0.47	0.45	
$D50_I$	**							**									
SOC_{gs_II}				***	***	***					0.69		-0.79	0.76	0.71	0.73	0.86
SOC_{gs_III}	*			***	***	***		**		***			-0.80	0.70	0.84	0.94	0.71
Slope	*														-0.43		
C-plan	*			***	***	***				***	***			-0.78	-0.84	-0.89	**-0.82**
C-prof	*			**	**	**				***	***		***		0.63	0.72	**0.79**
WI	**			***	***	***	*	*		***	***	*	***	**		0.90	**0.70**
SPI	*			***	***	***		*		***	***		***	***	***		**0.75**
E_{tot}	**			***	***	**				***	***		***	***	***	***	

4.4 DISCUSSION

The soil temperature dependent standardisation of soil respiration rates allowed to determine and to compare spatial variability of heterotrophic as well as combined autotrophic and heterotrophic respiration under arable land. Besides its advantages this standardisation also removed potential spatial variability of respiration due to a spatial variability of soil temperature. This should, however, be unproblematic as soil temperature differences on a field scale are relatively small and less important for spatial variability in soil respiration (Herbst et al., 2009; Kang et al., 2003). According to Herbst et al. (2009) differences in soil moisture are the most important drivers of spatial variability in heterotrophic respiration on a bare field, monitored at 48 locations between April and July. In contrast, in our data the spatial variability of soil moisture was neither significantly correlated in all years with soil respiration nor was it the most important reason for spatial variability in (heterotrophic) soil respiration. The relatively minor importance probably results from missing extremes (very dry or very wet) in our measured data, which proved to affect respiration in other studies (e.g. Davidson et al., 2000).

Only few studies relate spatial variability of soil respiration to terrain attributes or to soil redistribution patterns on agricultural land. For example Parkin et al. (2005) related *in situ* measured soil respiration to landscape positions (summit, side slope, and depressions) in three soybean (*Glycine max.* L.) and maize (*Zea mays* L.) fields. The authors measured under fully grown crops and found that root respiration, which is not directly related to the observed landscape positions, dominates overall respiration. Hence no significant correlation between overall CO_2 effluxes and landscape position could be determined. This result probably also explains the missing correlation between CO_2 effluxes and soil redistribution in the second phase of winter wheat in 2009 (Fig. 4.7B), when maximum respiration rates indicate the importance of root respiration.

In addition to the rare studies dealing with spatial variability of soil respiration on arable fields (Bajracharya et al., 2000; Han et al., 2007; Parkin et al., 2005; Rochette et al., 1991; Van Hemelryck et al., 2010b), our results give some insights into significant relations of soil respiration to soil properties, terrain attributes and soil redistribution. However, this is only the case for the first phase of both winter wheat years (plus second phase in 2008); while in the sugar beet year in 2007 no significant relations to any of the tested parameters (except

curvature) could be determined. The later might result from the small number of measurements (n=7), especially for the phase of heterotrophic respiration (n=2).

In the following discussion we therefore focus on the first phases of monitoring in the winter wheat years, as these phases correspond to heterotrophic respiration alone. Thus, spatial differences can be interpreted as indicators of spatial differences in overall SOC decomposition. Besides some texture parameters, heterotrophic respiration was best determined by terrain attributes and total soil erosion in 2008 and 2009. If total erosion increases (from negative values representing erosional sites to positive values representing depositional sites), heterotrophic soil respiration also increases. This is described by linear regressions representing 30 and 35% of the variation in respiration, respectively. When focusing separately on erosional and depositional sites no significant relation between soil respiration and soil erosion/deposition was found. This could result from the overall small number of measuring locations in each of the soil redistribution domains (max. n=13), which do not allow for a reasonable statistical analysis in case of the very variable data. However, it could also be an indicator that there is no substantial relation. However, it is important to note that the increase in respiration from locations with pronounced erosion (max. -4.1 mm a^{-1}) to pronounced deposition (max. 4.7 mm a^{-1}) can be described by a linear correlation. If the higher decomposition at the depositional sites was a direct result of lateral SOC input, the linear relation between soil respiration and soil redistribution would lead to a more or less balanced reduction of decomposition at erosional sites and corresponding increase of decomposition at depositional sites. This conclusions would follow Jacinthe and Lal (2001) and Van Hemelryck et al. (2010b) who argued that depositional sites gain large amounts of labile carbon from carbon rich eroded topsoil which can be respired more easily. However, a purely lateral C-input driven linear increase in respiration contradicts findings from comparisons of patterns in erosion and SOC, which indicated that decomposition at erosional sites decreases and leads to a dynamic replacement while no clear effect can be expected for depositional sites (Van Oost et al., 2007).

Moreover, higher decomposition rates at the depositional compared to non eroding sites are also inconsistent with a missing depletion of topsoil SOC at depositional sites in the catchment (Dlugoß et al., 2010; chapter 3). The increasing respiration at our test site could result from a number of interacting processes: (i) Following Berhe et al. (2007) the net primary productivity (NPP) at depositional sites may increase as a consequence of deposition of organic matter and nutrient rich topsoil and a subsequent increase in soil water holding

capacity. Regarding changes in nutrient status (N_I) and soil moisture (Tab. 4.4 and Tab. 4.5) there is some indication that depositional areas provide better growing conditions and hence increase gross primary productivity (GPP). However, there was no evidence of an increased crop growth at the depositional sites from the measured plant height, biomass and mixed respiration in the second phase of winter wheat monitoring (no amplified differences between erosional and depositional sites). (ii) Differences in soil moisture might affect C decomposition at the potentially wetter depositional sites in two ways. On the one hand slightly higher soil moisture during the vegetation period may prevent dryness limited respiration and therefore enhance decomposition, whereas during very wet periods, wetness limited respiration may stabilise SOC. Both cases should not substantially affect the spatial variability of the measured respiration (in phase one) as the differences in soil moisture between erosional and depositional sites were small (only significantly correlated in 2008) and conditions were neither very dry nor very wet (min: 20.8 and 28.1 vol.-%; max: 40.5 and 43.2 in 2008 and 2009, respectively). (iii) The depositional sites gain more labile carbon from eroded topsoil which can be respired more easily (e.g. Jacinthe and Lal, 2001; Van Hemelryck et al., 2010b). (iv) SOC buried underneath the plough layer is partly respired. This could be partly the case at the test site where soil respiration and soil redistribution are significantly correlated with subsoil SOC content (Tab. 4.4 and Tab. 4.5). However, SOC contents only decline very slowly with depth at the monitored depositional sites (Dlugoß et al., 2010; chapter 3) and therefore are relatively stable in time.

Overall, our measurements indicate an effect of soil redistribution on heterotrophic soil respiration in the observed winter wheat cultivations. Assuming that the relative differences of average standardised CO_2 effluxes are representative for differences in C decomposition between erosional and depositional sites, the C-sink function at erosional sites would be partly compensated by additional respiration at the depositional sites. Therefore, other processes must be at play preventing SOC depletion at depositional sites that cannot explicitly be identified from our data, but which are of major importance for a full C-balance of erosion and deposition processes.

4.5 CONCLUSION

Spatial variability of soil respiration was measured during three growing periods once under sugar beet and twice under winter wheat at 20-22 locations within a small agricultural catchment. Based on these data correlations between soil respiration and soil properties

(including soil moisture), terrain attributes and modelled soil redistribution were evaluated. Under sugar beet cultivation, in 2007, no correlation between soil respiration and any of the tested parameters (except curvature) was found. This points to the importance of comprehensive data sets for statistical analysis of spatial variability of soil respiration on arable land (only seven measuring days with one measurement at each collar were carried out under sugar beet). Under winter wheat significant correlations between heterotrophic respiration and soil redistribution in the first measurement phase could be found. These relations were not amplified in 2008 and even vanished in 2009 during the second phase of measurement, when heterotrophic and autotrophic respiration were combined, indicating that plant growth and hence root respiration was not affected at the test site by patterns of soil redistribution.

There were very few parameters correlated simultaneously with soil respiration and soil redistribution. Most prominent were terrain attributes, namely wetness index (*WI*) and stream power index (*SPI*). They showed significant correlations with heterotrophic respiration in 2008 and 2009 (in 2008 also with mixed heterotrophic and autotrophic respiration) and with soil redistribution. Regarding *SPI*, representing potential water erosion, this result is somewhat misleading because a high erosion potential is associated with highest soil respiration. Therefore, any meaningful analysis of soil respiration vs. soil redistribution on arable land must take into account the sum of water and tillage erosion (often overcompensating water erosion). Moreover, it is interesting to note that *WI* was always a better predictor of soil respiration than measured soil moisture. This might turn *WI* to be an interesting parameter for modelling soil respiration in agricultural catchments, as long as respiration is either dryness or wetness limited. Total topsoil nitrogen content was a significantly correlating parameter in the second phase of the winter wheat years with soil respiration and soil redistribution, indicating the importance of lateral sediment and water fluxes for nutrient supply, plant growth and hence root respiration. Moreover, subsoil SOC was highly correlated to soil redistribution and was also correlated to soil respiration in 2008 and 2009.

For the first phase of the 2008 and 2009 campaigns, heterotrophic respiration linearly increased from erosion to deposition (R^2 is 0.30 and 0.35; $p<0.05$ and $p<0.01$, respectively). Assuming that differences in heterotrophic respiration are an indicator for differences in overall soil C decomposition, this is important insofar as in case of a linear increase (including depositional areas) the C sink-function at erosional sites described in many studies

would be largely compensated by a C source-function of depositional sites. However, as no depletion in topsoil SOC was found at the depositional sites, but also no additional C sources could be clearly identified, a better process understanding regarding the C balance at depositional sites seems to be a key research issue determining the overall effects of erosion on CO_2 effluxes.

5 DEPTH DISTRIBUTION OF PARTICLE-SIZE SOIL ORGANIC CARBON FRACTIONS AND ^{14}C CONCENTRATION AT DIFFERENT LANDSCAPE POSITIONS

5.1 INTRODUCTION

The investigation of the role of soils in the global carbon cycle is generally exacerbated by the complex nature of SOC being composed of different decomposition and humification products resulting from the metabolic activities of the soil microbial biomass. The turnover of these different components varies continuously due to the complex interactions of biological, chemical and physical processes in soil (Christensen, 1992; Trumbore, 2009). In most dynamic SOC models, this continuum is conceptualised into several SOC pools with different turnover times. Principally, these encompass a fast or labile pool with a mean residence time of less than one year, a slow or passive pool with a mean residence time of decades or centuries and a refractory or inert pool with a mean residence time of millennia (Trumbore, 1996).

To characterise and quantify these pools and to gain further insights into the mechanisms leading to their decomposition and stabilisation, specific operational SOC fractions are often analysed, applying a range of different physical or chemical fractionation techniques (see review by Christensen (1992) and von Lützow et al. (2007)). Physical fractionation is often preferred, because chemical fractionation is potentially more destructive and moreover, the concepts of physical fractionation emphasise the role of soil minerals in the stabilisation and turnover of soil organic matter (Christensen, 1992). The basic physical methods are the separation by density (e.g. John et al., 2005; Paul et al., 2008; Rethemeyer et al., 2005) or particle-size (e.g. Amelung et al., 1998; Balesdent et al., 1998; Liang et al., 2009) of primary organo-mineral complexes, and the separation of aggregate classes (e.g. John et al., 2005; Six et al., 2001). All methods proved to at least separate a more labile pool, represented in the

light, sand-sized or the free SOC pool, respectively, from more passive components (von Lützow et al., 2007). In some studies more sophisticated fractionation schemes, combining physical and chemical methods, were developed, that specifically link measured to modelled SOC pools to improve process representation and validation of SOC dynamic models. For example, Zimmermann et al. (2007) successfully related measurable SOC pools to those applied in Roth-C (Coleman and Jenkinson, 2008).

In addition to SOC fractionation, radiocarbon (^{14}C) measurements by accelerator mass spectrometry (AMS) are increasingly used to study SOC dynamics (see review by Trumbore (2009)). The basic principles of radiocarbon dating are summarised in Hajdas (2008). Due to nuclear weapon testing, the atmospheric ^{14}C content increased significantly since the 1950s with a peak in 1963 (~180 pMC) that was almost double the atmospheric ^{14}C content of the period before 1950 (~100 pMC) (Levin and Kromer, 2004) (Fig. 5.1). This so-called bomb spike can be used as a time marker and to study SOC dynamics on decadal time scales (Trumbore, 2009). In combination with different SOC fractionation schemes, ^{14}C data were used to calculate turnover rates of SOC pools (e.g. Brovkin et al., 2008; Bruun et al., 2005; Leifeld et al., 2009) by means of various bomb ^{14}C turnover models (e.g. Bruun et al., 2005; Hahn and Buchmann, 2004; Harkness et al., 1986; Torn et al., 1997).

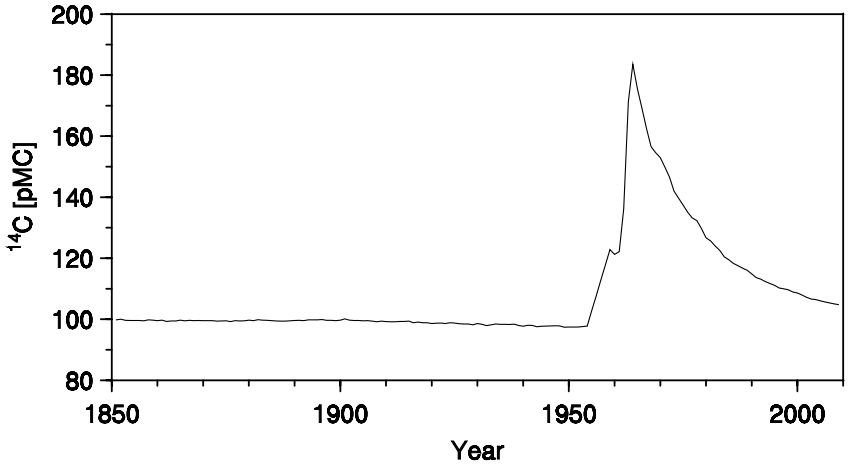

Fig. 5.1: Temporal evolution of atmospheric ^{14}C content in the northern hemisphere. Data are derived from Stuiver et al. (1998) and Levin and Kromer (2004).

While most studies including ^{14}C data are restricted to the topsoil (e.g. Leifeld et al., 2009; Leifeld and Fuhrer, 2009), few studies analyse the depth distribution of ^{14}C measured by AMS (e.g. Rethemeyer et al., 2005; Torn et al., 1997). On maize and wheat fields on flat terrain, Rethemeyer et al. (2005) showed that ^{14}C contents in the plough layer were in the same magnitude as the atmospheric ^{14}C content at the time of sampling. They attributed this

to high proportions of young carbon from recent plant residues. With increasing soil depth (maximum depth of 0.65 m) the ^{14}C age increased because of larger proportions of more stable SOC components.

Soil redistribution has a great impact on the spatial patterns of soil organic carbon (SOC) stocks as well as on lateral and vertical C fluxes between soil and atmosphere on sloped agricultural land (e.g. Berhe et al., 2008; Dlugoß et al., 2010; Ritchie et al., 2007; Zhang et al., 2006). However, in most studies considering the interaction of soil redistribution and SOC, SOC of bulk soil is analysed. The investigation of the impact of soil redistribution on different SOC pools and thus on different C quality might further improve the knowledge about the mechanisms controlling an erosion induced atmospheric C sink or source, that is discussed controversially (e.g. Berhe et al., 2007; Kuhn et al., 2009; Lal, 2003a; Van Oost et al., 2007). The studies of Jacinthe et al. (2004) and Van Hemelryck et al. (2010b) indicate that the labile SOC pool may be preferentially transported by water induced erosion, whereas Chaplot et al. (2005) found that black carbon, usually considered as an inert C pool, was preferentially eroded and deposited within the Mekong catchment in Vietnam. In a modelling approach considering soil redistribution, Liu et al. (2003) found that the labile pool decreased with depth, and that the distribution pattern might possibly be changed by soil redistribution. They concluded that omitting explicit consideration of specific SOC pools might lead to an overestimation of SOC mineralisation especially in the subsoil.

To our knowledge no studies were conducted so far that explicitly investigate the differences of the depth distribution of SOC fractions in combination with depth distributions of bulk ^{14}C at different landscape positions on sloped arable land. Hypothesising preferential erosion and/or deposition of specific SOC fractions, we expect spatial differences in the depth distribution of SOC fractions at different slope positions. As the influence of soil redistribution on soil texture was demonstrated in many soil erosion studies (e.g. Basic et al., 2002; Fiener et al., 2008; Malam Issa et al., 2006; Rosenbloom et al., 2001) and different soil texture classes were found to have different SOC quantities and quality (e.g. Amelung et al., 1998; Balesdent et al., 1998; Liang et al., 2009), in this study the particle-size fractionation following Amelung et al. (1998) was applied to investigate the effect of soil redistribution on the depth distribution of SOC fractions at different slope positions. Based on results of Berhe et al. (2008) being the only study that investigated ^{14}C depth distributions at different landscape positions, we assume an increased ^{14}C concentration below the actual plough layer in depositional profiles compared to reference or erosional profiles, since the material of the

plough layer imprinted with bomb ^{14}C was continuously superimposed. In erosional profiles, ^{14}C contents should be lower compared to reference sites in the same subsoil increment caused by truncation of the soil profile and an admixture of older subsoil SOC by tillage operations.

Besides giving further insights into SOC dynamics at different landscape positions, measured depth distributions of bulk soil ^{14}C at depositional sites might potentially be used to derive long-term deposition rates. In soil erosion studies, radiogenic nuclides, especially ^{137}Cs, are often used as tracers to analyse time integrating spatially distributed erosion and deposition patterns (e.g. Li et al., 2010; Walling et al., 2003). But the use of ^{137}Cs is exacerbated or even impossible in areas that, besides a contamination by nuclear weapon testing in the 1950s and 1960s, also experienced a ^{137}Cs contamination following the Chernobyl disaster, since these two contaminations can hardly be separated (e.g. Higgitt et al., 1992; Schimmack et al., 2001). In these regions, measurements of the $^{239+240}Pu$ activity proved to be successful in some studies (e.g. Schimmack et al., 2001), but these measurements are too expensive to be applied area-wide. Additionally, ^{210}Pb is often used (e.g. Li et al., 2006; Mabit et al., 2009; Walling and He, 1999), but as the differences of its activity at erosion and deposition sites are less pronounced than for ^{137}Cs (e.g. Vahrson and Frielinghaus, 1998), soil redistribution rates derived from ^{210}Pb were less precise. As there is a general need for further possibilities to derive spatially distributed soil redistribution rates in areas prone to Chernobyl fallout, the potential of bulk soil ^{14}C measurements to derive deposition rates is tested in this study.

Against this background, the objectives of this chapter are:

(i) To analyse preferential erosion and/or deposition of particle-size SOC fractions,
(ii) to investigate differences in the ^{14}C depth distribution of bulk soil at different slope positions in relation to depth profiles of SOC fractions, and
(iii) to estimate deposition rates by means of AMS ^{14}C profiles.

5.2 MATERIALS AND METHODS

5.2.1 Soil sampling and sample preparation

In 2009, soil profiles were taken in duplicates at slope positions representing depositional, erosional and reference (without deposition or erosion) sites (Fig. 5.2) at the Heiderhof test site. Their position was chosen by means of modelled total soil redistribution rates (comprising water and tillage induced soil redistribution) from an earlier study (Dlugoß et al., 2010; chapter 3). Two sampling points (D1 and D2) were situated in the area with highest modelled deposition rates near the outlet of the test site, and two were situated in an area with high modelled erosion rates (E1 and E2). As reference, two sampling points were chosen from grid cells showing less than 0.02 mm a^{-1} modelled erosion or deposition (R1 and R2). Each of the six soil sampling points was situated in the centre of the grid cell chosen out of the modelled total erosion map with a dGPS with a horizontal accuracy of less than 0.1 m (HiPer Pro, Topcon, Japan).

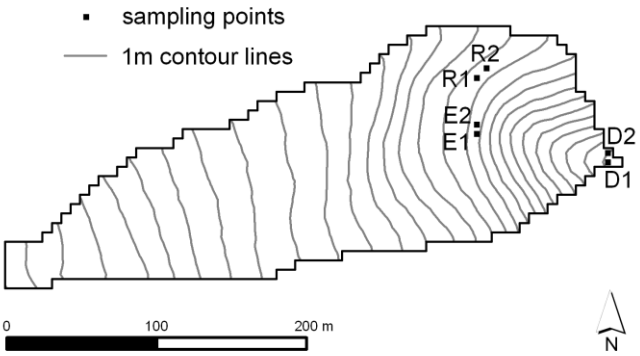

Fig. 5.2: Location of soil sampling points within the Heiderhof test site at reference (R), erosional (E) and depositional (D) sites. Flow direction is from west to east.

Soil cores were taken with a van der Horst soil auger (Eijkelkamp, Netherlands) with a diameter of 0.07 m and a length of 0.4 m. At depositional sites cores were taken up to a depth of 1.6 m, at reference sites up to 1.2 m and at erosional sites up to 0.8 m, respectively. To avoid compression effects and thus erroneous sampling depths, two cores were drilled at each sampling point offset by 0.2 m. Hence, except for the uppermost soil core, the upper and lower 0.1 m was neglected. Soil cores were divided into 0.05 m increments in the laboratory, except for the uppermost 0.15 m being the actual tillage depth. The samples were stored at -28°C.

For every second depth increment of each sampled profile starting with the topsoil layer (0-0.15 m), one half of each depth increment was prepared for the analysis of SOC and N content, pH value, and soil texture. Therefore, fine roots and other recognisable undecomposed organic matter particles were removed by hand picking before drying the soil samples at 105°C for 24 hours. After that they were ground, and coarse particles were

separated by 2 mm-sieving. Samples were treated with hydrochloric acid (10 %) to remove possible carbonates ($CaCO_3$).

The other half of each depth increment was prepared for AMS ^{14}C measurements and particle-size SOC fractionation. Roots and visible plant remains were removed more intensively by picking them with a forceps under a microscope (up to 40 fold magnification) for two to three hours in the topsoil layers (0-0.15 and 0.2-0.25 m) and for one hour in the subsoil layers, respectively. The fraction > 2 mm was removed by dry sieving, and soil samples were then freeze-dried.

The effect of different sample preparation on the amount of bulk SOC and SOC fractions was tested at one depositional profile up to a depth of 1 m by applying both preparation schemes and comparing results of the laboratory analysis. Student's T-tests ($p<0.05$) revealed that bulk SOC contents, sample weights and the SOC contents of the particle-size fractions did not differ significantly for the two methods of sample preparation. Thus, SOC fractions and radiocarbon data could be related to the other soil properties.

5.2.2 Soil properties

SOC and N content of bulk soil samples were determined by dry combustion using a CNS elemental analyser (vario EL, Elementar, Germany). Soil texture was determined by the combined sieve and pipette method (Deutsches Institut für Normung, 2002) using the following classification: Coarse sand (630-2000 µm), medium sand (200-630 µm), fine sand (63-200 µm), coarse silt (20-63 µm), medium silt (6.3-20 µm), fine silt (2-6.3 µm), and clay (<2 µm). The pH value was measured in a 0.01 M $CaCl_2$ solution (Deutsches Institut für Normung, 2006).

5.2.3 SOC fractionation

For one soil profile at each slope position (R2, E2 (chosen arbitrarily) and D1 (representing highest deposition)) four particle-size SOC fractions were separated for every second depth increment (starting with the topsoil layer) up to 1 m depth following the particle-size fractionation scheme of Amelung et al. (1998). In this approach boundaries of particle-size classes are based on the USDA (United States Department of Agriculture) system (USDA, 1999) with minor deviations. For this procedure two replicate samples of the freeze-dried fine soil (30 g, < 2 mm) were treated ultrasonically at 60 J ml^{-1} with a probe-type

sonicator (Branson Sonifier Model 250, Branson, USA) in 150 ml demineralised water to disperse macro aggregates (> 250 µm). The power output of the sonicator was calibrated calorimetrically every day following North (1976). A coarse-sized fraction (fraction 1: 250 to 2000 µm) was then isolated by wet sieving. The remnant was again treated ultrasonically at 440 J ml^{-1} in a soil/water ratio of 1:10 to disperse the samples completely. Wet sieving was again applied to separate an intermediate-sized fraction (fraction 2: 53-250 µm) and a fine-sized fraction (fraction 3: 20-53 µm). These particle-size classes were then dried at 40°C, weighted and ground for further CN analysis with a CNS elemental analyser (vario EL, Elementar, Germany). They were treated with hydrochloric acid (10 %) to remove possible carbonates ($CaCO_3$). The mass, SOC, and N content of the remaining very fine sized class (fraction 4: < 20 µm) was calculated by mass balancing assuming no loss of sample weight, SOC and N, as the studies of Amelung et al. (1998) showed that the loss of sample material after fractionation was relatively low. Recoveries averaged 97% of sample weight, 94% of SOC, and 79% of N (Amelung et al. 1998). The enrichment factor E (Christensen, 1992) that relates the C content of a specific particle-size fraction to that of bulk SOC was calculated for each particle-size fraction. Enrichment of a SOC pool results in $E > 1$, while $E < 1$ indicates depletion.

Black carbon (BC), a product of incomplete biomass and fossil fuel combustion (Goldberg, 1985), is generally considered to be a resistant or inert SOC pool (e.g. Bornemann et al., 2008; Brodowski et al., 2007; Rethemeyer et al., 2007). For the chosen soil samples, BC was determined by mid-infrared spectroscopy (MIRS) in combination with partial least squares regression (PLSR) (Bornemann et al., 2008) at the Institute of Crop Science and Resource Conservation (INRES), Bonn, Germany. For each sample, spectra were recorded on a Bruker Tensor 27 (Bruker Optik, Germany) equipped with an automated high throughput device (Bruker HTS-XT) from 8000 to 600 cm^{-1} at a resolution of 4 cm^{-1} for five replicates. Spectra were automatically corrected for absorptions of atmospheric water and CO_2. PLSR quantification was performed using the PLS 1 algorithm developed by Martens and Naes (1989) within the OPUS QUANT software (Bruker Optik, Germany). The PLSR model was calibrated to BC determined by the BPCA (benzene polycarboxylic acids) method (Brodowski et al., 2005) on soil samples from the US, Russia and Germany (Bornemann et al., 2008). For their complete data set, Bornemann et al. (2008) received a coefficient of determination of their model of 0.63 from cross-validation results. This model was also applied to the measured spectra in this study.

5.2.4 AMS ^{14}C measurements

The ^{14}C content of bulk soil samples of every second depth increment (starting with the topsoil layer) of the six soil profiles (R1, R2, E1, E2, D1, and D2) was measured by accelerator mass spectrometry (AMS) at the AMS facility of the Institute of Particle Physics of the Swiss Federal Institute of Technology, Zurich, Switzerland. Chemical pre-treatment at the AMS laboratory included the destruction of carbonates using 0.5 M HCl at 60 °C for 24 h. For further details on sample preparation for AMS measurement we refer to Hajdas et al. (2004). ^{14}C concentrations were calculated from the measured $^{14}C/^{12}C$ ratio of the sample compared to 95% of the NIST oxalic acid standard (NIST, National Institute of Standards and Technology, Gaithersburg, USA). Both were corrected for isotopic fractionation using the simultaneously measured $^{13}C/^{12}C$ ratio. Data are expressed according to Stuiver and Polach (1977) in percent modern carbon (pMC; 100 pMC = 1950 AD). The mean precision was 0.4 pMC.

5.2.5 Estimation of deposition rates

Exemplary ^{137}Cs measurements (GSF, Neuherberg, Germany) at our test site indicated a ^{137}Cs contamination due to nuclear weapon testing in the 1950s and 1960s as well as to fallout following the Chernobyl disaster in 1986. As the intensity of ^{137}Cs contamination in both periods is unknown, and as the Chernobyl ^{137}Cs was potentially deposited during a limited number of heavy rainfall events causing spatially heterogeneous deposition by surface runoff, it was not possible to use ^{137}Cs as a tracer of soil erosion at the test site. Hence, we used ^{14}C measured by AMS as a tracer for long-term deposition.

For a simple estimate of deposition, we assumed that the ^{14}C content of bulk soil in the plough layer resembled the atmospheric ^{14}C content (Rethemeyer et al., 2005) and that the ^{14}C content of overwhelmed material at depositional sites was relatively stable. Thus, at the depositional profiles, an increased ^{14}C concentration below the plough layer due to the burial of SOC imprinted with bomb-^{14}C since 1950, whose extend in depth corresponds to the deposition height since 1950, was expected. This increase was expected to own a similar shape as the developing of the atmospheric ^{14}C concentration (Fig. 5.1), being more or less attenuated depending on the turnover rate of the buried SOC. Under the above assumptions, the maximum deposition depth since 1950 can be derived from the depth increment below which ^{14}C contents are falling below the values attributed to the bomb spike.

In a more complex approach, we reconstructed the measured depth development of ^{14}C at the depositional sites based on the bomb carbon turnover model of Harkness et al. (1986). Following this model the ^{14}C activity A_t at time t of bulk SOC or a specific SOC fraction is calculated as

$$A_t = A_{(t-1)} \cdot e^{-k} + A_i \cdot (1 - e^{-k}) - A_{(t-1)} \cdot \lambda_{14C} \quad (5.1)$$

where $A_{(t-1)}$ is the ^{14}C activity of SOC of the previous year, A_i is the input ^{14}C activity of plant residue, k the turnover rate of SOC and λ_{14C} the ^{14}C decay constant (1/8268 a^{-1}). For agricultural plants no time lag for A_i has to be accounted for, so that atmospheric ^{14}C concentrations can be used directly as input.

We modified this model by integrating a loss of radiocarbon from the plough layer at eroding profiles proportional to the erosion rate and a gain of radiocarbon at deposition profiles proportional to the deposition rate. The eroded radiocarbon from the plough layer at the erosional site is transferred to the plough layer at the depositional site and replaced by the corresponding amount from the subsoil. At the depositional site the actual plough layer is buried deeper in the soil profile. Thus, this more complex approach, accounts for a depletion of ^{14}C in the plough layer of the parent material at erosion profiles, caused by an integration of older subsoil material by tillage operations. Following this, the ^{14}C activity at time t of bulk SOC in the plough layer at erosional profiles ($A_{t/Epl}$) is calculated as

$$A_{t/Epl} = \left[A_{(t-1/Epl)} \cdot e^{-k} + A_i \cdot (1 - e^{-k}) - A_{(t-1/Epl)} \cdot \lambda_{14C} \right] \cdot (1 - f_E) + A_{sub} \cdot f_E \quad (5.2)$$

and for the plough layer at depositional profiles ($A_{t/Dpl}$) it is calculated as

$$A_{t/Dpl} = \left[A_{(t-1/Dpl)} \cdot e^{-k} + A_i \cdot (1 - e^{-k}) - A_{(t-1/Dpl)} \cdot \lambda_{14C} \right] \cdot (1 - f_D) + A_{t/Epl} \cdot f_D \quad (5.3)$$

respectively. For the buried plough layer at depositional profiles the ^{14}C activity $A_{t/Dbur}$ is calculated as

$$A_{t/Dbur} = A_{(t-1/Dpl)} \cdot e^{-k} + A_i \cdot (1 - e^{-k}) - A_{(t-1/Dpl)} \cdot \lambda_{14C} \quad (5.4)$$

$A_{(t-1/Epl,\ Dpl)}$ is the ^{14}C activity in the plough layer at erosion and depositional profiles of the previous year. A_{sub} is the ^{14}C activity of bulk SOC in the subsoil which is set to 80 pMC derived from measurements on undisturbed sites by Rethemeyer et al. (2005). The variables f_E and f_D represent the fraction of eroded and deposited soil of the plough layer. Different erosion rates (0.1, 1, and 2 mm a^{-1}) were applied to account for differences in the origin and

hence ^{14}C depletion of the deposited soil. The turnover rate *k* was set to 0.006, corresponding to the turnover rate of the passive pool of SPEROS-C (chapter 6.2.2), and was assumed to remain stable with depth and slope position. As it does not affect the depth interval of buried bomb^{14}C at deposition profiles, but just the extent of the increase, the derivation of deposition is not sensitive to the chosen turnover rate. The atmospheric ^{14}C activity was derived from Stuiver et al. (1998) for the period 1511 to 1954 and from Levin and Kromer (2004) for 1959 to 2003 (stations Vermunt and Schauinsland). The exponential decrease of the ^{14}C activity at Schauinsland was used to extrapolate to our sampling year 2009. The period between 1954 and 1959 was linearly interpolated. The deposition rate was then iteratively adjusted, so that the reconstructed ^{14}C depth distribution qualitatively fitted the measured one.

5.3 RESULTS AND DISCUSSION

5.3.1 Depth distribution of soil properties

The analysed bulk soil properties (SOC, N, C/N ratio, texture) show substantial differences in their depth distribution at the different slope positions (reference, erosion, and deposition profiles) except for the pH value (Fig. 5.3). Maximum values of bulk SOC at all observed profiles were found in the actual plough layer (0-0.15 m). Here, SOC was highest for the reference profiles and declined from depositional to erosional profiles. At erosional profiles the topsoil layer was slightly depleted in SOC corresponding to results from the analysis of SOC in a regular grid in the test site (Dlugoß et al., 2010, chapter 3). The slightly lower SOC contents in the topsoil at depositional compared to reference profiles might be caused by higher rates of heterotrophic decomposition (chapter 4) at depositional sites or by the fact that the labile SOC pool was preferentially exported out of the test site (Jacinthe et al., 2004). Additionally, the deposited material was potentially already depleted in SOC because it originated from depleted erosion sites. At the reference profiles, SOC content declined from about 1.5 wt% in the topsoil layer to 0.4 wt% in 0.5 m depth. From this depth downward SOC remained relatively stable. At the two eroding profiles, this decline of SOC with depth was much steeper, as SOC contents of approximately 0.2 wt% already occured at a depth of 0.4 m. In contrast, at depositional profiles, SOC declined slowly to still relatively high values between 0.8 and 1.0 wt% in the layers directly beyond the actual tillage depth and then remained relatively constant up to a depth of 1 m. This corresponds to the results of Berhe et al. (2008), who also analysed the depth distribution of SOC and other soil properties at different landscape positions. From 1 m depth downwards SOC decreased below 0.5 wt% at

D2, while it increased again to values of ~1.5 wt% at D1 between 1.1 and 1.4 m depth. This difference was potentially caused by groundwater influence, observed in the borehole at D1 during sampling, hampering the decomposition of SOC by the microbial biomass. Another explanation might be the re-precipitation of dissolved organic carbon that was transported into this soil depth by infiltration processes.

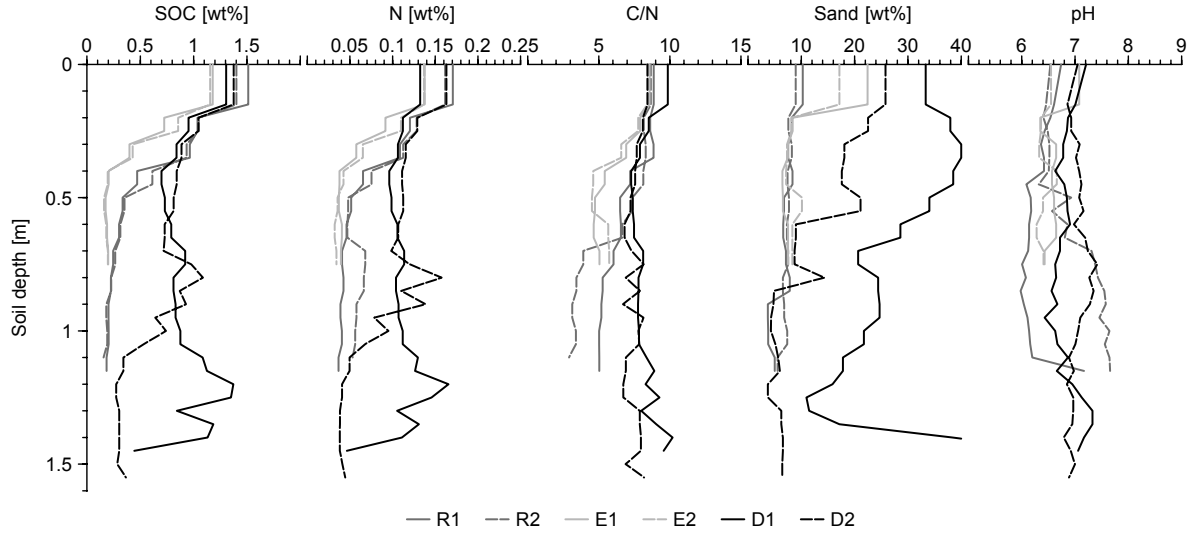

Fig. 5.3: Depth distribution of SOC, N, C/N ratio, sand content (63-2000 µm) and pH value for reference (R), erosional (E) and depositional (D) profiles.

Similar results were apparent for the depth profiles of the N content (Fig. 5.3). Highest values of approximately 0.15 wt% occurred in the topsoil layer at the profiles of each slope position. The descent of N content with increasing soil depth up to 0.5 m depth was steeper at erosion than at reference profiles, whereas values were relatively similar from 0.5 m depth downwards at the two slope positions. In contrast, at depositional profiles the N content remained at a relatively high level without substantial change to a depth of 1 m. From there on, the same phenomenon as for the SOC content was observed. At the depositional profile D2 N decreased to values of 0.05 wt% being in the same magnitude as in the subsoil layers at reference and erosional profiles, whereas at depositional profile D1 N increased again from 1 m downwards. This again might be ascribed to a reduced metabolism by soil microorganisms due to groundwater influences.

As SOC and N content had a similar behaviour concerning their depth distribution at the sampled slope positions, the same behaviour was also observed for the C/N ratio. In general, the C/N ratio is an indicator of the abundance of relatively fresh plant residues. It decreased with increasing soil depth indicating an increasing humification accompanied by the consumption of N with increasing soil depth (Berhe et al., 2008).

Sand content (63-2000 µm) at the two reference profiles amounted to approximately 10 wt% throughout the entire soil profile (Fig. 5.3). At the eroding profiles, the sand content in the plough layer was enlarged (18 to 22 wt%) indicating a preferential detachment of smaller grain sizes by water induced erosion (e.g. Basic et al., 2002), while it was again reduced to ~10 wt% in the subsoil layers. The two depositional profiles were generally enriched in sand compared to the reference and erosional profiles. At D1 the sand content was higher than 20 wt% up to a depth of 1.1 m, then also decreased to almost 12 wt% in 1.4 m depth, but then steeply increased again to more than 40 wt% below 1.4 m depth. At D2 sand content at the surface was approximately 26 wt%, and remained more than 20 wt% up to 0.4 m depth. Deeper down the soil profile the sand content corresponded with 10 wt% to that of the profiles at reference and erosional sites. The general higher abundance of sand at the two depositional profiles indicated that deposition by water is selective in nature. Small sized particles were transported out of the test site, while coarse particles were preferentially deposited especially during winter events when soils are less aggregated than during the summer (e.g. Wang et al., 2010). Water induced deposition in the test site is primarily caused by the backwater effect introduced by the adjacent grassland and was observed during some large erosion events in 2007 to 2009 especially at D1 being next to the outlet of the test site (Fig. 5.2). The general higher sand content of D1 compared to D2 indicated a higher water induced deposition at D1. However, the steep increase below 1.4 m depth could not be explained by depositional processes but might be caused by a coarser parent material as this sampling point lies closest to the Dissenbach.

The pH value that was recognised to have an impact on soil CO_2 efflux in some studies (e.g. Luo and Zhou, 2006; Reth et al., 2005b) did not exhibit any substantial differences with depth or between the different slope positions in our test site. Values ranged between 6.5 and 7.5 considering all profiles, being in the neutral region typical for Luvisols under agricultural use. Thus, the pH value could not be determined to be an important factor for soil organic carbon dynamics under the influence of soil redistribution in this study. This corresponds to the results of Berhe et al. (2008) who also did not find and significant differences in their toposequence.

5.3.2 Depth distribution of particle-size SOC fractions

As already shown for the bulk soil properties, distinct differences also existed for particle-size fractions between reference, erosional and depositional profiles (R2, E2, and D1; Fig.

5.4). The proportion of sample weight, combining mineral and organic constituents, of fraction 1 (250-2000 µm) was with ~2 wt% relatively stable throughout the entire soil profile at the reference and erosion site. In contrast, it was generally enlarged throughout the whole soil profile at the depositional site. At some depth increments it was even more than 10 wt%. This enrichment indicates a preferential deposition of this coarse sized class mainly by water induced processes. The same was true for the medium-sized fraction 2 (53-250 µm). These results correspond to the already described depth distribution of the sand content (63-2000 µm) (Fig. 5.3), comprising these two size classes. However, SOC content in fractions 1 and 2 in the depositional profile was generally depleted compared to bulk SOC (Fig. 5.4) with a mean profile-integrated enrichment factor of 0.12.

Substantial differences in SOC in fraction 1 were observed for the topsoil layer at the different slope positions, whereas below 0.2 m depth no differences were found. In contrast to the erosional and depositional profile, SOC in fraction 1 at the reference site was slightly enriched (E = 1.2) compared to bulk SOC in the topsoil. This hints to a preferential erosion of SOC in that fraction, since its proportion of sample weight was equal at the reference and the erosional site. At the depositional site, SOC in this fraction was even more reduced in the topsoil, indicating either a mineralisation of this SOC pool during transport or rapidly after deposition, contributing to an increased mineralisation at deposition sites (chapter 4), or a preferential export out the test site.

Following Amelung et al. (1998), fraction 1 represents a labile SOC pool. They observed large amounts of undecomposed plant residues in this fraction by electron microscopy and a high C/N ratio. For the reference profile at our test site, the C/N ratio in the plough layer was with a value of 19 in the same magnitude as that found by Amelung et al. (1998). This supports that this fraction represents a labile SOC pool. However, the C/N ratio was significantly reduced at our erosion profile, whereas the depositional profile was in a medium position. This again suggests a preferential erosion and deposition of this coarse-sized SOC fraction. Our results support the findings of Jacinthe et al. (2004) who found the labile pool to be preferentially transported by surface runoff, with enrichment factors of 18 to 40 in the exported sediment.

However, the observed enrichment in fraction 1 in the topsoil of our reference profile was much lower than the enrichment of 3.54 found by Amelung et al. (1998) on undisturbed sites in native grasslands of North America. On the one hand, this indicates the influence of land

use, and on the other hand, on arable land the enrichment of C in the labile SOC fraction is also highly dependent on the date of sampling. For example Jacinthe et al. (2004) reported a general increase of mineralisable C in soils during the growing season in cropped systems due to variations of C inputs. A similar result was reviewed in Christensen (1992) for the light fraction from density separation. As our soil samples were taken at the beginning of March 2009, when winter wheat plants had a height of less than 0.1 m in the test site, one can assume that the abundance of the labile SOC in fraction 1 was relatively low. Hence, a larger effect of soil erosion on that fraction can be expected, when more labile SOC is available throughout the growing period.

SOC in fraction 2 was depleted compared to bulk SOC throughout the entire soil profile at all sample locations in the test site (Fig. 5.4). In the plough layer it decreased in the order reference, erosion and deposition site, again suggesting a preferential erosion and export of SOC in that particle-size fraction. At the depositional site, a relatively stable SOC content was observed at depth, indicating that the buried SOC remained relatively stable. But one has to notice that SOC was generally very low in that fraction.

In contrast to fractions 1 and 2, the proportion of sample weight of fraction 3 (20-53 μm) was reduced throughout the whole depositional profile compared to reference and erosion profiles. There it ranged between 46 and 48 wt% (Fig. 5.4). Compared to bulk SOC, SOC in this fraction was substantially depleted for all analysed soil profiles corresponding to the results of Amelung et al. (1998). This indicates that this fraction is of less importance for SOC dynamics in our test site. According to Amelung et al. (1998), fractions 2 and 3 mainly contain altered and decomposed organic debris, but they also found unaltered plant residues in these fractions. The increasing abundance of more decomposed organic substances was reflected in our measured C/N ratios. These were reduced compared to those of fraction 1 for the reference and the depositional profile.

Considering fraction 4 (< 20 μm), the proportion of sample weight was decreased by ~10 wt% at the erosion and deposition profile up to 0.6 m depth compared to the reference one (Fig. 5.4) suggesting a preferential detachment and export of the silt and clay sized fractions. SOC in this fraction encompassed more than 80% of bulk SOC in each profile and was generally enriched by a factor of 2.4 to 2.8 at the three landscape positions. This

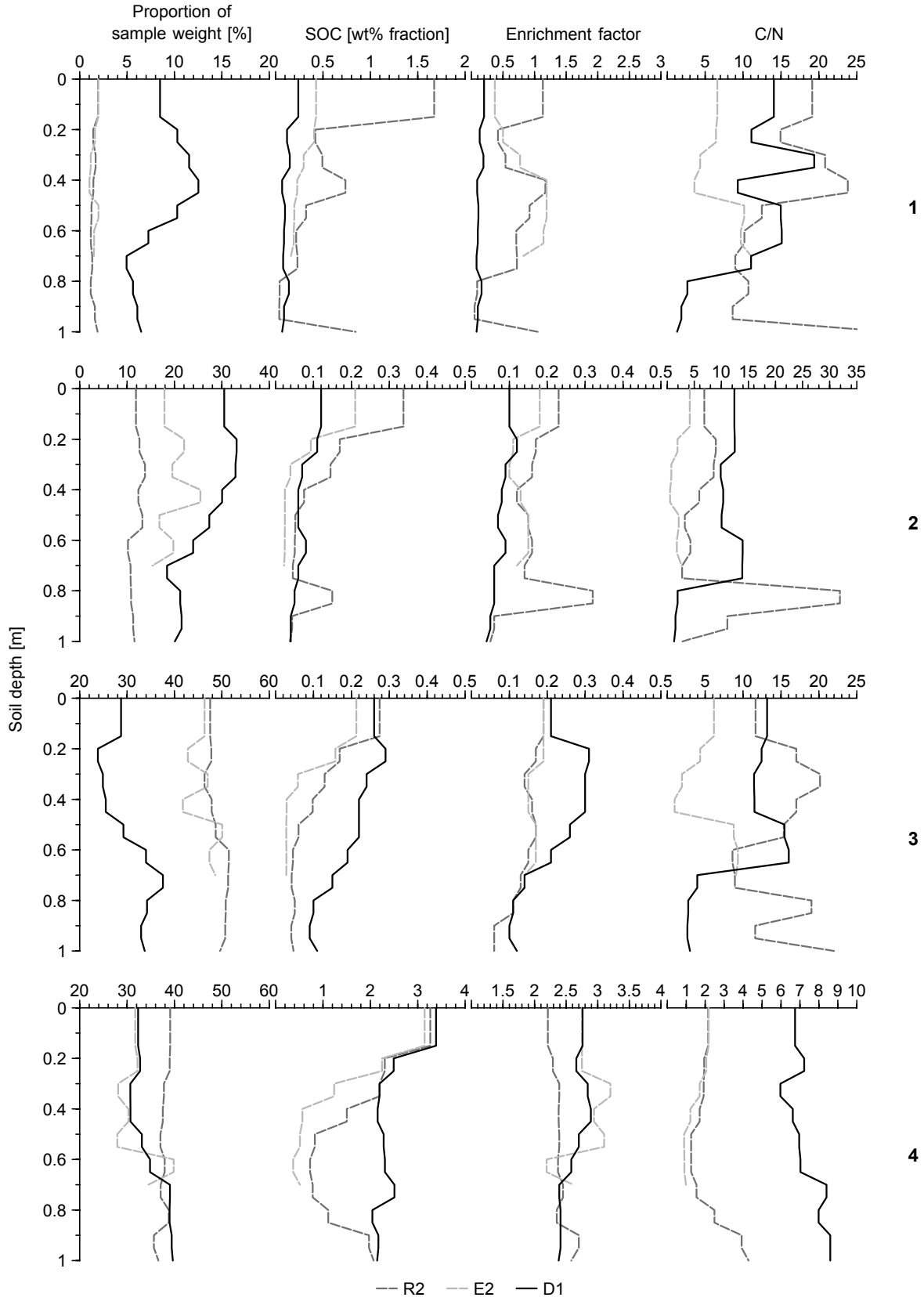

Fig. 5.4: Depth distribution of proportion of sample weight, SOC content, enrichment factor, and C/N ratio of particle-size classes at reference (R), erosional (E) and depositional (D) sites. Fraction 1 represents a coarse-sized class (250-2000 µm), fraction 2 an intermediate-sized class (53-250 µm), fraction 3 a fine-sized class (20-53 µm), and fraction 4 a very fine-sized class (< 20µm), respectively. The enrichment factor relates the SOC content of the specific fraction to bulk SOC.

enrichment was much higher than for the grassland topsoil samples investigated by Amelung et al. (1998). However, it corresponds to results summarised in Christensen (1992) where C enrichment was highest for silt and clay sized fractions. The C/N ratios were lowest for this fraction at all slope positions indicating the abundance of a large proportion of humified substances and thus a more passive quality of this SOC pool. Notably, the C/N ratio was much higher throughout the whole soil profile at the deposition site compared to the erosion and reference site indicating a stabilisation of SOC in the depositional profile.

5.3.3 Depth distribution of ^{14}C concentration

The measured ^{14}C contents of bulk soil at all sampling positions showed a decrease of ^{14}C activity with increasing soil depth (Fig. 5.5) corresponding to observed depth profiles on flat terrain (e.g. Rethemeyer et al., 2005; Torn et al., 1997). But in contrast to other results in literature (Berhe et al., 2008; Leifeld et al., 2009; Leifeld and Fuhrer, 2009; Rethemeyer et al., 2005), where ^{14}C contents in the topsoil layer resembled the atmospheric ^{14}C content at the time of sampling due to the dominance of relatively fresh plant material, ^{14}C concentrations in the topsoil layer of our profiles were less than 104.7 pMC (atmospheric ^{14}C concentration in 2009; extrapolated from the data provided by Levin and Kromer (2004)) and even less than 100 pMC. This suggests that besides fresh plant residues, substantial amounts of passive SOC with low ^{14}C contents were abundant in the plough layer of our soil profiles. This assumption was verified by measurements of BC, proven to represent an inert SOC pool (e.g. Rethemeyer et al., 2007), at three of the six soil profiles (Fig. 5.6). In the topsoil, BC contributed to 6-7% of bulk SOC at each observed profile.

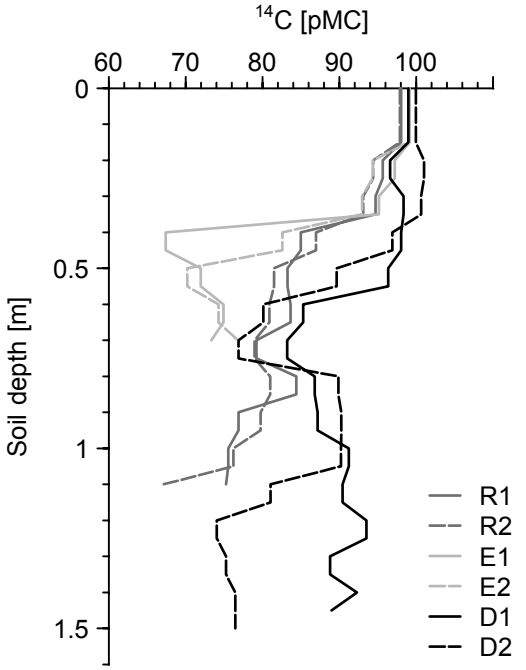

Fig. 5.5: Depth distribution of ^{14}C content at reference (R), erosional (E) and depositional (D) sites.

The general decrease of bulk ^{14}C with depth was potentially caused by a higher relative abundance of old SOC pools at depth (Rethemeyer et al., 2005). Assuming that SOC in fraction 4 represents a relatively passive SOC pool, this could not be verified for our observed profiles (Fig. 5.4). But the consideration of measured BC profiles verified this assumption (Fig. 5.6). BC increased with depth at our three sampled profiles. This increase was continuously and only slight at the reference and erosion profile reaching a value of ~15% BC in 1 m depth at the reference profile. In contrast, at the depositional profile a steep increase up to ~15% at 0.5 m depth was observed, whereas below this depth the black carbon content decreased again to values between 7 and 10%.

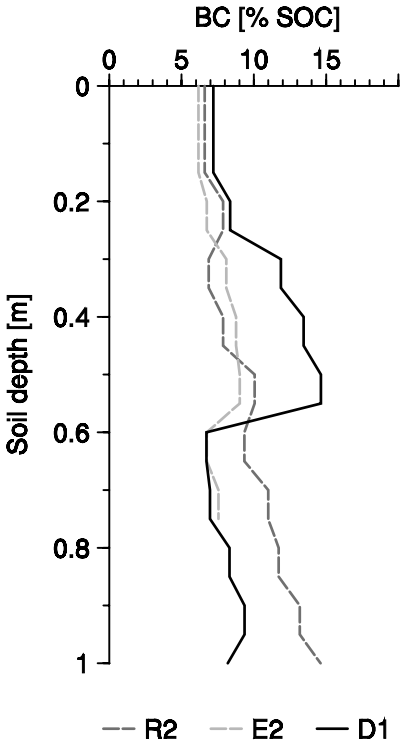

Fig. 5.6: Depth distribution of black carbon at reference (R), erosional (E) and depositional (D) sites.

The extent of the decrease of bulk radiocarbon showed obvious differences between the studied landscape positions (Fig. 5.5). As was the case for the other analysed bulk soil properties, the two profiles from the reference sites were in an intermediate position with relatively high ^{14}C contents (> 90 pMC) up to a depth of 0.35 m, followed by a steeper decline in the next depth increment. Beyond 0.50 m depth ^{14}C concentrations at the two reference profiles tended to stabilise at around 80 pMC. The depth distribution of the two erosional profiles showed a similar decrease of radiocarbon up to a depth of 0.35 m, followed by a much steeper decrease, compared to the reference profiles, to values of approximately 70 pMC at 0.50 m soil depth. This indicates a higher relative abundance of old SOC at the same depth increment at erosional compared to the reference profiles caused by the truncation of the soil profile by erosional processes and the corresponding admixture of formerly deeper subsoil material. However, this was not verified, considering SOC in fraction 4 (Fig. 5.4) as well as BC content (Fig. 5.6) at three of our observed profiles.

In the two depositional profiles, ^{14}C contents remained relatively high (> 90 pMC) up to a larger depth (up to 0.6 m) compared to the reference profiles, indicating the burial of topsoil material imprinted with bomb ^{14}C below the actual plough layer by depositional processes and

its relative stabilisation. At D1 ^{14}C remained relatively stable up to a depth of 0.6 m, whereas at D2 ^{14}C first increased with depth and then decreased again similar to the developing of atmospheric ^{14}C since the 1950s. This difference between the two depositional profiles was potentially caused by remarkably high amounts of black carbon with relatively low ^{14}C concentrations and a low turnover rate below the actual tillage depth at D1 (Fig. 5.6). Hence, we assume that BC contents are not that high at D2, but this assumption could not yet be verified. Further down the soil profile, the ^{14}C concentration at the two depositional profiles also declined to ~80 pMC at D2 and to ~86 pMC at D1 at 0.8 m depth, but then increased again to values > 90 pMC. At D2 ^{14}C concentration decreased again from 1.1 m downwards, whereas it remained relatively stable between 94 and 96 pMC up to 1.5 m depth at D1. This indicates a relatively high amount of relatively young SOC at the deeper subsoil layers of the depositional profiles that might result from the re-precipitation of infiltrated dissolved organic carbon of recent age in these layers.

5.3.4 Soil redistribution estimate

As both depositional soil profiles exhibited an increased ^{14}C concentration below the actual tillage depth (0.15 m) compared to reference sites (Fig. 5.5), they fulfilled the requirements necessary to estimate deposition height since 1950. Simply estimating deposition from the depth interval with increased ^{14}C contents below the plough layer (Fig. 5.5) revealed that deposition had not exceeded 0.45 m at D1 (deposition rate: 7.5 mm a^{-1}) and 0.3 m at D2 (deposition rate: 5 mm a^{-1}) since 1950. The reconstruction of the depth interval with increased ^{14}C concentrations at the depositional profiles resulted in similar estimates (Fig. 5.7). The measured ^{14}C depth distributions were best reproduced using a deposition rate of 7 mm a^{-1} and 5 mm a^{-1} at D1 and D2, respectively, in the modified (integration of modelled erosion and deposition rates) version of the bomb ^{14}C model of Harkness et al. (1986). The application of different erosion rates (Fig. 5.7) showed, that the depth interval of increased ^{14}C contents did not depend on the origin of the deposited soil and hence its depletion in ^{14}C, but just on the deposition rate.

However, the ^{14}C depletion of the source material from the erosion sites and the assumed turnover rate influence the extent of the ^{14}C increase in the subsoil. A high erosion rate resulted in a high depletion of ^{14}C in the topsoil layer at the two reconstructed depositional profiles (Fig. 5.7) and subsequently in a more pronounced extent of the ^{14}C increase with depth. In contrast, low erosion led to high ^{14}C contents in the topsoil of the depositional

profiles. Hence, the increase of ^{14}C with depth was less pronounced. The same was true for the assumed turnover rate in the reconstruction model. A high turnover rate led to a pronounced increase with depth, whereas the increase was only slight when assuming a low turnover rate. As the origin of the deposited material and the turnover rate did not affect the depth increment of increased ^{14}C contents, our results showed that deposition rates can easily be derived from measured ^{14}C depth distributions at depositional sites for the time period since 1950 without further knowledge of SOC dynamics.

5.4 CONCLUSION

In this chapter the depth distribution of bulk soil properties, including ^{14}C concentrations, and of specific SOC fractions (particle-size fractions and black carbon) was investigated for intensively sampled soil profiles at erosion, deposition and reference sites.

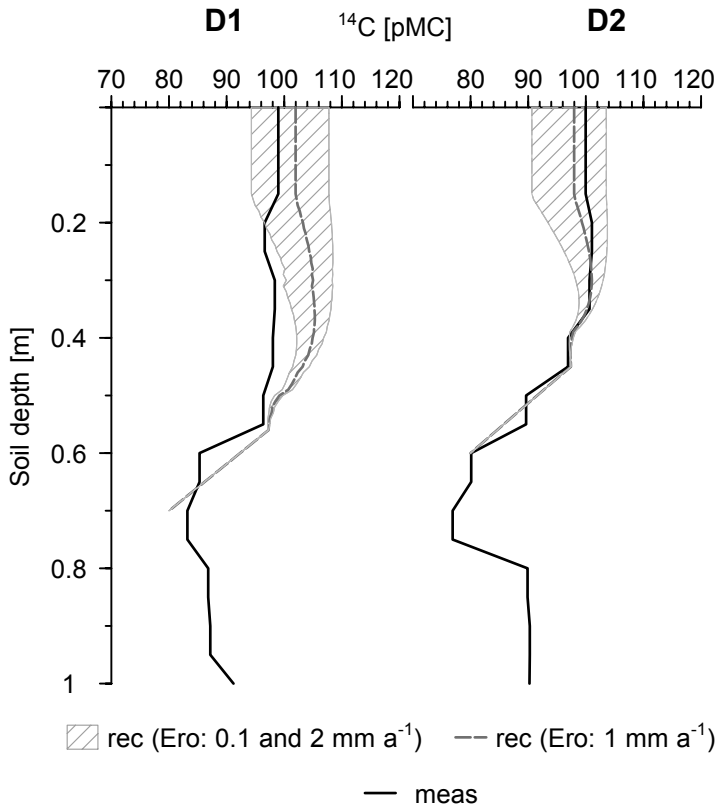

Fig. 5.7: Depth profiles of measured (meas) and reconstructed (rec) ^{14}C content at the two depositional sites D1 and D2. For the reconstructed depth distributions different erosion rates (Ero) were applied.

Soil redistribution exhibited a substantial effect on all measured bulk soil properties, except for pH value, with a general enrichment throughout the depositional profiles and a steeper decrease with depth at the erosional profiles, compared to references without erosion or deposition. Furthermore, this study also revealed an impact of soil redistribution on particle-size SOC fractions. The coarse-sized fraction, representing the labile SOC pool, was preferentially eroded. As it was also depleted in the topsoil at the depositional profile compared to the reference, it was either mineralised during transport or after deposition, or it was preferentially exported out of the test site. SOC in the intermediate-sized and fine-sized fractions was generally depleted, suggesting a minor importance of these fractions for SOC dynamics in our test site. Highest amounts of SOC were found in the very

fine-sized fraction in all soil profiles with a mean enrichment of 2.4 to 2.8 compared to bulk SOC. As this fraction contained large amounts of humified substances, proven by low C/N ratios, its relative high abundance in the subsoil of depositional sites indicated a stabilisation of SOC especially in these layers.

Although these findings were based on the analysis of only three soil profiles, our results gave first insights into the influence of soil redistribution on operational SOC fractions that substantially improve the knowledge of SOC dynamics under the impact of soil redistribution processes. Previous studies were concerned with different SOC pools under a conceptual point of view only.

Since our results also exhibited substantial differences in the depth distribution of ^{14}C at different slope positions, the usefulness of AMS ^{14}C measurements to study SOC dynamics under the impact of soil erosion was proven. The enrichment of bomb ^{14}C below the actual plough layer at depositional profiles was used to derive estimates of deposition since 1950. Results indicated that ^{14}C can be used to derive deposition rates in areas, where the use of ^{137}Cs as a tracer for soil redistribution is not possible, without further knowledge of the origin of the deposited material or its turnover. But it is important to measure the ^{14}C concentration in a fine resolution with respect to the amount of depth increments, to be able to precisely locate the depth in which ^{14}C concentrations start to decrease below values attributable to the bomb curve. Besides AMS ^{14}C measurements of bulk soil, ^{14}C concentrations of specific SOC fractions might further advance future research of the impact of agricultural soil erosion on SOC dynamics.

6 MODEL BASED ANALYSIS OF LATERAL AND VERTICAL SOIL C FLUXES INDUCED BY SOIL REDISTRIBUTION PROCESSES*

6.1 INTRODUCTION

On sloped arable land, SOC stocks and soil-atmosphere C fluxes are highly spatially variable, as their interaction with soil redistribution is manifold and highly complex. Thus, the application of coupled and spatially explicit SOC and soil redistribution models is useful for spatially integrated approaches that link sediment and C budgets at erosional and depositional sites across the landscape (e.g. Polyakov and Lal, 2004; Van Oost et al., 2005a; Yadav and Malanson, 2009).

Several approaches of combined modelling of soil redistribution and soil carbon cycling have been presented in literature, but mostly approaches were restricted to single points at different landscape positions using erosion and/or deposition rates derived either from measurements or separate erosion modelling (e.g. Gregorich et al., 1998; Harden et al., 1999; Pennock and Frick, 2001). The simulation of SOC dynamics in these studies relied on the CENTURY (Parton et al., 1987) model that was restricted to the simulation of the topsoil layer in its early versions. But as significant amounts of SOC are stored in deeper soil layers especially at depositional sites, a depth explicit model must be applied for systems including soil redistribution. Thus, Liu et al. (2003) used a modified version of CENTURY, the EDCM (Erosion-Deposition-Carbon-Model), and Billings et al. (2010) developed the spread-sheet model SOrCERO (Soil Organic Carbon, Erosion, Replacement, and Oxidation). Both models simulate several soil layers with explicit controls on the depth variation of SOC formation and

* Based on: Dlugoß, V., P. Fiener, K. Van Oost, and K. Schneider. Model based analysis of lateral and vertical soil C fluxes induced by soil redistribution processes in a small agricultural watershed. Submitted to Earth Surface Processes and Landforms.

decomposition. However, these models fail to include spatial integration as they are also limited to single soil profiles at different slope positions.

In recent advances, models allow for an improved integrated spatial analysis of the impact of soil redistribution on SOC dynamics at the catchment scale by combining spatially explicit geomorphic models, including soil redistribution, with models of SOC dynamics (Rosenbloom et al., 2001; Van Oost et al., 2005a; Yadav and Malanson, 2009; Yoo et al., 2005). While the models presented by Rosenbloom et al. (2001) and Yoo et al. (2005) focus on the long-term hillslope response due to diffusive geomorphic processes on grasslands, the SPEROS-C (Van Oost et al., 2005a) and the combined CENTURY and GeoWEPP (Renschler, 2003) model presented by Yadav and Malanson (2009) focus on contemporary soil redistribution on arable land. They focus on the catchment scale C balance and allow for an integrated spatial analysis of the impact of soil erosion on SOC at eroding sites, the burial of SOC at depositional sites, and the fate of eroded C during transport in terrestrial ecosystems. Both models consider different soil layers and explicitly simulate changing controls on C input and decomposition with depth. The only model that also considers soil redistribution by tillage operations, a phenomenon that has been recognised in soil erosion research since the 1990s (e.g. Govers et al., 1994; Lindstrom et al., 1992), is the model SPEROS-C (Van Oost et al., 2005a). A consideration of tillage erosion is obligatory as it can be more important than water erosion on sloped arable fields and as it substantially changes soil redistribution patterns (Govers et al., 1994).

SPEROS-C (Van Oost et al., 2005a) combines the Introductory Carbon Balance Model (ICBM, Andrén and Kätterer, 1997) with the soil erosion model SPEROS (Van Oost et al., 2003). Its main characteristics are the three-dimensional representation of the landscape and its dynamic evolution of the soil and SOC profile under erosion and deposition. The current version of the model represents the upper 1 m soil profile using four depth layers (Van Oost et al., 2009). Since previous studies proved the suitability of SPEROS-C to simulate soil carbon dynamics for the last 50 years in small agricultural catchments (~4 ha) under conventional tillage in Denmark and Great Britain (Van Oost et al., 2005a), we chose this model for our study. In our test site, a change of land management occurred in the 1980s, providing the opportunity to analyse the interaction of soil redistribution and SOC dynamics introduced by changes in land management. Although land management is known to have a large effect on both SOC stocks (e.g. Eynard et al., 2005; Gregorich et al., 1998; Jarecki et al., 2005) and soil erosion rates (expressed, e.g. in the crop management factor of the Universal Soil Loss

Equation (USLE) (Wischmeier and Smith, 1978)) on arable land, these processes were mostly studied in isolation.

Against this background, the objectives of this chapter are:

(i) To modify the SPEROS-C model for analysing the relative contribution of lateral and vertical soil C fluxes induced by soil redistribution processes in a small arable catchment in Germany,
(ii) to explore the integrated effect of changes in land management on soil redistribution and on the soil carbon balance, and
(iii) to investigate the sensitivity of the simulated C fluxes to uncertainties in model inputs.

6.2 Materials and Methods

6.2.1 Field measurements

Spatially distributed soil properties

In 2006 and 2007, an intensive soil sampling campaign was carried out in the test site. Soil samples were taken in a regular 17 by 17 m grid (n = 144) (Fig. 3.1) at three depths (I: 0-0.25; II: 0.25-0.50 m; III: 0.50-0.90 m) (for a further description of soil sampling and sample analysis refer to chapter 3.2.1). For each of these samples, SOC was determined with a CNS elemental analyser (vario EL, Elementar, Germany) and soil texture was determined by the combined sieve and pipette method (Deutsches Institut für Normung, 2002). Soil bulk density was measured on 15 of these sampling points by weighing the soil samples after oven drying at 105°C (volumetric core method).

Spatially distributed SOC inventories (n = 1030) were interpolated from the measured data by means of geostatistics for each soil layer (Dlugoß et al., 2010; chapter 3). In each layer, the best interpolation result (produced by ordinary kriging in soil layer I and by regression kriging in layers II and III) was taken as validation data for the modelled SOC distributions. Soil texture and soil bulk density data were used for model implementation.

Runoff, sediment and carbon delivery

In March 2006, a San Dimas flume (Grant and Dawson, 1997; Kilpatrick and Schneider, 1983) was installed at the outlet of the Dissenbach catchment (Fig. 2.1). Here, precipitation

and water-level are measured continuously, and runoff is derived by a calibrated stage-discharge equation (Grant and Dawson, 1997; Kilpatrick and Schneider, 1983). An automatic sampler (AWS, EcoTech, Germany) continuously takes water samples once a day as well as event-driven samples, i.e., when a critical water-level, which is varied seasonally, is exceeded. The sediment content of the sampled water is determined by filling two aliquots of 100 ml into beakers after carefully shaking the sample bottles for two minutes. The samples are then oven-dried at 105 °C and weighed. If sediment content is approximately > 2 g l^{-1}, its SOC content is determined by dry combustion using a CNS elemental analyser (vario EL, Elementar, Germany).

Based on these sediment and SOC samples, the sediment and carbon delivery of the Dissenbach catchment was calculated for the years 2007 to 2009. However, it must be noted that SOC delivery could just be determined for large erosion events constituting ~35% of the total sediment yield in 2007 and 2008 and ~54% in 2009, respectively. Hence, we estimated total SOC delivery assuming that the average carbon content in sediment during large events can be applied to total sediment output, even if this seems to be a conservative estimate (Wang et al., 2010). Based on these data, the average enrichment of C in sediments, as compared to the parent soil material, was calculated using topsoil SOC information from the entire Dissenbach catchment derived from a digital soil map provided by the Geological Survey of North-Rhine Westphalia.

The data measured at the Dissenbach outlet were used to analyse the results from erosion and SOC modelling at the Heiderhof sub-catchment. The focus was the comparison of the overall erosion on both scales and especially the enrichment of C in delivered sediment.

6.2.2 Model description SPEROS-C

Soil redistribution

The soil redistribution component of SPEROS-C consists of a water and a tillage erosion component that can be run separately. In order to apply the model at our test site, we replaced the original calculation of potential water erosion with the one of the WaTEM model (Van Oost et al., 2000; Van Rompaey et al., 2001). The RUSLE-type erosion component allows (i) to account for a change in land management during the simulation period, and (ii) to avoid a site-specific calibration necessary for the original water erosion component (Van Oost et al., 2003; 2005a) since the use of tracer data like ^{137}Cs was not possible in our test site.

To apply the RUSLE in a two dimensional landscape, the slope length factor was replaced in WaTEM/SEDEM using the unit contributing area following Desmet and Govers (1996a). To account for sediment transport and deposition, sediment transport is calculated using the flux decomposition approach by Desmet and Govers (1996b). Deposition is controlled by the local transport capacity *TC* (kg m^{-1} a^{-1}) calculated for each grid cell following Verstraeten et al. (2006):

$$TC = ktc \cdot R \cdot K \cdot (LS - 4.1s^{0.8}) \quad (6.1)$$

where *ktc* is the transport capacity coefficient (m), *s* is the slope (m m^{-1}) and R, K, L and S are the RUSLE factors. R is the rainfall erosivity factor (N h^{-1} a^{-1}), K the soil erodibility factor (kg h m^{-2} N^{-1}), L the slope length factor (-), and S the slope gradient factor (-).

If the sediment inflow plus the local potential erosion calculated by RUSLE at a grid cell exceeds the transport capacity, net deposition occurs. The amount of material leaving this grid cell then equals the transport capacity. The transport capacity coefficient *ktc* depends on land use. It was originally calibrated for a 20 m grid resolution based upon data from 21 catchments in the Belgian Loess Belt, yielding 75 m for non-erodible surfaces (forest and pasture) and 250 m for arable land use (Verstraeten et al., 2006). Different grid sizes require a re-calibration of the transport capacity coefficients. Van Oost et al. (2003) found an optimum value of 150 m for cropland for a 5 m grid resolution.

On tilled fields, runoff direction is affected by tillage induced oriented roughness, causing runoff to flow along tillage instead of topographic direction (Desmet and Govers, 1997; Souchère et al., 1998; Takken et al., 1999). To account for a resulting change in runoff and erosion patterns, the logistic regression model developed by Takken et al. (2001) was implemented in the calculation of the contributing area as well as that of the water induced sediment and SOC routing. The model includes the slope *s* (%), the angle between tillage orientation and aspect direction α (°) and the oriented roughness *Ro* (cm) and is applied to calculate the probability *p* of runoff flowing in topographic direction:

$$\text{logit}(p) = -5.92 + 0.133 \cdot s + 0.102 \cdot \alpha - 0.417 \cdot R_O \quad (6.2)$$

The flow direction is predicted to be topographic if the calculated probability is greater than 0.5, and flow is predicted to be in tillage direction if $p < 0.5$.

Tillage erosion is calculated following the diffusion approach of Govers et al. (1994) (Eq. 3.4 in chapter 3.2.3).

In previous studies (e.g. Poesen et al., 2001; Ruysschaert et al., 2004; 2005), the importance of soil loss due to crop harvesting of root crops has become apparent. According to Auerswald (2006), average losses of soil adhering to sugar beet range from 5 to 8 t ha^{-1} a^{-1} in Germany with large annual fluctuations. Since this is in the same dimension as soil losses caused by water or tillage erosion and sugar beet provides 33% of the crop rotation in the test site, harvest erosion was also considered for C balancing in this study. It was assumed, that E_{har} is spatially uniform and that the SOC content of the adhering soil equals the SOC content of the plough layer. Thus, the amount of SOC removed from the plough layer (SOC_{loss}, (g m^{-2})) is proportional to the ratio between harvest erosion E_{har} (m) and the depth of the plough layer PD (m):

$$SOC_{loss} = \frac{E_{har}}{PD} \cdot SOC_{plough} \tag{6.3}$$

Assuming a mean harvest erosion of ~7 t ha^{-1} a^{-1} found for North Rhine-Westphalia (1980-2000) (Auerswald, 2006), E_{har} was set to 5.6×10^{-4} m for each sugar beet year in the model.

Soil organic carbon dynamics

The Introductory Carbon Balance Model (ICBM, Andrén and Kätterer (1997)) describes SOC dynamics using two SOC pools, a so-called young pool, mainly consisting of undecomposed plant residues and roots, and a so-called old pool, comprising the slow and passive pool. Four carbon fluxes alter the pools: (i) The C input from plants to soil, (ii) the mineralisation from the young and (iii) the old pool, and (iv) the humification, i.e. transformation from the young to the old pool. The dynamics of the two SOC pools are described as:

$$\frac{\Delta Y}{\Delta t} = i - k_Y r Y \tag{6.4}$$

$$\frac{\Delta O}{\Delta t} = h_{c/m} k_Y r Y - k_O O \tag{6.5}$$

where Y and O are the young and the old SOC pool (g C m^{-2}) in each soil layer, respectively, and k_Y and k_O are the corresponding turnover rates (a^{-1}). The C input (g C m^{-2} a^{-1}) is i, $h_{c/m}$ is the humification coefficient (-), and r is a climate coefficient (-), which is assumed to equally affect the decomposition of the young and old pool. The humification coefficient depends on the source of C input and on clay content cl (%):

$$h_{c/m} = \frac{i_c h_c + i_m h_m}{i} \cdot e^{0.0112(cl-36.5)} \quad (6.6)$$

$$i = i_c + i_m \quad (6.7)$$

where i_c are inputs of C from crop residues, roots, and rhizodeposition and i_m are inputs from organic manure (g C m^{-2} a^{-1}), while h_c and h_m are the corresponding humification coefficients. The climate effect accounted for by r primarily depends on mean annual air temperature T (°C) that is assumed to be spatially uniform. The spatially variable relative *wetness* value derived from the wetness index *WI* (Beven and Kirkby, 1979) was integrated into the calculation of the climate effect:

$$r = 2.07^{\frac{T-5.4}{10}} \cdot \frac{1}{wetness} \quad (6.8)$$

The wetness index is highest at depositional sites in our test site (Fig. 3.3). Its integration thus accounts for a reduced SOC mineralisation under wetter conditions often found in deposits (e.g. Berhe et al., 2007). Since the Q_{10} value of 2.07 (Kätterer et al., 1998) did not differ significantly from the mean Q_{10} value derived from measured soil respiration and soil temperature data in our test site (chapter 4), it was not changed from the original model implementation. Also its dependency on temperature, based on the mean annual air temperature of 5.4°C for the test site in Sweden, was adopted. In that study, Andrén and Kätterer (1997) estimated the turnover rates for the plough layer that were set to k_Y = 0.8 a^{-1} and k_O = 0.006 a^{-1}. The humification coefficients were set to $h_c = 0.125$ and $h_m = 0.31$, respectively.

The turnover rates of the young and the old pool exponentially decrease with increasing soil depth following Rosenbloom et al. (2001):

$$k_{Y/Oz} = k_{Y/Os} \cdot e^{(-u \cdot z)} \quad (6.9)$$

where $k_{Y/Oz}$ and $k_{Y/Os}$ are the turnover rates (a^{-1}) at depth z and at the soil surface, respectively. The exponent u needs to be calibrated in an inverse modelling approach. The C input by roots into the soil profile is modelled by an exponential root density function (Van Oost et al., 2005a). Additionally, the C input by plant residues, cover crops and/or organic manure is specified.

SOC redistribution and profile evolution

SOC erosion from the topsoil layer for the young and the old pool ($C_{ero,Y/O}$) is modelled using the results of the water and tillage erosion component as well as those from the soil loss due to crop harvesting routine. It is calculated as

$$C_{ero,Y/O} = SOC_{plough,Y/O} \cdot \frac{M_{ero}}{M_{plough}} \tag{6.10}$$

with $SOC_{plough,Y/O}$ being the amount of SOC in the plough layer (g), M_{ero} being the mass of eroded soil (g) and M_{plough} being the total mass of the plough layer (g).

At erosion sites, a fraction of SOC from the first subsoil layer proportional to the erosion height is incorporated into the plough layer, since plough depth is maintained during the whole simulation period. Accordingly, SOC from the second subsoil layer is assigned to the first subsoil layer, etc. At depositional sites, the deposition height is used to simulate a change in soil depth. Since plough depth is maintained, a fraction of the SOC proportional to the deposition height is transferred to a buried plough layer that is dynamic and equals the total deposition height. The subsoil layers are also buried in the soil profile.

Since the transport of SOC during water erosion may result in an additional mineralisation of SOC and thus in a source of atmospheric C (Lal, 2003a), a fixed fraction of the C transported in runoff ($C_{ero,wat}$) is assumed to be mineralised. Thus, the C loss caused by mineralisation of SOC in soil eroded by water (C_{oxi}) (g C m^{-2} a^{-1}) can be calculated as

$$C_{oxi} = f_{oxi} \cdot C_{ero,wat} \tag{6.11}$$

with f_{oxi} being in the range of 0 to 1. A possible enrichment of C in transported sediment is not accounted for.

6.2.3 Model implementation

The simulation period was set from 1950, when arable agriculture in the region was intensified due to the introduction of more powerful machinery, to 2007, when SOC inventory measurements were carried out. During this period, a constant crop rotation of sugar beet, winter wheat and winter barley was assumed, although this has been only explicitly documented by the farmer since the 1970s. In 1980, management changed from conventional to conservation agriculture accompanied by the introduction of chisel instead of mouldboard

ploughing and a cover crop after sugar beet. The model operates in a yearly time step, and the spatial resolution is 6.25 × 6.25 m.

Soil redistribution

The RUSLE factors were determined as follows:

i. A K factor map was derived from a digital soil map (scaled 1:50000) provided by the Geological Survey of North Rhine-Westphalia, where it was calculated following Deutsches Institut für Normung (2005). It ranges between 0.058 and 0.061 kg h m^{-2} N^{-1}.
ii. The annual R factor and its seasonality were calculated using precipitation data (1975-2007; 5 min temporal resolution) from the precipitation station Bockeroth situated about 2.5 km east of the test site (151 m a.s.l.) (Fig. 2.1) provided by the Landesamt für Natur, Umwelt und Verbraucherschutz Nordrhein-Westfalen following an approach of Schwertmann et al. (1987). The annual R factor is 88.96 N h^{-1} a^{-1} with a pronounced seasonality owning highest values in May and June.
iii. The calculation of the C factor for the crop rotation in the test site was also based on Schwertmann et al. (1987). Regional sowing and harvesting dates were taken from meteorological yearbooks (average of 1995 to 2004) provided by the German Weather Service. The calculated C factor for the modelled period of conventional tillage amounts to 0.142, and for the period of conservation tillage to 0.028, respectively.
iv. The L factor is replaced by the unit contributing area calculated following(Desmet and Govers, 1996a) Desmet and Govers (1996a), and the S factor is calculated following McCool et al. (1987). Both are simulated throughout the model run based on a digital elevation model with a 6.25 × 6.25 m grid. The DEM was interpolated from Lidar data (2–3 m point distance) provided by the Landesvermessungsamt North Rhine-Westphalia using ordinary kriging (spherical model; nugget: 0.6; sill: 46.2; range: 237 m) within the Geostatistical Analyst of the Geographical Information System ArcGis 9.2 (ESRI Inc., USA).
v. Since contour ploughing is carried out in the test site, a P factor map is calculated during the model run accounting for the local slope of each grid cell following Schwertmann et al. (1987). The P factor in our test site ranges between 0.5 and 0.7.

As no spatially distributed measured soil redistribution data were available for our test site, the transport capacity coefficient (Eq. 6.1) could not be calibrated accordingly. Thus, it was reduced to the optimum value of 150 m derived for a 5 m grid in Van Oost et al. (2003).

Takken et al. (2001) derived characteristic measures of oriented roughness per crop type in a three-year monitoring period of an agricultural catchment in the Belgian Loess Belt. Following this, the oriented roughness (Eq. 6.2) for winter wheat and winter barley was set to 2 cm and that for sugar beet to 3 cm. The tillage transport coefficient (Eq. 3.4) was set to 600 kg m^{-1} a^{-1} from 1950 up to 1979 when tillage depth by mouldboard ploughing was 0.25 m, and from 1980 onwards it was set to 400 kg m^{-1} a^{-1}, when tillage depth was reduced to 0.15 m by cultivator tillage. For both time periods, 2-3 tillage operations per year were assumed. This results in an average of 500 kg m^{-1} a^{-1} for the whole simulation period corresponding to average tillage erosion intensities over the last 35-45 years derived for various sites across Europe (Van Oost and Govers, 2006).

Soil organic carbon

The C input from plant to soil at the time of harvest is estimated from yield observation in each simulation year. Since yield data were not explicitly available for the test site, data for winter wheat and winter barley were adopted from the agricultural research station Gut Frankenforst (Universität Bonn; approximately 1.5 km south-east of the test site), which have been available since 1965. The data represent mean values of 2 to 10 fields in each year. Since sugar beet is not cultivated by the research station, corresponding yield data were taken from statistical data of IT NRW (Information und Technik, Nord-Rhein Westfalen) for the administrative unit Rhein-Sieg Kreis, which have been available from 1950 until today. The gap from 1950 to 1965 for winter cereals was filled by regression equations between the Frankenforst and the Rhein-Sieg Kreis data with Pearson correlation coefficients of 0.88 for winter wheat and 0.82 for winter barley, respectively.

The parameterisation of the C input from yield data for cereal crops was adopted from Van Oost et al (2005b), where the proportion of carbon allocated to roots is assumed to constitute 30% of total carbon assimilation. The grain dry matter yield is assumed to constitute 45% of above ground dry matter, and stubble and other losses of above ground crop residues is set to 15% of above ground biomass. Following this, the root dry matter corresponds to 95% of grain dry matter, and stubble dry matter corresponds to 33% of grain dry matter. To more explicitly consider sugar beet, which contributes 33% to the crop rotation in the test site, the model was extended by the C input for sugar beet calculated every third year, in which C input by sugar beet leaves can be specified. Following Draycott (2006), the proportion of fibrous roots and storage roots of total dry matter weight before harvest was set to 3% and 66.5%, respectively. Thus, the dry matter content of fibrous roots corresponds to

4.5% of the storage root and above ground biomass corresponds to 45% of the storage root. When specifying mustard as a cover crop before sugar beet, the C input by this cover crop is added to the C input in each sugar beet year. Following Gan et al. (2009), mustard roots contribute approximately 23% to total dry matter content, which was set to 40 dt/ha (Aigner, 1998; Frede and Dabbert, 1999). The carbon content in dry matter for all crops was set to 45%. As the estimation of C input is derived from relationships at harvesting date, it does not consider carbon released by rhizodeposition (including exudates) (Hütsch et al., 2002) during crop growth. Following Ludwig et al. (2007) this input was set to 50% of the C input by crop and root residues for cereals and to 35% of the C input by crop and root residues for sugar beet.

The soil carbon dynamics model needed to be calibrated in an inverse modelling approach without running the soil redistribution component for the described land management history. Modelled SOC inventories in each soil layer were compared with measured ones at reference sites (n = 65) chosen from earlier erosion modelling in the test site (Dlugoß et al. 2010; chapter 3). In several set-up runs, the C input by manure and roots as well as the decline of the turnover rate with depth were iteratively adjusted so that the modelled SOC inventories fit the measured ones. Mean values at reference sites could be well met in the first and second soil layer, but a higher deviation, still within the range of ± one standard deviation, was achieved for the deepest soil layer (Fig. 6.1). Adjustments resulted in C input by manure of 10 g C m^{-2} and 60% of roots being in the topsoil layer. The exponent for the reduction of turnover rate with depth *u* (Eq. (6.9) was set to 2.8, resulting in a mean residence time of ~10 years for the young and ~1360 years for the old SOC pool in the deepest soil layer.

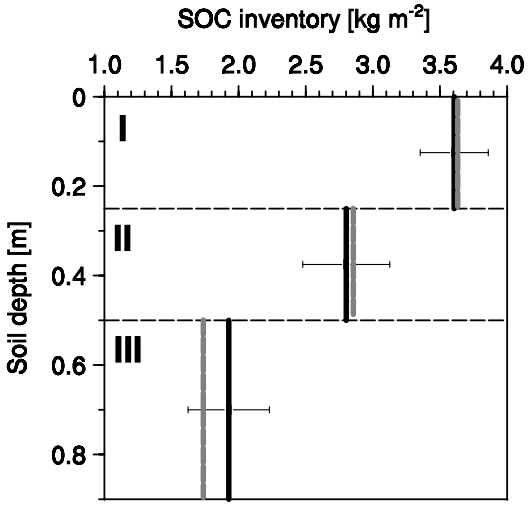

Fig. 6.1: SOC inventories at reference sites (sites without erosion or deposition) for three soil layers (I: 0-0.25 m; II: 0.25-0.50 m; III: 0.50-0.90 m). The black solid line represents the measured arithmetic mean at reference sites (n = 65) ± one standard deviation (error bar) for each soil layer. The grey dashed line represents the corresponding modelled value resulting from calibration in an inverse modelling approach.

An average, spatially uniform soil bulk density of 1.31 g cm^{-3} in the plough layer and 1.53 g cm^{-3} for the two subsoil layers was implemented. The clay content influencing the humification coefficient was also set as a spatially uniform value of 19% in each soil layer since spatial variability was not very distinct.

At the start of the simulation, a spatially uniform SOC start value at steady state was assumed for each soil layer, since no data of the initial SOC distribution were available. The results of Van Oost et al. (2005a) showed that neglecting the pre-existing erosion history leads to conservative estimations of the erosion induced vertical C fluxes. This model run is referred to as reference run.

6.2.4 Sensitivity analysis

A sensitivity analysis was performed to test the effects of the following uncertainties and assumptions on the mean lateral and vertical C fluxes resulting from soil redistribution processes compared to the reference run.

i. To test if the modelled C fluxes are sensitive to the assumption of a spatially uniform SOC value at steady state at the start of the simulation, the simulation period was enhanced for 100 years meaning that pre-existing land management and corresponding erosional processes were considered. A relatively low soil redistribution rate (C factor = 0.02; ktil = 100) derived from a crop rotation solely consisting of small grains and non-mechanised agriculture and a constant yield were assumed for the period before 1950.
ii. As C inputs to the soil rely on yield data not directly measured at our test site and on relatively simple average relations between yield and C input, we varied the C input by adding and subtracting up to 50% of the estimated C input in each simulation year without recalibrating the soil organic carbon dynamics model.
iii. To account for the fact that modelled soil erosion rates could not be validated against an independent spatially distributed erosion data set, the total soil redistribution rate was changed by varying the tillage transport coefficient and the potential water erosion calculated by RUSLE by up to +/- 50% for the two simulation periods. Potential water erosion was changed by changing the USLE C factor, since the calculation of this factor is most tentative and since it is related to land management.
iv. As USLE based model approaches assume a constant yearly erosion rate as long as the USLE factors do not change, the model cannot take into account the fact that soil

erosion by water is not a continuous process, but is dominated by a few large events, especially at the catchment scale (Edwards and Owens, 1991; Fiener and Auerswald, 2007). In order to explore the importance of temporal variability of water erosion, we performed a simulation where soil erosion by water occurred every 10 simulation years with a 10-fold magnitude of the USLE potential erosion.

For each sensitivity model run, the C fluxes of the two periods (conventional and conservation tillage) were analysed separately to consider possible effects between different land management and the effect of a change from conventional to conservation agriculture.

6.3 Results and Discussion

6.3.1 Soil redistribution

The map of modelled cumulative total erosion (Fig. 6.2), comprising water and tillage induced soil redistribution as well as soil loss due to crop harvesting simulated every third year, shows that the test site can be divided into two parts with regards to the intensity of the erosional processes. The western part of the test site with slopes between 1 and 2° is dominated by relatively low erosion and deposition rates between -0.05 and 0.05 m per 58 years. In contrast, in the steeper eastern part (slopes up to 9.5°) a spatially distinct pattern of erosion and deposition sites is observed.

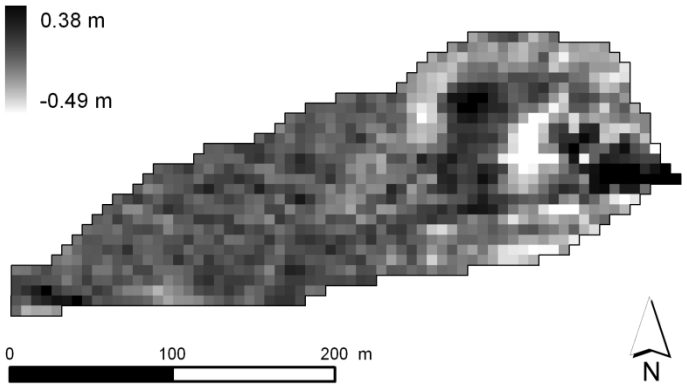

Fig. 6.2: Map of modelled cumulative total erosion rate [m 58 a^{-1}]; positive values indicate deposition, and negative values indicate erosion.

Highest cumulative total erosion rates (> 0.2 m per 58 years) mainly caused by water erosion occur in the small thalweg area. As no deposition by water was modelled within the test site, the colluvial area (deposition > 0.2 m per 58 years) near the outlet of the test site was formed by tillage induced deposition. Highest erosion rates caused by tillage operations are located at the shoulders of the north-south-facing slope in the eastern part of the test site. This corresponds to other results in literature (e.g. Govers et al., 1994), where tillage induced erosion generally occurs on convexities and on the down slope sides of field boundaries,

whereas deposition caused by tillage processes occurs on concavities and on the upslope sides of field boundaries.

Due to the change from conventional to conservation agriculture in 1980, a distinct reduction of water and tillage erosion was modelled in the second simulation period. Mean net water erosion dropped from 0.66 to 0.13 mm a^{-1} for 1950-1979 and 1980-2007, while the net tillage erosion was reduced from 0.79 to 0.55 mm a^{-1} (Tab. 6.1). While the individual spatial patterns of both erosion processes remained stable for the two simulation periods, the spatial pattern of total erosion combining both processes changed, leading to an increase of the depositional area from 26% to 39% within the test site (Tab. 6.1).

Tab. 6.1: Statistics of modelled water (E_{wat}), tillage (E_{til}) and total erosion (E_{tot}) within the test site (n = 1030) for the modelled period of conventional (1950-1979) and conservation tillage (1980-2007), as well as for the whole simulation period (1950-2007) differentiated into erosional (Ero) and depositional (Depo) sites.

		Soil erosion [mm a^{-1}]					
		Ewat		Etil		Etot	
		Ero	Depo	Ero	Depo	Ero	Depo
1950-1979	Mean	0.66	---	0.79	1.11	1.11	0.68
	SD‡	1.37	---	0.65	1.55	1.23	0.96
	Max	16.88	---	3.17	10.25	14.32	7.30
	n	1030	0	588	442	761	269
1980-2007	Mean	0.13	---	0.52	0.74	0.57	0.62
	SD	0.27	---	0.43	1.03	0.47	0.86
	Max	3.33	---	2.11	6.83	2.38	6.25
	n	1030	0	588	442	632	398
1950-2007	Mean	0.41	---	0.66	0.93	0.85	0.61
	SD	0.84	---	0.54	0.96	0.82	0.87
	Max	10.33	---	2.66	7.30	8.18	6.79
	n	1030	0	588	442	700	330

‡ SD: standard deviation
n: number of grid cells in the test site

Similar to the two test sites in Van Oost et al. (2005), erosion by tillage was the dominant process, accounting for ~71% in the phase of conventional tillage and ~91% in the phase of conservation tillage, respectively. Since SPEROS-C is not capable of modelling the backwater effect near the outlet of the test site caused by a change in land use, no deposition by water was modelled within our test site. Sediment transport was also not limited by transport capacity. Thus all water eroded sediment is exported out of the test site. In contrast, sediment eroded by tillage operations was completely deposited within the same field, i.e., the area weighted mean of erosion and deposition equals zero.

The modelled cumulative deposition rates at two profiles in the colluvial area near the outlet of the test site (D1 and D2 (Fig. 5.2); 6.5 mm a^{-1} and 2.3 mm a^{-1}) are in qualitative agreement with measured radiocarbon and corresponding SOC and sand contents (Fig. 5.3 and Fig. 5.5). Measured ^{14}C depth distributions indicate that deposition has not exceeded 0.45 m at D1 and 0.30 m at D2 since 1950. Iteratively varying the deposition rate in a modified bomb ^{14}C model of Harkness et al. (1986) to reconstruct the measured ^{14}C depth distribution results in a deposition rate of 7 mm a^{-1} at D1 and 5 mm a^{-1} at D2 (chapter 5.3.4).

Thus, SPEROS-C slightly underestimated deposition at both profiles. This might be caused by the fact that no deposition by water was simulated.

6.3.2 Soil organic carbon stocks

In general, measured SOC inventory patterns in each soil layer (Fig. 6.3A) were linked to modelled soil redistribution patterns with low SOC contents at the erosional sites and high SOC contents at the depositional sites, as was already shown in an earlier study within the test site (Dlugoß et al., 2010; chapter 3). This pattern was more pronounced in deep soil layers and led to a higher spatial variability of measured SOC in the two subsoil layers as compared to the plough layer. This result was confirmed by the coefficients of variation of SOC, which equal 8% in the plough layer and 20% and 44% in the two subsoil layers, respectively. Another area of relatively high measured SOC contents, primarily in the two upper soil layers, was located in the upper part near the southern boundary of the test site (Fig. 6.3A). At this relatively flat slope position, these high values cannot be attributed to soil redistribution processes, but we assume that they were caused by former dung or sugar beet storage.

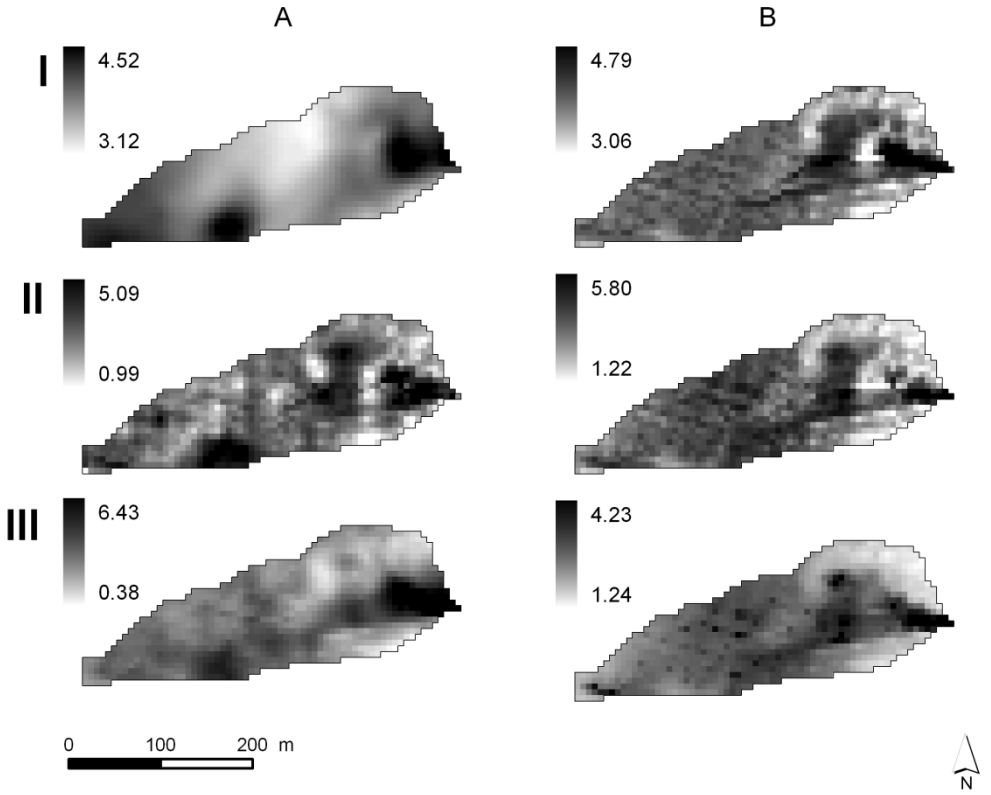

Fig. 6.3: Maps of measured (A) and modelled (B) SOC inventories [kg m^{-2}] for the three soil layers (I: 0-0.25 m; II: 0.25-0.50 m; III: 0.50-0.90 m).

Modelled SOC inventory patterns of the three soil layers (Fig. 6.3B) were generally in good agreement with the measured patterns. Lowest values were found along the thalweg (water erosion) and on the shoulders of the north-south facing slope (tillage erosion), whereas highest SOC contents in each soil layer were located in the modelled depositional area near the outlet of the test site. The other area of relatively high observed SOC contents in soil layers I and II was potentially related to processes not included in the model and could therefore not be reproduced by SPEROS-C, resulting in moderate modelled SOC contents in this area.

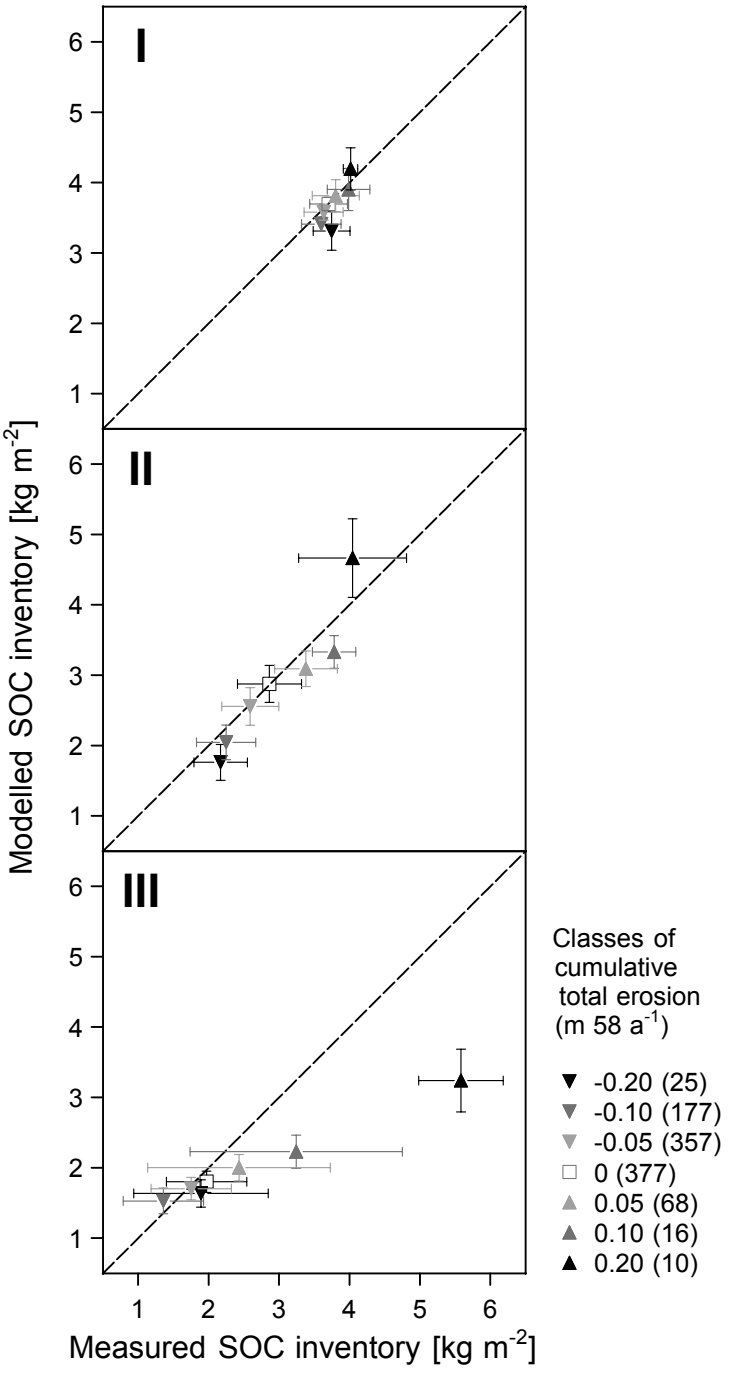

Fig. 6.4: Scatter plots of modelled vs. measured SOC inventories for three soil layers (I: 0-0.25 m; II: 0.25-0.50 m; III: 0.50-0.90 m). Data are summarised to classes of cumulative total erosion. The number of grid cells within each class is given in brackets. Data points represent arithmetic means for each erosion class ± one standard deviation. The dashed line represents the 1:1 line.

To more explicitly analyse which areas were well described by SPEROS-C and which ones showed potential gaps in process description, we divided the measured and modelled SOC stocks into classes of cumulative (1950-2007) total erosion (Fig. 6.4). These comprise two classes of moderate to high erosion (< -0.1 m 58 a^{-1}), two classes of moderate to high deposition (> 0.1 m 58 a^{-1}), and three classes of low erosion or deposition (between -0.05 and 0.05 m 58 a^{-1}).

In the plough layer, modelled mean SOC inventories lie close to the 1:1 line (Fig. 6.4) except for the maximum erosion (<-0.2 m 58 a^{-1}) class, where depletion of SOC was slightly overestimated. On the one hand, this might indicate a slight overestimation of erosion or an underestimation of dynamic replacement at sites of extreme erosion. On the other hand, this maximum erosion class is dominated by five grid cells located along the thalweg of the catchment. In case of a raster based model, the high erosion rates resulting from concentrated erosion along the thalweg are attributed to the total area of this grid cell, while point measurements of SOC within the grid cell might or might not represent a linear feature smaller than the overall grid cell.

Hence, we assume that the mismatch between measured and modelled SOC stocks in this erosion class potentially results from the relatively small number of grid cells and from differences representing space in SPEROS-C compared to the measured SOC stock. In the first subsoil layer, SOC in the maximum erosion class was also slightly underestimated, whereas SOC in the maximum deposition class was overestimated by SPEROS-C. This is in contrast to the results of Van Oost et al. (2005a), who found an underestimation of SOC accumulation in this soil depth. However, as the maximum deposition class just comprised ~1% of the total catchment area and the mean values of all other classes lie close to the 1:1-line, SPEROS-C reproduced the spatial variability of SOC contents in the first and second soil layers very well.

In the deepest soil layer especially high measured SOC values of the high deposition classes were underestimated by the model (Fig. 6.4). On the one hand, this underestimation might be attributed to a general slight underestimation resulting from inverse estimation of the SOC model parameters at reference sites in this soil layer (Fig. 6.1). This is also visible in Fig. 6.4, where the mean of the class without erosion or deposition is situated slightly below the 1:1 line for the deepest soil layer, whereas this class is perfectly represented in the two upper layers. On the other hand, the underestimation of C storage by deposition in that soil layer might be caused by the fact that our simulation started in 1950 with a spatially uniform start value. Pre-existing soil redistribution history was thus not considered, which might date back to ~1500 AD when agricultural use began in the region (Preston, 2001). Our detailed profile data from two depositional sites (Fig. 5.3 and Fig. 5.5) indicate historic deposition below 0.5 m depth, as they show a substantial enrichment in sand, SOC and ^{14}C, when compared to the reference and erosional profiles. Reconstructing the measured ^{14}C depth distribution at the two depositional profiles (Fig. 5.7) also reveals an underestimation of deposition especially at

D2. In their experimental study Van Hemelryck et al. (2010a) hypothesised that turnover of SOC might be lower at depositional compared to erosional sites, especially in the deeper soil layers because of the production of a dense sediment layer capping the soil surface and thus hampering gas exchange. Hence, turnover of SOC might also be overestimated in this subsoil layer. In concordance to the modelled results of the two upper soil layers, the mean SOC inventory of the maximum erosion class was underestimated in the deepest soil layer compared to the measured data. Again this can be deduced to the fact, that this class is dominated by five grid cells lying in a line of concentrated flow.

The overall spatial variability of SOC as expressed in the range of data (Fig. 6.3) was well met in the two upper soil layers, whereas it was significantly reduced in the deepest soil layer with a modelled coefficient of variation of ~15%. The same was true for the variability within one soil erosion class (Fig. 6.4), indicating that further spatially differentiating processes need to be considered, especially within the deepest soil layer.

Tab. 6.2: Values describing the goodness-of-fit (ME: mean error; RMSE: root mean square error; MEF: model efficiency (Nash and Sutcliffe, 1970); R: Pearson correlation coefficient; for calculation refer to chapter 3.2.5) between measured and modelled SOC inventories for the three soil layers (I: 0-0.25 m; II: 0.25-0.50 m; III: 0.50-0.90 m) (n=1030).

	I	II	III
ME	0.06	0.07	0.12
RMSE	0.31	0.51	0.70
MEF	-0.13	0.15	0.28
R	0.27	0.53	0.64

However, values describing the goodness-of-fit between measured and modelled SOC inventories (Tab. 6.2) display a better overall representation of the modelled results in the two subsoil layers compared to the plough layer. This suggests a close relationship between spatial patterns of soil redistribution and SOC stocks in the deeper soil layers, supporting previous results by Dlugoß et al. (2010) (chapter 3). In layer II, 28% and in layer III 41% of the SOC variance can be ascribed to the variance of simulated soil redistribution processes. In the plough layer, this relationship is less pronounced due to homogenisation by tillage operations, the relatively high turnover rates in that soil layer, and the site-specific high SOC contents in the southern part of the test site resulting from former dung or sugar beet deposits. The specification of the modelled spatial variability is dominated by the redistribution of the old SOC pool, whereas high turnover rates lead to a relatively low spatial variability of the young pool in each soil layer. This is due to the fact that the young pool only comprises about 10% of the total organic carbon pool throughout the soil profile. In contrast, the mean error and the root mean square error increase with increasing soil depth (Tab. 6.2), indicating that the modelled SOC inventories are more biased in the deepest soil layer. In general, the overall representation of the measured SOC inventories by the application of SPEROS-C is good,

indicating a good process representation concerning the interaction of soil redistribution and soil C dynamics in the model. However, the goodness-of-fit is significantly degraded by a few grid cells that undergo extreme erosion and deposition as well as by the fact, that the area of high SOC contents caused by dung or sugar beet storage was not related to processes integrated in the model and could thus not be reproduced.

6.3.3 Lateral and vertical C fluxes

To determine the long-term (1950-2007) development of net vertical C fluxes between soil and atmosphere resulting from land management and generally increasing yields and to separate these C fluxes from those induced by soil redistribution, a first model run was performed without taking erosion into account. In general, the cultivation of sugar beet (starting in 1953, then every third year) led to a depletion of SOC in the test site, whereas the following cultivation of winter cereals again increased SOC contents (Fig. 6.5). Since yields did not significantly increase between 1950 and 1970, the applied crop rotation acted as a source of atmospheric CO_2 under conventional farming in those years. In the following decade, a rapid increase in yields generated a C sequestration in the formerly depleted soils. Thus, the entire period of conventional agriculture was modelled as a small sink of atmospheric C (mean vertical C flux 1950-1979: 1.8 g C $m^{-2}a^{-1}$).

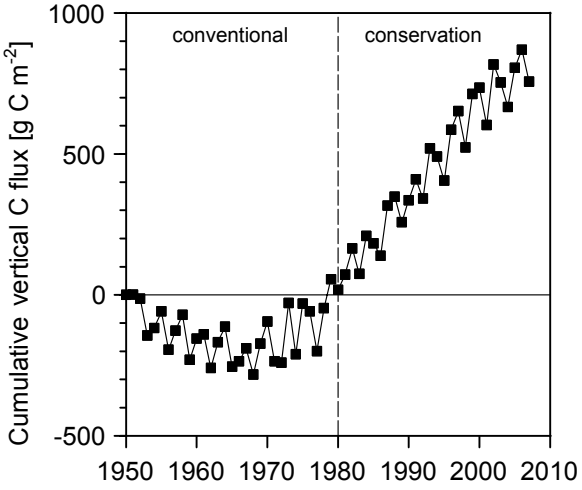

Fig. 6.5 Temporal evolution of the test site integrated cumulative vertical C flux without simulating soil redistribution; negative fluxes represent a loss, and positive fluxes represent a gain. The modelled time span encompasses a period of conventional (1950-1979) and a period of conservation (1980-2007) agriculture.

From 1980 to 2007 (period of conservation agriculture), the system became a stronger C sink caused by further increasing yields on the one hand and by the incorporation of mustard as a cover crop on the other hand (mean vertical C flux 1980-2007: 25.2 g C $m^{-2}a^{-1}$). The biomass and its allocated C of the cover crop were completely incorporated into the soil in each sugar beet year before sowing of the winter cereals. Aboveground biomass of mustard contributes to two thirds of the total biomass and was completely incorporated into the plough

layer so that the sink term was mainly caused by an increase of SOC in the plough layer. Single sugar beet years still acted as a C source to the atmosphere in this period of conservation tillage, but this source term was less pronounced than in the period before. The increasing sink term due to increasing yields might be somewhat overestimated since the relation between yields and C input into the soil remained constant throughout our simulated period. This may not be realistic because an increase in yield due to e.g., the cultivation of new crop species does not necessarily result from higher photosynthesis but from allocating more C to harvestable plant parts, thus reducing the C input into the soil (Billings et al., 2010; Janzen, 2006). However, there were no data available that took this aspect into account.

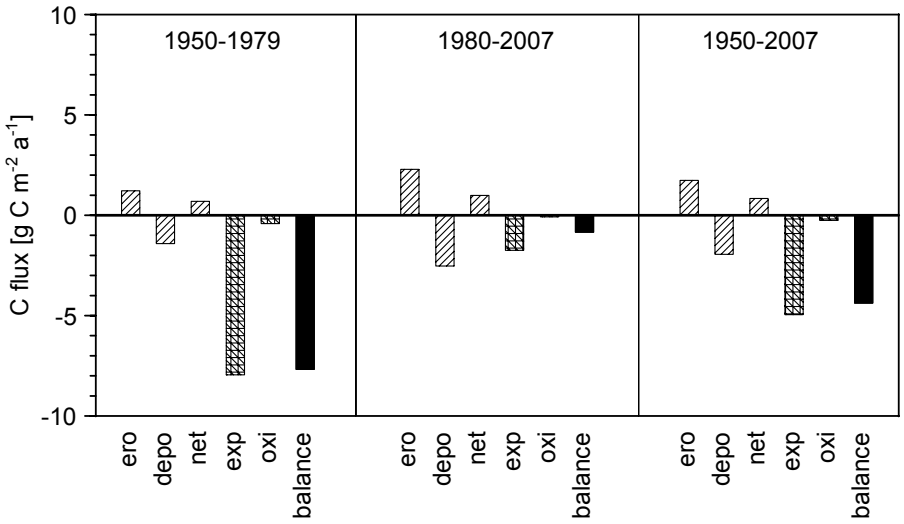

Fig. 6.6 Test site integrated mean lateral and vertical C fluxes induced by soil redistribution processes for the modelled period of conventional (1950-1979) and conservation tillage (1980-2007) as well as for the whole simulation period (1950-2007). Negative fluxes represent a loss, and positive fluxes represent a gain. (ero: mean vertical C flux at erosional sites; depo: mean vertical C flux at depositional sites; net: mean vertical C flux for the whole catchment; exp: C exported by water erosion; oxi: oxidised C during transport; balance: sum of mean vertical C flux, oxidised and exported C)

Compared with the catchment integrated mean vertical C flux caused by the applied land management for the whole simulation period (1950-2007: 13.1 g C $m^{-2}a^{-1}$), the net vertical C flux induced by soil redistribution processes (including the catchment averaged vertical C flux as well as the amount of C oxidised during transport by water) for the whole simulation period constituted with 0.8 g C $m^{-2}a^{-1}$ to only ~6% of the total vertical C flux (Fig. 6.6). For the period of conventional tillage, the soil redistribution associated net vertical C flux contributed to 27% of the total vertical C flux being reduced to approximately 4% in the period of conservation tillage. This corresponds to results of Yadav and Malanson (2009) who found that the vertical C flux associated with erosion or deposition varies with the type of management practice. In cases with conservation practices, the soil redistribution induced

C flux was less than 10% of the total C flux, whereas it contributed to almost 50% for non conservation practices in their test site (Yadav and Malanson, 2009).

Despite its relatively low mean contribution to the catchment averaged net vertical C flux, in concordance to the results of Van Oost et al. (2005a), the net vertical C flux induced by soil redistribution exhibited a very distinct spatial pattern of sink and source areas (Fig. 6.7). Areas with highest deposition rates constituted the largest sources to the atmosphere (maximum C efflux of ~15 g C $m^{-2}a^{-1}$) mainly by the enhanced mineralisation of buried C below the plough layer, whereas areas with high erosion rates acted as C sinks due to dynamic replacement (maximum C sequestration of ~15 g C $m^{-2}a^{-1}$). Thus, the catchment averaged net vertical C flux is generally highly dependent on the relation of erosional and depositional sites. Considering the entire simulation period, on average, total erosion occurred on almost two thirds of the test site area with a mean vertical C flux into the soil of 1.7 g C $m^{-2}a^{-1}$, whereas the depositional areas had a mean vertical C flux from soil to atmosphere of 1.9 g C $m^{-2}a^{-1}$ (Fig. 6.6). Thus, the net soil redistribution induced vertical C flux within the whole catchment acted as a small C sink. Only a small amount of modelled C was oxidised during transport by water (0.3 g C $m^{-2}a^{-1}$). Integrating the loss of C due to the export by water erosion, the overall mean C balance (1950-2007) of our test site became negative (-4.4 g C $m^{-2}a^{-1}$). This was mainly caused by the fact that erosion by water was not transport limited in our test site, so that all eroded sediment and C was exported out of the test site.

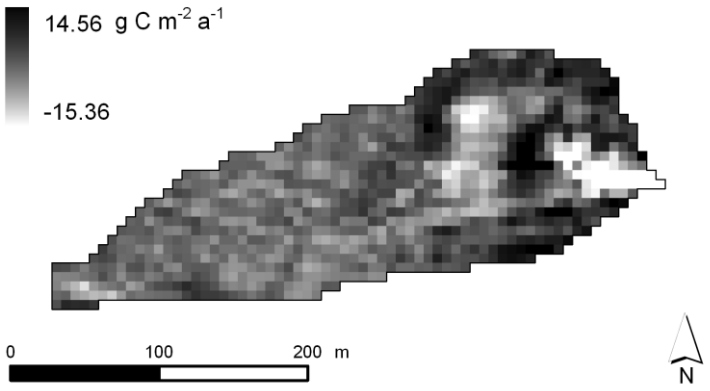

Fig. 6.7: Spatial distribution of mean annual (1950-2007) vertical C flux caused by soil redistribution. Negative fluxes represent a loss, and positive fluxes represent a gain.

The reduction of the amount of exported C from ~8 g C $m^{-2}a^{-1}$ during conventional tillage to less than 2 g C $m^{-2}a^{-1}$ during conservation tillage indicates that it is strongly affected by land management practices (Fig. 6.6). Mainly this reduction of water exported C led to a less pronounced negative C balance (-0.85 g C $m^{-2}a^{-1}$) under conservation agriculture, as compared to conventional practices. In addition, the mean C balance under conservation tillage was reduced due to the fact that the net vertical C flux induced by soil redistribution was more

positive in the period of conservation tillage compared to that of conventional tillage (Fig. 6.6). This was caused by higher negative fluxes at depositional sites and higher positive fluxes at erosional sites. On the one hand, this is a consequence of the transient nature of the vertical C fluxes (Van Oost et al., 2009) and on the other hand of land management change. The period of conservation tillage was dominated by vertical C fluxes, whereas the period of conventional tillage was dominated by a C loss due to the export by water.

Our results correspond to the findings of Izaurralde et al. (2007). Soil respiration contributed to 96% of the total C loss at their two test sites under no-till treatment. These two test sites were C sinks, whereas the test site under conventional tillage acted as a C source. Even more differentiated results were derived by Billings et al. (2010) who found that soil management practices that maintain low erosion rates and high C inputs result in a minimal C exchange with the atmosphere at sites with low SOC content or a small net C sink at sites with higher SOC contents. In contrast, management practices promoting high erosion rates and low C input into the soil represented a strong C source at sites with low SOC contents, whereas at sites with higher SOC contents, soil redistribution might act as a C source or sink.

In general, the C sink or source term of soil redistribution strongly depends on the fate of the exported C by water erosion (e.g. Berhe et al., 2007; Van Oost et al., 2007). Following Stallard (1998), two thirds of the eroded sediment are stored in the same catchment, in local wetlands or other depositional sites. In the test sites analysed in Van Oost et al. (2007), up to 95% of the eroded carbon was redeposited within the catchments. Since a grass buffer strip of ca. 50 m width adjoins our test site near the outlet (Fig. 2.1), we assume that most of the sediment and associated C exported by water is trapped there (e.g. Fiener and Auerswald, 2003). Additionally, evidence of water induced deposition near the outlet is given by a change in soil texture owing to an increased sand content of up to 35-40% (Fig. 5.3), as compared to a mean sand content of ~12% for the whole catchment.

Our measured flume data for the super-ordinate Dissenbach catchment (~150 ha) exhibited a mean annual sediment yield of 205 g m^{-2} a^{-1} (2007-2009), being in the same magnitude as the amount of modelled exported sediment from the Heiderhof test site for the period of conservation tillage (mean 1980-2007: ~170 g m^{-2} a^{-1}), although grass buffer strips exist along the whole Dissenbach brook. This is caused by the fact that most fields in the Dissenbach catchment are tilled conventionally, leading to large internal dynamics as compared to the Heiderhof test site. The mean C content of the exported sediment at the San Dimas flume was ~4%, constituting an enrichment factor of 2.7, as compared to a mean SOC

content in the plough layer of ~1.5% within the Dissenbach catchment (data derived from a digital soil map (1:50000) of North-Rhine Westphalia; Geological Survey). This resulted in a mean C export of 8 g m^{-2} a^{-1} for the whole Dissenbach catchment in the period 2007 to 2009. The fact that the water exported sediment was enriched with SOC was not accounted for in our model run. Thus, C loss by water export of the Heiderhof catchment was potentially underestimated even under conservation tillage.

6.3.4 Sensitivity of lateral and vertical C fluxes

Non-uniform SOC contents at the beginning of the investigated time period (1950), introduced by a prolonged simulation period (1850-2007), did not substantially change the mean C balance in the considered period of conventional (1950-1979: -7.41 g C $m^{-2}a^{-1}$) and conservation agriculture (1980-2007: -0.53 g C $m^{-2}a^{-1}$). This is caused by the fact, that the C balance in our test site was dominated by the C export by water. Considering the vertical C fluxes, the C sink strength of erosion sites (mean vertical C flux 1950-2007: 2.21 g C $m^{-2}a^{-1}$) and the C source strength of deposition sites (mean vertical C flux 1950-2007: -2.28 g C $m^{-2}a^{-1}$) increased with a prolonged simulation period due to the transient nature of these fluxes. However, the extent of this effect was highly dependent on the land management assumptions that affect C inputs as well as soil redistribution for the period before 1950. Assuming extensive grain crop rotations and thereby relatively small erosion rates and C inputs did not change the results for the test site substantially. Hence, it seemed to be reasonable to start the simulation in 1950 and to ignore long-term erosion due to historic land management of which no profound data were available.

In contrast, the lateral and vertical C fluxes associated with soil redistribution exhibited a more pronounced sensitivity to changes of C inputs from plant to soil (Fig. 6.8A). The sink term of the erosion sites as well as the source term at the depositional sites increased with higher C inputs, whereas they were smaller with lower C inputs. This corresponds to results of Billings et al. (2010) who found that increasing the SOC production increased the potential C sink at eroding sites as a result of enhanced dynamic replacement. Since the proportion of erosional to depositional sites remained constant, the catchment averaged net vertical C flux increased with increasing C input. However, the overall changes of the vertical C fluxes due to changes in C input were relatively low, whereas the change in the amount of water-exported C, especially under conventional agriculture, was more pronounced. This indicates

that under constant soil erosion an increase in soil C inputs increases the C loss of our test site.

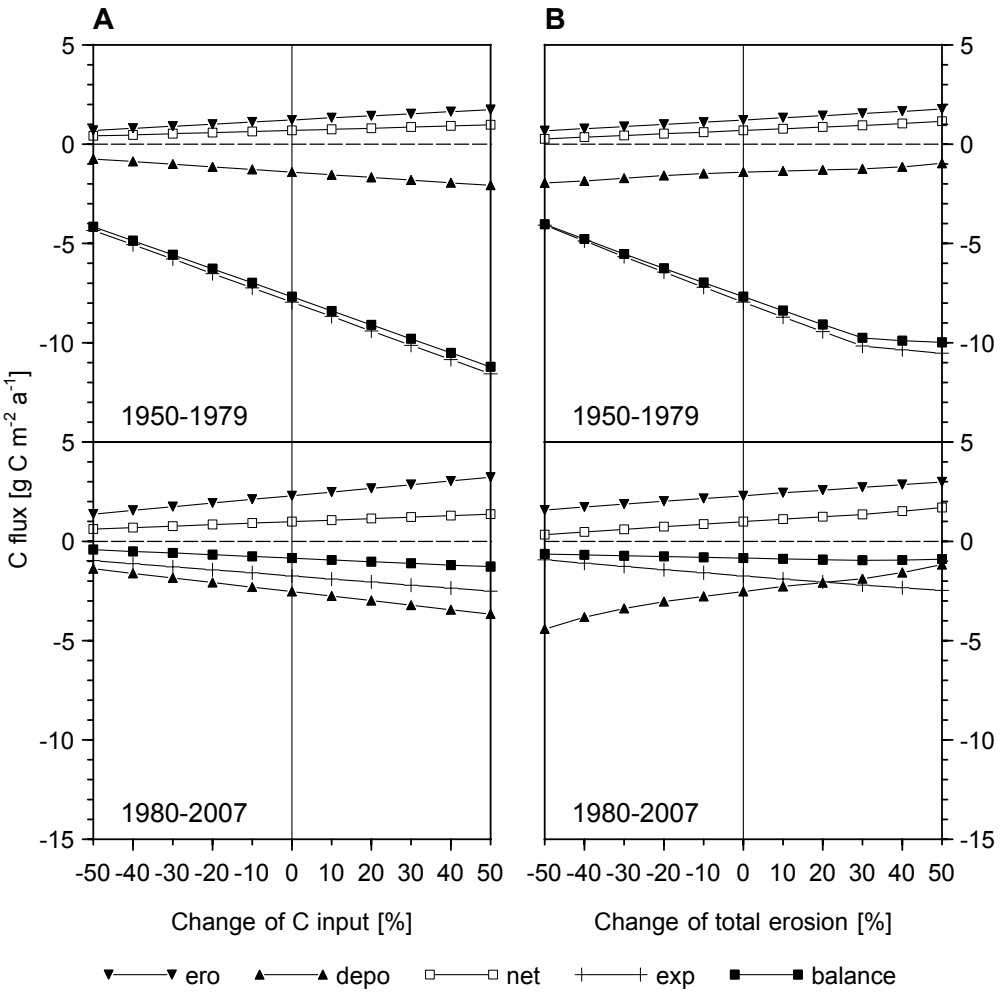

Fig. 6.8: Sensitivity of test site integrated mean lateral and vertical C fluxes [g C $m^{-2}a^{-1}$] induced by soil redistribution processes to changes of C input [%] (A) and changes of potential total erosion [%] (B) for the modelled period of conventional (1950-1979) and conservation tillage (1980-2007). Negative fluxes represent a loss, and positive fluxes represent a gain. Zero change in C input and total erosion represents the results of the reference run. (ero: mean vertical C flux at erosional sites; depo: mean vertical C flux at depositional sites; net: mean vertical C flux for the whole catchment; exp: C exported by water erosion; balance: sum of mean vertical C flux, oxidised and exported C).

The change of the C fluxes caused by the change of total erosion showed a more distinct picture (Fig. 6.8B). The overall C balance of our test site exhibited a linear development in relation to changes in total erosion, i.e., an increase of the C loss with increasing total erosion. Increasing the potential total erosion by more than 30% resulted in transport limitation under conventional tillage in our test site, which led to deposition by water and thus a reduction of the C export. Such behaviour was not found under conservation tillage. In each of the two land management periods, the sink function of erosional sites became stronger with increased erosion rates. This indicates that the absolute dynamic replacement rate increases with increasing soil erosion as long as yields do not decline. At depositional sites the source term

decreased with enhanced soil erosion rates. This results from the deposition of C depleted soil originating from the erosional sites where subsoil material was also eroded with enhanced erosion rates.

In general, changes of total erosion again had a higher impact on the lateral than on the vertical C fluxes especially in the first model period. Especially a change in water erosion processes, i.e., the introduction of deposition by water, clearly shifted the linear behaviour of the C balance. Since under conservation agriculture the overall C balance was dominated by the vertical C fluxes, its sensitivity to changes in erosion rates was less pronounced.

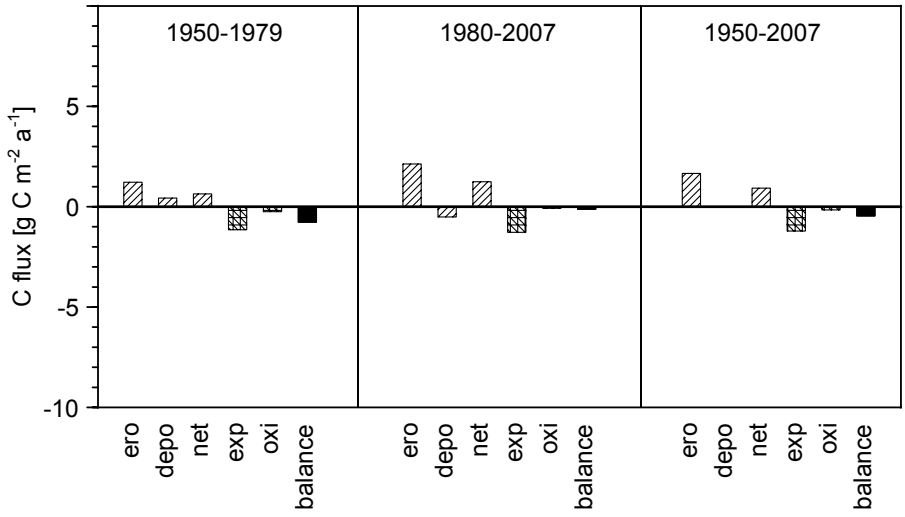

Fig. 6.9: Test site integrated mean lateral and vertical C fluxes induced by soil redistribution processes for the modelled period of conventional (1950-1979) and conservation tillage (1980-2007) as well as for the whole simulation period (1950-2007) when water erosion is restricted to every tenth simulation year. Negative fluxes represent a loss, and positive fluxes represent a gain. (ero: mean vertical C flux at erosional sites; depo: mean vertical C flux at depositional sites; net: mean vertical C flux for the whole catchment; exp: C exported by water erosion; oxi: oxidised C during transport; balance: sum of mean vertical C flux, oxidised and exported C).

The restriction of water erosion to every tenth simulation year had a strong effect on the lateral and vertical C fluxes in both simulation periods. In contrast to the reference run, under conventional tillage, the depositional sites were characterised by a positive vertical C flux to the soil. In the period of conservation tillage, the source strength at depositional sites was significantly reduced compared to the reference run (Fig. 6.9). This can be explained by the fact that in years when water erosion occurred, the depositional sites exhibited a strong sink term, whereas in years when just tillage erosion occurred they acted as a C source to the atmosphere. As was the case in the runs with increased total erosion, restricting water erosion to a few large events, led to a lateral transfer of C depleted subsoil material that was

redeposited at the depositional sites and thus reduced mineralisation. Since the mean C export by water erosion was significantly reduced especially under conventional tillage (-1.15 g C $m^{-2}a^{-1}$) due to transport limited conditions in case of extreme erosion events, and since the mean vertical C flux at depositional sites was almost zero considering the whole simulation period, the overall C balance at our test site was reduced by almost 90%. This is an important finding in so far that many studies (e.g. Stallard, 1998) that deal with (global) estimations of the effect of soil redistribution on SOC are based on mean soil erosion rates derived from field measurements or modelling. It also indicates that the mean C exported by water erosion might be overestimated in our reference run.

6.4 CONCLUSION

At our test site, measured spatial patterns of SOC stocks in three soil layers (0-0.9 m) were closely linked to soil redistribution patterns. In general, SOC was depleted at erosional sites and accumulated at depositional sites. Thus, the application of SPEROS-C, which dynamically couples a spatially distributed soil erosion model (including tillage and water erosion) and a SOC model, allowed for the analysis of the spatial patterns of SOC stocks as well as their lateral and vertical fluxes in our test site. The model was applied from 1950 to 2007 in a one-year time step, comprising a period of conventional tillage (1950-1979) followed by a period of conservation tillage (1980-2007) with reduced soil erosion rates and an additional C input by the cultivation of a cover crop.

In general, modelled SOC patterns corresponded well with measured ones in each soil layer, although there were some discrepancies on areas with extreme erosion or deposition. However, these areas only represent ~3% of the total test site area. Two measured AMS ^{14}C depth profiles in the colluvial area indicate that modelled deposition is slightly underestimated, possibly caused by the fact that no deposition by water is modelled near the outlet of the test site.

The lateral and vertical C fluxes induced by soil redistribution show a strong relation to land management practices. Whereas the period of conventional tillage is dominated by lateral C fluxes leading to an overall C loss of 7.7 g C $m^{-2}a^{-1}$, the period of conservation tillage is dominated by vertical C fluxes reducing the C balance to a loss of 0.9 g C $m^{-2}a^{-1}$.

Although it can be expected that the main part of the water exported C from the Heiderhof test site is deposited in an adjacent grass buffer strip, which is the case for almost every field

in the super-ordinate Dissenbach catchment, sediment export from the Dissenbach catchment is in the same magnitude as that from the Heiderhof test site under conservation agriculture. Nevertheless, C exported from the Dissenbach catchment exhibits a SOC enrichment factor of 2.7 that was not accounted for in the model. This implies that the overall C loss from our test site might be higher even under conservation agriculture.

Analysing the sensitivity of C sources and sinks to changes in C input reveals that all C fluxes associated with soil redistribution are enhanced with increasing C input and attenuated with decreasing C input. This indicates that an increase in C input solely does not increase SOC pools when soil erosion rates remain constant, but that for the sequestration of C in soils, soil erosion has to be reduced correspondingly. Changes in total erosion also exhibit a strong effect on the soil redistribution induced C fluxes. Especially when restricting the occurrence of water erosion to every tenth simulation year, lateral C loss by water and the atmospheric C source at depositional sites are significantly reduced. This indicates that estimates of the erosion induced sink or source strength are overestimated when mean annual soil erosion rates are used.

All model runs showed a substantial carry over effect of the period of conventional to the following period of conservation agriculture concerning the C fluxes caused by the applied crop rotation as well as those caused by soil redistribution. The applied crop rotation led to a depletion of SOC in our field in the first model phase, whereas this depletion was compensated in the following phase due to increasing yields and conservation practices. The erosion induced vertical C fluxes were pronounced, whereas the lateral C fluxes were reduced under conservation agriculture (encompassing a reduction of soil redistribution and an increase in soil C input), both leading to a stronger net atmospheric C sink and a lower lateral C loss.

In general, the spatially distributed SOC and soil redistribution model SPEROS-C proved to be reasonably applicable at the small scale Heiderhof catchment. The adaptations of the model carried out in this study allow for the integration of different land management, which is important with respect to erosion induced lateral and vertical SOC fluxes. Thus, the model will be applicable to larger spatial scales with spatial variances of land management as well as complex management histories, expanding the possibilities to analyse the soil redistribution induced SOC fluxes at the catchment scale.

7 SUMMARY OF RESULTS AND CONCLUSIONS

Impacts of soil redistribution processes on SOC stocks and fluxes were studied in the Heiderhof catchment (4.2 ha) in Germany, being representative for loess covered and intensively used agricultural regions in Central Europe. By intense field measurements of SOC stocks, bulk ^{14}C, particle-size SOC fractions, and CO_2 effluxes at different landscape positions prone to differing erosional processes, this thesis seeks to improve the knowledge about the mechanisms involved in the interplay of soil redistribution and SOC dynamics. In a spatially integrated three-dimensional modelling approach at the catchment scale, the questions are solved whether soil redistribution constitutes a C sink or source for the atmosphere in the test site and how the vertical and lateral soil C fluxes are influenced by a change in land management.

Spatial patterns of SOC stocks

The lateral redistribution of SOC and subsequent spatial patterns of SOC stocks were studied by analysis of soil samples from the plough layer (0-0.25 m) and two subsoil layers (0.25-0.5 m and 0.5-0.9 m) arranged in a 17 x 17 m grid. Mean SOC contents decreased with depth (1.14, 0.71, and 0.34 wt%, respectively), while the spatial variability, expressed as the coefficient of variation increased (14.9, 31.0, and 62.6%, respectively). The spatial patterns of SOC revealed a significant correlation to modelled spatial patterns of tillage and total erosion in the three soil layers also increasing with depth. In the plough layer the impact of soil erosion on SOC stocks was generally weakened due to homogenisation of management practices and due to a general faster turnover of SOC at the soil surface. In the two subsoil layers, a substantial accumulation of SOC in the colluvial area of the test site was observed.

The study shows that the integration of subsoil layers substantially improves C budgeting in agricultural landscapes prone to soil redistribution. Using topsoil SOC data alone, e.g. from remote sensing techniques, might lead to a misinterpretation of total SOC stocks in catchments prone to erosion. As the investigation of subsoil SOC is cost and time consuming, this study also introduces a new method for the derivation of detailed SOC maps in the subsoil. By integrating covariables in the geostatistical interpolation (regression kriging) of

SOC, substantial improvements were achieved in map quality compared to ordinary kriging without covariables that allow for a reduction of sampling density. This improvement increased with depth and with process relation of the chosen covariables. In the medium soil layer, the integration of modelled patterns of tillage and total erosion improved SOC interpolation best, whereas in the deepest soil layer, besides soil redistribution patterns, also the wetness index representing soil moisture improved interpolation results. As these covariables can easily be derived from topographic information or from simple erosion models like the WaTEM/SEDEM, this result can be conferred on the investigation of SOC stocks on larger spatial scales.

Soil respiration and erosion

Soil erosion laterally redistributed SOC in our test site leading to distinct spatial patterns of SOC stocks. However, it remained unclear whether soil and SOC redistribution had an additional effect on soil respiration, being the major vertical CO_2 efflux from soils to atmosphere, and either enhanced or attenuated spatial patterns of SOC. *In situ* measurements of soil respiration, soil moisture (at 6 cm depth), and soil temperature (at 3 cm depth) were carried out bi-weekly on 20 to 22 locations during three vegetation periods (2007: sugar beet; 2008 and 2009: winter wheat) in the most dynamic area with respect to soil redistribution within the test site. Mean temperature-standardised CO_2 effluxes of each measuring location were calculated for a first phase of heterotrophic respiration and a second phase of combined heterotrophic and autotrophic respiration. Besides modelled soil redistribution patterns, further parameters (soil properties, plant parameters, and terrain attributes) were analysed for their impact on the spatial variability of soil respiration and their potential to alter SOC stocks. However, no universal relation between soil respiration and the tested parameters was found for all three vegetation periods, underlining the large variability of soil respiration. In the sugar beet year, when only one measurement was carried out at each location per measuring day, no significant correlation between soil respiration and any of the tested parameters was found. However, in the winter wheat years, with three to four measurements per location and day, a significant linear relation with modelled total soil erosion (comprising water and tillage erosion) for phase one in both years (R^2 is 0.30 and 0.35; $p<0.05$ and $p<0.01$, resp.) and for phase two in one of the two years (R^2 is 0.47; $p<0.001$) was found. Heterotrophic soil respiration, representing the overall decomposition of SOC, under winter wheat was also related to soil texture and SOC in the subsoil layers, while no relation to topsoil SOC was found. Measured topsoil moisture, found to be an important driver of the

spatial variability of soil respiration in many studies, did also not show any significant relation to soil respiration, potentially caused by missing extremes (very dry or very wet) in the measured data. On the one hand, as no evidence for spatial differences in C input was found by our measured plant parameters, the linear increase of heterotrophic respiration with decreasing erosion and increasing deposition supported the mechanism of dynamic replacement with a reduced decomposition and a continued C input by plants at erosion sites. On the other hand, it indicated that the C sink at erosion sites was partly compensated by a C source at depositional sites due to enhanced mineralisation. In the test site, this resulted from the decomposition of subsoil SOC and/or the preferential deposition of labile SOC that was rapidly mineralised.

In general, our results stress the need for multiple measurements and comprehensive data sets necessary for a statistical analysis of the spatial variability of soil respiration on arable land prone to erosion. Further investigations of *in situ* soil respiration measurements need to be conducted, as laboratory experiments do not represent 'real-world' conditions and as the processes leading to spatially differing soil respiration proved to be highly complex.

SOC fraction and ^{14}C profiles

Most studies dealing with the interaction of soil redistribution and SOC dynamics investigate bulk SOC. However, this study shows that the understanding of the involved processes can generally be improved by investigating specific SOC fractions, and hence SOC quality, in combination with ^{14}C concentrations. Particle-size SOC fractions exhibited differing depth distributions for erosion, deposition, and reference profiles in our test site. In the topsoil of the erosion profile, SOC was depleted in the coarse-sized fraction (250-2000 µm) representing the labile SOC pool, compared to the topsoil layer of the reference profile, suggesting a preferential erosion of this SOC fraction. As SOC in this fraction was also depleted in the topsoil layer of the depositional profile, the labile SOC pool was either mineralised during transport or rapidly after deposition, supporting an enhanced decomposition in our test site, or it was preferentially exported out of the test site leading to enrichment of the labile pool. SOC in the intermediate-sized (53-250 µm) and fine-sized (20-53 µm) fractions was generally depleted compared to bulk SOC for all profiles, thus playing a negligible role for SOC dynamics. More than 80% of bulk SOC in the observed profiles was stored in the very fine-sized fraction (< 20 µm) representing a passive SOC pool. This fraction was enriched in C by a factor of 2.4 to 2.8 compared to bulk SOC for all profiles. SOC content in this fraction was relatively similar in the topsoil of the observed profiles, while it

substantially differed in the subsoil layers. Throughout the depositional profile SOC content in this fraction remained relatively high, whereas it decreased with depth at the reference and erosion profile. This proves a substantial stabilisation of SOC especially in the subsoil of the depositional profile.

Depth distributions of bulk ^{14}C measured by accelerator mass spectrometry for erosion, deposition, and reference profiles also revealed a close relation to soil redistribution processes in our test site. In the reference profiles, ^{14}C concentrations decreased with depth indicating a relatively high amount of young plant residues in the topsoil and increasing amounts of more passive components in the subsoil. This decrease was more pronounced at the erosion profiles, whereas ^{14}C concentrations remained relatively high up to a certain depth at the depositional profiles. This hints to burial and preservation of relatively recent SOC below the actual plough layer. In a new approach, the increased ^{14}C concentration below the plough layer was employed to estimate soil and SOC deposition since the 1950s by applying a modified bomb radiocarbon model. Results revealed that the depth increment of this increase only depended on deposition. Hence, ^{14}C concentrations measured by AMS can be used to estimate deposition since the 1950s.

Modelled lateral and vertical C fluxes

For an integrated spatial analysis of the impact of soil redistribution on SOC dynamics at the catchment scale, the combined soil redistribution and SOC dynamics model SPEROS-C was modified and applied to our test site. The model was run for the period between 1950 (intensification of agricultural land use) and 2007 (availability of validation data) covering a period of conventional tillage (1950-1979) and a period of conservation tillage (1980-2007). Measured SOC stocks in the three sampled soil depths (0-0.25 m, 0.25-0.5 m, and 0.5-0.9 m, resp.) could be satisfactorily reproduced except for a few grid cells experiencing extreme erosion or deposition (representing ~3% of the test site area). This indicates a good process representation with respect to the interaction of SOC dynamics and soil erosion within the model. Modelled deposition was validated by two measured ^{14}C depth profiles near the outlet of the test site. Deposition rates derived from the measurements with a modified bomb radiocarbon model were slightly higher than the modelled ones (7 and 5 mm a^{-1} compared to 6.5 and 2.3 mm a^{-1}, respectively). This underestimation of deposition by SPEROS-C was possibly caused by a lack of modelled deposition by water.

Only 6% of the overall net vertical C flux into the soil between 1950 and 2007 was caused by soil redistribution. A more pronounced C sink effect in the test site was caused by the applied crop rotation and the general increase in yields during the simulated period. However, substantial spatial differences of the erosion induced net vertical C flux existed with depositional sites acting as a C source to the atmosphere due to mineralisation of buried C (mean vertical C flux to the atmosphere: 1.9 g C m^{-2} a^{-1}) and with erosional sites acting as a C sink due to dynamic replacement (mean vertical C flux to the soil: 1.7 g C m^{-2} a^{-1}). As the erosion sites constitute approximately two thirds of the test site area, the catchment integrated net vertical C flux induced by soil redistribution of the entire simulation period results in a small C sink of 0.8 g C m^{-2} a^{-1}. However, with respect to the lateral C flux, our test site experienced a substantial C loss due to the export by water erosion, resulting in an overall negative C balance of 4.4 g C m^{-2} a^{-1}. Land management had a profound effect on the lateral and vertical C fluxes, leading to a predominance of lateral C export under the period of conventional tillage and of vertical C fluxes under the period of conservation tillage. The export of C was substantially reduced due to decreased erosion, while the C sink function was slightly increased, leading to a less pronounced negative C balance under conservation tillage (0.9 g C m^{-2} a^{-1} compared to 7.7 g C m^{-2} a^{-1}).

Modelling an increase in C input by plants suggests that additional C sequestration in the test site can only be achieved when the C loss due to water erosion is simultaneously reduced. A modelled increase in total erosion reduced the sediment delivery ratio, as the system was getting partly transport limited. Hence, the C export increased more slowly than the internal C redistribution. In consequence, dynamic replacement increased with higher erosion, and the burial of SOC at depositional sites was more effective due to the deposition of C depleted subsoil from the erosion sites. A similar effect was found when water erosion was restricted to a few large events instead of applying long-term mean soil erosion rates. The overall negative C balance of our test site was then reduced by almost 90% indicating that global estimates of the erosion induced C sink or source might be biased when relying on mean long-term soil erosion rates.

Although we assume most of the exported C to be deposited in the adjacent grass buffer strip in all model runs, the analysis of suspended sediment yield at a runoff monitoring station in the Dissenbach brook revealed a mean C enrichment factor of 2.7 for the period 2007 to 2009 that has to be considered in future investigations. As the sink or source function of the exported C depends on its fate after leaving the test site, there is need for further research at

the larger catchment scale, like e.g. the Dissenbach catchment, including cascading C sinks in colluvia and alluvia as well as C dynamics in the river network. As the model adaptations performed in this study allow for the integration of spatial and temporal differences in land management, the model will be suitable for application to larger spatial scales in future research. A site specific calibration of the erosion model is no longer necessary.

General conclusions

In general, this thesis substantially improves the knowledge about the impacts of soil redistribution on SOC stocks and fluxes at the small catchment scale. Soil redistribution led to a distinct spatial pattern of SOC stocks by lateral SOC redistribution with a substantial accumulation and stabilisation of SOC in the colluvial area due to the burial of C rich topsoil. The spatial pattern of SOC stocks was partly attenuated by an increase of mineralisation at depositional sites and a decrease of mineralisation at erosion sites proven by *in situ* measurements of soil respiration and a catchment integrated modelling approach of combined soil erosion and SOC dynamics. As no spatial differences in C input were found by measured plant parameters and hence C input was also implemented spatially uniform in the model, measured and modelled results supported the abundance of (partial) dynamic C replacement at erosion sites turning them to act as atmospheric C sinks. In contrast, the depositional sites acted as C sources to the atmosphere, albeit a substantial sequestration of SOC in the subsoil. Comparing particle-size SOC fractions at different slope positions indicated that the observed differences in C mineralisation did not just result from a general lateral redistribution of SOC, but also differences in SOC pool composition contributed to this effect. As the labile SOC pool was preferentially eroded and potentially also deposited in our test site, the abundance of more passive components at erosion sites led to reduced mineralisation, whereas at deposition sites the labile SOC pool was rapidly mineralised after deposition.

Overall, soil redistribution constituted a sink for atmospheric CO_2 for the observed period between 1950 and 2007 with respect to the net vertical C flux in the test site. However, the test site experienced a substantial lateral C loss due to the export by water erosion resulting in an overall negative C balance. Sediment and carbon delivery measurements in the super-ordinate Dissenbach catchment indicate that the exported sediment is possibly enriched in C. A change in land management from conventional to conservation practices throughout the simulated period had a profound effect on the erosion induced vertical and lateral soil C fluxes. The net vertical C fluxes at erosion and deposition sites were pronounced, whereas the lateral C fluxes were reduced under conservation agriculture, leading to a stronger net

atmospheric C sink and a lower lateral C loss. Hence, a change from conventional to conservation practices has the potential to increase the erosion induced C sink as long as crop production can be maintained and as long as erosion is not completely impeded. Overall, our results show that soil redistribution has a substantial impact on the C balance of agricultural soils that has to be considered when managing agricultural land for C sequestration purposes.

REFERENCES

Ahmed, S. and G. DeMarsily. 1987. Comparison of geostatistical methods for estimating transmissivity using data on transmissivity and specific capacity. *Water Resources Research* 23:1717-1737.

Aigner, A. 1998. Zwischenfruchtbau. *In* BLV mbH (Ed.). *Die Landwirtschaft 1. Pflanzliche Erzeugung*. BLV mbH, München. pp. 495-500.

Amelung, W., W. Zech, X. Zhang, R.F. Follett, H. Tiessen, E. Knox and K.W. Flach. 1998. Carbon, nitrogen, and sulfur pools in particle-size fractions as influenced by climate. *Soil Science Society of America Journal* 62:172-181.

Andrén, O. and T. Kätterer. 1997. ICBM: The introductory carbon balance model for exploration of soil carbon balances. *Ecological Applications* 7:1226-1236.

Auerswald, K. 2006. Germany. *In* J. Boardman and J. Poesen (Eds.). *Soil erosion in Europe*. Wiley, Chichester. pp. 213-230.

Bajracharya, R.M., R. Lal and J.M. Kimble. 2000. Diurnal and seasonal CO_2-C flux from soil as related to erosion phases in central Ohio. *Soil Science Society of America Journal* 64:286-293.

Balesdent, J., E. Besnard, D. Arrouays and C. Chenu. 1998. The dynamics of carbon in particle-size fractions of soil in a forest-cultivation sequence. *Plant and Soil* 201:49-57.

Bartels, H., G. Malitz, S. Asmus, F.M. Albrecht, B. Dietzer, T. Günther and H. Ertel. 1997. *Starkniederschlaghöhen für Deutschland - KOSTRA*. Deutscher Wetterdienst, Offenbach a. Main.

Basic, F., I. Kisic, O. Nestroy, M. Mesic and A. Butorac. 2002. Particle size distribution (texture) of eroded soil material. *Journal of Agronomy and Crop Science* 188:311-322.

Berhe, A.A., J.W. Harden, M.S. Torn and J. Harte. 2008. Linking soil organic matter dynamics and erosion-induced terrestrial carbon sequestration at different landform positions. *Journal of Geophysical Research* 113:G04039.

Berhe, A.A., J. Harte, J.W. Harden and M.S. Torn. 2007. The significance of the erosion-induced terrestrial carbon sink. *BioScience* 57:337-346.

Beven, K. and M. Kirkby. 1979. A physically based, variable contributing area model of basin hydrology. *Hydrological Sciences Bulletin* 24:43-69.

Billings, S.A., R.W. Buddemeier, D. Richter, K. Van Oost and G. Bohling. 2010. A simple method for estimating the influence of eroding profiles on atmospheric CO_2. *Global Biogeochemical Cycles* 24:doi:10.1029/2009GB003560.

Borken, W., Y.-J. Xu, E.A. Davidson and F. Beese. 2002. Site and temporal variation of soil respiration in European beech, Norway spruce, and Scots pine forests. *Global Change Biology* 8:1205-1216.

Bornemann, L., G. Welp, S. Brodowski, A. Rodionov and W. Amelung. 2008. Rapid assessment of black carbon in soil organic matter using mid-infrared spectroscopy. *Organic Geochemistry* 39:1537-1544.

Brodowski, S., W. Amelung, L. Haumaier and W. Zech. 2007. Black carbon contribution to stable humus in German arable soils. *Geoderma* 139:220-228.

Brodowski, S., A. Rodionov, L. Haumaier, B. Glaser and W. Amelung. 2005. Revised black carbon assessment using benzene polycarboxylic acids. *Organic Geochemistry* 36:1299-1310.

Brovkin, V., A. Cherkinsky and S. Goryachkin. 2008. Estimating soil carbon turnover using radiocarbon data: a case study for European Russia. *Ecological Modelling* 216:178-187.

Bruun, S., J. Six, L.S. Jensen and K. Paustian. 2005. Estimating turnover of soil organic carbon fractions based on radiocarbon measurements. *Radiocarbon* 47:99-113.

Cambardella, C.A., T.B. Moorman, J.M. Novak, T.B. Parkin, D.L. Karlen, R.F. Turco and A.E. Konopka. 1994. Field-scale variability of soil properties in central Iowa soils. *Soil Science Society of America Journal* 58:1501-1511.

Chai, X., C. Shen, X. Yuan and Y. Huang. 2008. Spatial prediction of soil organic matter in the presence of different external trends with REML-EBLUP. *Geoderma* 148:159-166.

Chaplot, V.A.M., C. Rumpel and C. Valentin. 2005. Water erosion impact on soil and carbon redistributions within uplands of Mekong River. *Global Biogeochemical Cycles* 19:GB4004.

Chen, F., D.E. Kissel, L.T. West and W. Adkins. 2000. Field-scale mapping of surface soil organic carbon using remotely sensed imagery. *Soil Science Society of America Journal* 64:746-753.

Christensen, B.T. 1992. Physical fractionation of soil and organic matter in primary particle size and density separates. *In* B.A. Stewart (Ed.). *Advances in soil science. Volume 20.* Springer, New York. pp. 1-90.

Cole, J.J. and N.F. Caraco. 2001. Carbon in catchments: connecting terrestrial carbon losses with aquatic metabolism. *Marine and Freshwater Research* 52:101-110.

Coleman, K., Jenkinson, D.S., 2008. ROTHC-26.3. A model for the turnover of carbon in soil. Model description and windows user guide. http://www.rothamsted. bbsrc.ac.uk/aen/carbon/rothc.htm.

Davidson, E.A., I.A. Janssens and Y. Luo. 2006. On the variability of respiration in terrestrial ecosystems: moving beyond Q_{10}. *Global Change Biology* 12:154-164.

Davidson, E.A., L.V. Verchot, J. Henrique Cattanio, I.L. Ackerman and J.E.M. Carvalho. 2000. Effects of soil water content on soil respiration in forests and cattle pastures of eastern Amazonia. *Biogeochemistry* 48:53-69.

De Gryze, S., J. Six, H. Bossuyt, K. Van Oost and R. Merckx. 2008. The relationship between landform and the distribution of soil C, N and P under conventional and minimum tillage. *Geoderma* 144:180-188.

Desmet, P.J.J. and G. Govers. 1996a. A GIS procedure for automatically calculating the USLE LS factor on topographically complex landscape units. *Journal of Soil and Water Conservation* 51:427-433.

Desmet, P.J.J. and G. Govers. 1996b. Comparison of routing algorithms for digital elevation models and their implications for predicting ephemeral gullies. *International Journal of Geographic Information Systems* 10:311-331.

Desmet, P.J.J. and G. Govers. 1997. Two-dimensional modelling of the within-field variation in rill and gully geometry and location related to topography. *Catena* 29:283-306.

Deutsches Institut für Normung. 1996. *DIN 18129: 1996-11 Baugrund, Untersuchung von Bodenproben - Kalkgehaltsbestimmung*. Beuth Verlag, Berlin.

Deutsches Institut für Normung. 2002. *DIN ISO 11277: 2002-08 Bodenbeschaffenheit - Bestimmung der Partikelgrößenverteilung in Mineralböden - Verfahren mittels Siebung und Sedimentation*. Beuth Verlag, Berlin.

Deutsches Institut für Normung. 2005. *DIN 19708 - Bodenbeschaffenheit - Ermittlung der Erosionsgefährdung von Böden durch Wasser mit Hilfe der ABAG*. Beuth Verlag, Berlin.

Deutsches Institut für Normung. 2006. *DIN ISO 10390:2005 Bodenbeschaffenheit - Bestimmung des pH-Wertes*. Beuth Verlag, Berlin.

Dlugoß, V., P. Fiener and K. Schneider. 2010. Layer-specific analysis and spatial prediction of soil organic carbon using terrain attributes and erosion modeling. *Soil Science Society of America Journal* 74:922-935.

Draycott, A.P. 2006. *Sugar Beet*. Blackwell, Oxford.

Edwards, W.M. and L.B. Owens. 1991. Large storm effects on total soil erosion. *Journal of Soil and Water Conservation* 46:75-78.

Epron, D., A. Bosc, D. Bonal and V. Freycon. 2006. Spatial variation of soil respiration across a topographic gradient in a tropical rain forest in French Guiana. *Journal of Tropical Ecology* 22:565-574.

Eshel, G. and P. Fine. 2007. Total soil carbon and water quality: An implication for carbon sequestration. *Soil Science Society of America Journal* 71:397-405.

Eynard, A., T.E. Schumacher, M.J. Lindstrom and D.D. Malo. 2005. Effects of agricultural management systems on soil organic carbon in aggregates of Ustolls and Usterts. *Soil & Tillage Research* 81:253-263.

Fang, C., J.B. Moncrieff, H.L. Gholz and L.C. Kenneth. 1998. Soil CO_2 efflux and its spatial variation in a Florida slash pine plantation. *Plant and Soil* 205:135-146.

FAO. 1998. *World reference base for soil resources*. United Nations, Rome.

Fiener, P. and K. Auerswald. 2003. Concept and effects of a multi-purpose grassed waterway. *Soil Use and Management* 19:65-72.

Fiener, P. and K. Auerswald. 2007. Rotation effects of potato, maize and winter wheat on soil erosion by water. *Soil Science Society of America Journal* 71:1919-1925.

Fiener, P., G. Govers and K. Van Oost. 2008. Evaluation of a dynamic multi-class sediment transport model in a catchment under soil-conservation agriculture. *Earth Surface Processes and Landforms* 33:1639-1660.

Flessa, H., W. Amelung, M. Helfrich, G.L.B. Wiesenberg, G. Gleixner, S. Brodowski, J. Rethemeyer, C. Kramer and P.M. Grootes. 2008. Storage and stability of organic matter and fossil carbon in a Luvisol and Phaeozem with continuous maize cropping: A synthesis. *Journal of Plant Nutrition and Soil Science* 171:36-51.

Frede, H.-G. and S. Dabbert. 1999. *Handbuch zum Gewässerschutz in der Landwirtschaft*. ecomed, Landsberg.

Gan, Y.T., C.A. Campbell, H.H. Janzen, R.L. Lemke, P. Basnyat and C.L. McDonald. 2009. Carbon input to soil from oilseed and pulse crops on the Canadian prairies. *Agriculture Ecosystems & Environment* 132:290-297.

Geologischer Dienst NRW. 2001. *Bodenkarte NRW 1:50000*. Geologischer Dienst NRW, Krefeld.

Geologisches Landesamt Nordrhein-Westfalen. 1975. *Geologische Karte von Nordrhein-Westfalen 1:25000. Blatt 5209 Siegburg*. Geologisches Landesamt Nordrhein-Westfalen, Krefeld.

Goldberg, E.D. 1985. *Black carbon in the environment*. Wiley, New York.

Govers, G., T.A. Quine and D.E. Walling. 1993. The effect of water erosion and tillage movement on hillslope profile development: a comparison of field observation and model results. *In* S. Wicherek (Ed.). *Farm land erosion in temperate plains environments and hills*. Elsevier, Amsterdam. pp. 285-300.

Govers, G., K. Vandaele, P. Desmet, J. Poesen and K. Bunte. 1994. The role of tillage in soil redistribution on hillslopes. *European Journal of Soil Science* 45:469-478.

Graf, A., N. Prolingheuer, A. Schickling, M. Schmidt, K. Schneider, D. Schüttemeyer, M. Herbst, J.A. Huisman, L. Weihermüller, B. Scharnagl, C. Steenpass, R. Harms and H. Vereecken. 2010. Temporal downscaling of soil carbon dioxide efflux measurements based on time-stable spatial patterns. *Vadose Zone Journal* 9:1-13.

Grant, D.M. and B.D. Dawson. 1997. *Isco open channel flow measurement handbook*. Lincoln.

Gregorich, E.G., K.J. Greer, D.W. Anderson and B.C. Liang. 1998. Carbon distribution and losses: erosion and deposition effects. *Soil & Tillage Research* 47:291-302.

Grunert, J. 1988. Geomorphologische Entwicklung des Bonner Raumes. *Arbeiten zur Rheinischen Landeskunde* 58:165-180.

Hahn, V. and N. Buchmann. 2004. A new model for soil organic carbon turnover using bomb carbon. *Global Biogeochemical Cycles* 18:GB1019.

Hajdas, I. 2008. Radiocarbon dating and its applications in Quaternary studies. *Eiszeitalter und Gegenwart* 57:2-24.

Hajdas, I., G. Bonani, J. Thut, G. Leone, R. Pfenniger and C. Maden. 2004. A report on sample preparation at the ETH/PSI AMS facility in Zurich. *Nuclear Instruments & Methods in Physics Research B Beam Interactions with Materials and Atoms* 223-224:267-271.

Han, G., G. Zhou, Z. Xu, Y. Yang, J. Liu and K. Shi. 2007. Biotic and abiotic factors controlling the spatial and temporal variation of soil respiration in an agricultural ecosystem. *Soil Biology & Biochemistry* 39:418-425.

Hanson, P.J., S.D. Wullschleger, S.A. Bohlmann and D.E. Todd. 1993. Seasonal and topographic patterns of forest floor CO2 efflux from an upland oak forest. *Tree Physiology* 13:15.

Harden, J.W., J.M. Sharpe, W.J. Parton, D.S. Ojima, T.L. Fries, T.G. Huntington and S.M. Dabney. 1999. Dynamic replacement and loss of soil carbon by eroding cropland. *Global Biogeochemical Cycles* 13:885-901.

Harkness, D.D., A.F. Harrison and P.J. Bacon. 1986. The temporal distribution of `bomb` ^{14}C in a forest soil. *Radiocarbon* 28:328-337.

Heckrath, G., J. Djurhuus, T.A. Quine, K. Van Oost, G. Govers and Y. Zhang. 2005. Tillage erosion and its effect on soil properties and crop yield in Denmark. *Journal of Environmental Quality* 34:312-324.

Hengl, T., G.B.M. Heuvelink and D.G. Rossiter. 2007. About regression-kriging: From equations to case studies. *Computers & Geosciences* 33:1301-1315.

Hengl, T., G.B.M. Heuvelink and A. Stein. 2004. A generic framework for spatial prediction of soil variables based on regression-kriging. *Geoderma* 120:75-93.

Henningsen, D. and G. Katzung. 1998. *Einführung in die Geologie Deutschlands*. Enke, Stuttgart.

Herbst, M., B. Diekkrüger and H. Vereecken. 2006. Geostatistical co-regionalization of soil hydraulic properties in a micro-scale catchment using terrain attributes. *Geoderma* 132:206-221.

Herbst, M., H.J. Hellebrand, J. Bauer, J.A. Huisman, J. Simunek, L. Weihermüller, A. Graf, J. Vanderborght and H. Vereecken. 2008. Multi-year heterotrophic soil respiration: Evaluation of a coupled CO_2 transport and carbon turnover model. *Ecological Modelling* 214:271-283.

Herbst, M., N. Prolingheuer, A. Graf, J.A. Huisman, L. Weihermüller and J. Vanderborght. 2009. Characterization and understanding of bare soil respiration spatial variability at plot scale. *Soil Science Society of America Journal* 8:762-771.

Higgitt, D.L., W. Froehlich and D.E. Walling. 1992. Applications and limitations of Chernobyl radiocaesium measurements in a Carpathian erosion investigation, Poland. *Land Degradation and Rehabilitation* 3:15-26.

Hütsch, B.W., J. Augustin and W. Merbach. 2002. Plant rhizodeposition - an important source for carbon turnover in soils. *Journal of Plant Nutrition and Soil Science* 165:397-407.

IPCC. 2000. *Special report on emissions scenarios*. Cambridge University Press, Cambridge.

IPCC. 2007. *Climate Change 2007: The Physical Science Basis - Summary for Policymakers*. 4: 1-18.

Isaaks, E.H. and R.M. Srivastava. 1989. *Applied geostatistics*. Oxford University Press, New York.

Izaurralde, R.C., J.R. Williams, W.M. Post, A.M. Thomson, W.B. McGill, L.B. Owens and R. Lal. 2007. Long-term modeling of soil C erosion and sequestration at the small watershed scale. *Climatic Change* 80:73-90.

Jacinthe, P.A. and R. Lal. 2001. A mass balance approach to assess carbon dioxide evolution during erosional events. *Land Degradation & Development* 12:329-339.

Jacinthe, P.A., R. Lal, L.B. Owens and D.L. Hothem. 2004. Transport of labile carbon in runoff as affected by land use and rainfall characteristics. *Soil & Tillage Research* 77:111-123.

Janzen, H.H. 2006. The soil carbon dilemma: Shall we hoard it or use it? *Soil Biology & Biochemistry* 38:419-424.

Jarecki, M.K., R. Lal and R. James. 2005. Crop management effects on soil carbon sequestration on selected farmers' fields in northeastern Ohio. *Soil & Tillage Research* 81:265-276.

John, B., T. Yamashita, B. Ludwig and H. Flessa. 2005. Storage of organic carbon in aggregate and density fractions of silty soils under different types of land use. *Geoderma* 128:63-79.

Kang, S., S. Doh, D. Lee, D. Lee, V.L. Jin and J.S. Kimball. 2003. Topographic and climatic controls on soil respiration in six temperate mixed-hardwood forest-slopes, Korea. *Global Change Biology* 9:1427-1437.

Kang, S., S. Kim, S. Oh and D. Lee. 2000. Predicting spatial and temporal patterns of soil temperature based on topography, surface cover and air temperature. *Forest Ecology and Management* 136:173-184.

Kätterer, T., M. Reichstein, O. Andrén and A. Lomander. 1998. Temperature dependence of organic matter decomposition: a critical review using literature data analyzed with different models. *Biology and Fertility of Soils* 27:258-262.

Kerry, R. and M.A. Oliver. 2007a. Determining the effect of asymmetric data on the variogram. I. Underlying asymmetry. *Computers & Geosciences* 33:1212-1232.

Kerry, R. and M.A. Oliver. 2007b. Determining the effect of asymmetric data on the variogram. II. Outliers. *Computers & Geosciences* 33:1233-1260.

Kilpatrick, F.A. and V.R. Schneider. 1983. *Use of flumes in measuring discharge*. United States Government Printing Office, Washington.

Kuhn, N.J. 2010. Erosion and climate. *Nature Geoscience* 3:738.

Kuhn, N.J., T. Hoffmann, W. Schwanghart and M. Dotterweich. 2009. Agricultural soil erosion and global carbon cycle: controversy over? *Earth Surface Processes and Landforms* 34:1033-1038.

Kutsch, W.L., M. Bahn and A. Heinemeyer. 2009. Soil carbon relations: an overview. *In* W.L. Kutsch, M. Bahn, and A. Heinemeyer (Eds.). *Soil carbon dynamics. An integrated methodology*. Cambridge University Press, Cambridge. pp. 1-15.

Lal, R. 2001. Soil degradation by erosion. *Land Degradation & Development* 12:519-539.

Lal, R. 2003a. Soil erosion and the global carbon budget. *Environment International* 29:437-450.

Lal, R. 2003b. Importance of inorganic carbon in sequestering carbon in soils of the dry regions. *Current Science* 84:864-865.

Lal, R. 2004a. Soil carbon sequestration impacts on global climate change and food security. *Science* 304:1623-1627.

Lal, R. 2004b. Soil carbon sequestration to mitigate climate change. *Geoderma* 123:1-22.

Lal, R. 2008. Soil carbon stocks under present and future climate with specific reference to European ecoregions. *Nutrient Cycling in Agroecosystems* 81:113-127.

Lal, R. 2009. Challenges and opportunities in soil organic matter research. *European Journal of Soil Science* 60:158-169.

Lal, R. 2010. Beyond Copenhagen: mitigating climate change and achieving food security through soil carbon sequestration. *Food Security* 2:169-177.

Lal, R., M.L. Griffin, J. Apt, L. Lave and M.G. Morgan. 2004. Managing soil carbon. *Science* 304:5669.

Lark, R.M., B.R. Cullis and S.J. Welham. 2006. On spatial prediction of soil properties in the presence of a spatial trend: the empirical best linear unbiased predictor (E-BLUP) with REML. *European Journal of Soil Science* 57:787-799.

Leifeld, J. and J. Fuhrer. 2009. Long-term management effects on soil organic matter in two cold, high-elevation grasslands: clues from fractionation and radiocarbon dating. *European Journal of Soil Science* 60:230-239.

Leifeld, J., M. Zimmermann, J. Fuhrer and F. Conen. 2009. Storage and turnover of carbon in grassland soils along an elevation gradient in the Swiss Alps. *Global Change Biology* 15:668-679.

Lessmann-Schoch, U., R. Kahrer and G.W. Brümmer. 1991. Pollenanalytische und ^{14}C-Untersuchungen zur Datierung der Kolluvienbildung in einer lößbedeckten Mittelgebirgslandschaft (Nördlicher Siebengebirgsrand). *Eiszeitalter und Gegenwart* 41:16-25.

Levin, I. and B. Kromer. 2004. The tropospheric $^{14}CO_2$ level in mid-latitudes of the northern hemisphere (1959-2003). *Radiocarbon* 46:1261-1272.

Li, S., D.A. Lobb, K.H.D. Tiessen and B.G. McConkey. 2010. Selecting and applying Cesium-137 conversion models to estimate soil erosion rates in cultivated fields. *Journal of Environmental Quality* 39:204-219.

Li, Y., Q.W. Zhang, D.C. Reicosky, L.Y. Bai, M.J. Lindstrom and L. Li. 2006. Using ^{137}Cs and $^{210}Pb_{ex}$ for quantifying soil organic carbon redistribution affected by intensive tillage on steep slopes. *Soil & Tillage Research* 86:176-184.

LI-COR. 2006. *LI-8100 automated soil CO_2 flux system & LI-8150 Multiplexer*. Lincoln.

Liang, A., X. Yang, X. Zhang, N. McLaughlin, Y. Shen and W. Li. 2009. Soil organic carbon changes in particle-size fractions following cultivation of Black soils in China. *Soil & Tillage Research* 105:21-26.

Lindstrom, M.J., W.W. Nelson and T.E. Schumacher. 1992. Quantifying tillage erosion rates due to moldboard plowing. *Soil & Tillage Research* 24:243-255.

Liu, G. and B.C. Si. 2009. Multi-layer diffusion model and error analysis applied to chamber-based gas fluxes measurements. *Agricultural and Forest Meteorology* 149:178.

Liu, S., N. Bliss, E. Sundquist and T.G. Huntington. 2003. Modeling carbon dynamics in vegetation and soil under the impact of soil erosion and deposition. *Global Biogeochemical Cycles* 17:1074.

Liu, Y., S.Q. Li, S.J. Yang, W. Hu and X.P. Chen. 2010. Diurnal and seasonal soil CO_2 flux patterns in spring maize fields on the Loess Plateau, China. *Acta Agriculturae Scandinavica Section B: Soil and Plant Science* 60:245-255.

Ludwig, B., E. Schulz, J. Rethemeyer, I. Merbach and H. Flessa. 2007. Predictive modelling of C dynamics in the long-term fertilization experiment at Bad Lauchstädt with the Rothamsted Carbon Model. *European Journal of Soil Science* 58:1155-1163.

Luo, Y. and X. Zhou. 2006. *Soil respiration and the environment*. Elsevier, Amsterdam.

Mabit, L., C. Bernard, M. Makhlouf and M.R. Laverdière. 2008. Spatial variability of erosion and soil organic matter content estimated from ^{137}Cs measurements and geostatistics. *Geoderma* 145:245-251.

Mabit, L., A. Klik, M. Benmansour, A. Toloza, A. Geisler and U.C. Gerstmann. 2009. Assessment of erosion and deposition rates within an Austrian agricultural watershed by combining ^{137}CS, $^{210}Pb_{ex}$ and conventional measurements. *Geoderma* 150:231-239.

Malam Issa, O., Y. Le Bissonnais, O. Planchon, D. Favis-Mortlock, N. Silvera and J. Wainwright. 2006. Soil detachment and transport on field- and laboratory-scale interrill

areas: erosion processes and the size-selectivity of eroded sediment. *Earth Surface Processes and Landforms* 31:929-939.

Marschner, B., S. Brodowski, A. Dreves, G. Gleixner, A. Gude, P.M. Grootes, U. Hamer, A. Heim, G. Jandl, R. Ji, K. Kaiser, K. Kalbitz, C. Kramer, P. Leinweber, J. Rethemeyer, A. Schäffer, M.W.I. Schmidt, L. Schwark and G.L.B. Wiesenberg. 2008. How relevant is recalcitrance for the stabilization of organic matter in soils? *Journal of Plant Nutrition and Soil Science* 171:91-110.

Martens, H. and T. Naes. 1989. *Multivariate calibration*. Wiley, Chichester.

Martin, J.G. and P.V. Bolstad. 2009. Variation of soil respiration at three spatial scales: Components within measured, intra-site variation and patterns on the landscape. *Soil Biology & Biochemistry* 41:530-543.

Matheron, G. 1963. Principles of geostatistics. *Economic Geology* 58:1246-1266.

McCarty, G.W. and J.C. Ritchie. 2002. Impact of soil movement on carbon sequestration in agricultural ecosystems. *Environmental pollution* 116:423-430.

McCool, D.K., L.C. Brown, G.R. Foster, C.K. Mutchler and L.D. Meyer. 1987. Revised slope steepness factor for the Universal Soil Loss Equation. *Transactions of the American Society of Agricultural Engineers* 30:1387-1396.

Minasny, B. and A.B. McBratney. 2007a. Spatial prediction of soil properties using EBLUP with the Mátern covariance function. *Geoderma* 140:324-336.

Minasny, B. and A.B. McBratney. 2007b. Corrigendum to "Spatial prediction of soil properties using EBLUP with the Mátern covariance function" [Geoderma 140 (2007) 324-336]. *Geoderma* 142:357-358.

Montgomery, D.R. 2007. Soil erosion and agricultural sustainability. *Proceedings of the National Academy of Sciences of the United States of America* 104:13268-13272.

Moore, I.D., P.E. Gessler, G.A. Nielsen and G.A. Peterson. 1993. Soil attribute prediction using terrain analysis. *Soil Science Society of America Journal* 57:443-452.

Moyano, F.E. 2008. *Soil respiration fluxes and controlling factors in temperate forest and cropland ecosystems*. PhD thesis, Universität Tübingen, Tübingen, Germany.

Mueller, T.G. and F.J. Pierce. 2003. Soil carbon maps: Enhancing spatial estimates with simple terrain attributes at multiple scales. *Soil Science Society of America Journal* 67:258-267.

Mueller, T.G., F.J. Pierce, O. Schabenberger and D.D. Warncke. 2001. Map quality for site-specific fertility management. *Soil Science Society of America Journal* 65:1547-1558.

Mueller, T.G., N.B. Pusuluri, K.K. Mathias, P.L. Cornelius and R.I. Barnhisel. 2004. Site-specific soil fertility management: A model for map quality. *Soil Science Society of America Journal* 68:2031-2041.

Nash, J.E. and J.V. Sutcliffe. 1970. River flow forecasting through conceptual models: Part I. A discussion of principles. *Journal of Hydrology* 10:282-290.

Nearing, M.A., F.F. Pruski and M.R. O'Neal. 2004. Expected climate change impacts on soil erosion rates: A review. *Journal of Soil and Water Conservation* 59:43-50.

North, P.F. 1976. Towards an absolute measurement of soil structural stability using ultrasound. *Journal of Soil Science* 27:451-459.

Odeh, I.O.A., A.B. McBratney and D.J. Chittleborough. 1994. Spatial prediction of soil properties from landform attributes derived from a digital elevation model. *Geoderma* 63:197-214.

Odeh, I.O.A., A.B. McBratney and D.J. Chittleborough. 1995. Further results on prediction of soil properties from terrain attributes: heterotopic cokriging and regression-kriging. *Geoderma* 67:215-226.

Oldeman, L.R., R.T.A. Hakkeling and W.G. Sombroek. 1991. *World map of the status of human-induced soil degradation. Global Assessment of soil degradation*. ISRIC and UNEP, Wageningen.

O´Neal, M.R., M.A. Nearing, R.C. Vining, J. Southworth and R. Pfeifer. 2005. Climate change impacts on soil erosion in Midwest United States with changes in crop management. *Catena* 61:165-184.

Pacific, V.J., B.L. McGlynn, D.A. Riveros-Iregui, D.A. Welsch and H.E. Epstein. 2008. Variability in soil respiration across riparian-hillslope transitions. *Biogeochemistry* 91:51-70.

Papiernik, S.K., M.J. Lindstrom, T.E. Schumacher, J.A. Schumacher, D.D. Malo and D.A. Lobb. 2007. Characterization of soil profiles in a landscape affected by long-term tillage. *Soil & Tillage Research* 93:335-345.

Parkin, T.B., T.C. Kaspar, Z. Senwo, J.H. Prueger and J.L. Hatfield. 2005. Relationship of soil respiration to crop and landscape in the Walnut Creek watershed. *Journal of Hydrometeorology* 6:812-824.

Parton, W.J., D.S. Schimel, C.V. Cole and D.S. Ojima. 1987. Analysis of factors controlling soil organic matter levels in Great Plains grasslands. *Soil Science Society of America Journal* 51:1173-1179.

Paul, S., E. Veldkamp and H. Flessa. 2008. Soil organic carbon in density fractions of tropical soils under forest - pasture - secondary forest land use changes. *European Journal of Soil Science* 59:359-371.

Pebesma, E.J. 2004. Mutivariable geostatistics in S: the gstat package. *Computers & Geosciences* 30:683-691.

Pennock, D.J. and A.H. Frick. 2001. The role of field studies in landscape-scale applications of process models: an example of soil redistribution and soil organic carbon modelling using CENTURY. *Soil & Tillage Research* 58:183-191.

Pimentel, D. 2000. Soil erosion and the threat to food security and the environment. *Ecosystem Health* 6:221-226.

Pimentel, D. 2006. Soil erosion: A food and environmental threat. *Environment, Development and Sustainability* 8:119-137.

Ping, J.L. and A. Dobermann. 2006. Variation in the precision of soil organic carbon maps due to different laboratory and spatial prediction methods. *Soil Science* 171:374-387.

Poesen, J.W.A., G. Verstraeten, R. Soenens and L. Seynaeve. 2001. Soil losses due to harvesting of chicory roots and sugar beet: an underrated geomorphic process? *Catena* 43:35-47.

Polyakov, V. and R. Lal. 2004. Modeling soil organic matter dynamics as affected by soil water erosion. *Environment International* 30:547-556.

Polyakov, V. and R. Lal. 2008. Soil organic matter and CO_2 emission as affected by water erosion on field runoff plots. *Geoderma* 143:216-222.

Preston, N. 2001. *Geomorphic response to environmental change: The imprint of deforestation and agricultural land use on the contemporary landscape of the Pleiser Hügelland, Bonn, Germany*. PhD thesis, Rheinische Friedrich-Wilhelms-Universität, Bonn, Germany.

Pruski, F.F. and M.A. Nearing. 2002. Runoff and soil-loss responses to changes in precipitation: a computer simulation study. *Journal of Soil and Water Conservation* 57:7-16.

Quine, T.A. and K. Van Oost. 2007. Quantifying carbon sequestration as a result of soil erosion and deposition: Restrospective assessment using caesium-137 and carbon inventories. *Global Change Biology* 13:2610-2625.

Quinn, P., K. Beven, P. Chevallier and O. Planchon. 1991. The prediction of hillslope flow paths for distributed hydrological modelling using digital terrain models. *Hydrological Processes* 5:59-79.

Quinton, J.N., J.A. Catt, G.A. Wood and J. Steer. 2006. Soil carbon losses by water erosion: Experimentation and modeling at field and national scales in the UK. *Agriculture Ecosystems & Environment* 112:87-102.

Quinton, J.N., G. Govers, K. Van Oost and R.D. Bardgett. 2010. The impact of agricultural soil erosion on biogeochemical cycling. *Nature Geoscience* 3:311-314.

R Development Core Team, 2007. R: A language and environment for statistical computing. http://www.R-project.org.

Renard, K.G., G.R. Foster, G.A. Weesies, D.K. McCool and D.C. Yoder. 1996. *Predicting soil erosion by water: A guide to conservation planning with the Revised Universal Soil Loss Equation (RUSLE)*. USDA-ARS, Washington DC.

Renschler, C.S. 2003. Designing geo-spatial interfaces to scale process models: the GeoWEPP approach. *Hydrological Processes* 17:1005-1017.

Renwick, W.H., S.V. Smith, R.O. Sleezer and R.W. Buddemeier. 2004. Comment on "Managing soil carbon" (II). *Science* 305:5690.

Reth, S., M. Göckede and E. Falge. 2005a. CO_2 flux from agricultural soil in eastern Germany: Comparison of a close chamber system with eddy covariance measurements. *Theoretical and Applied Climatology* 80:105-120.

Reth, S., M. Reichstein and E. Falge. 2005b. The effect of soil water content, soil temperature, soil pH-value and the root mass on soil CO_2 efflux - A modified model. *Plant and Soil* 268:21-33.

Rethemeyer, J., P.M. Grootes, S. Brodowski and B. Ludwig. 2007. Evaluation of soil ^{14}C data for estimating inert organic matter in the RothC model. *Radiocarbon* 49:1079-1091.

Rethemeyer, J., C. Kramer, G. Gleixner, B. John, T. Yamashita, H. Flessa, N. Andersen, M.J. Nadeau and P.M. Grootes. 2005. Transformation of organic matter in agricultural soils: radiocarbon concentration versus soil depth. *Geoderma* 128:94-105.

Ritchie, J.C., G.W. McCarty, E.R. Venteris and T.C. Kaspar. 2007. Soil and soil organic carbon redistribution on the landscape. *Geomorphology* 89:163-171.

Rochette, P., R.L. Desjardins and E. Pattey. 1991. Spatial and temporal variability of soil respiration in agricultural fields. *Canadian Journal of Soil Science* 71:189-196.

Rodeghiero, M. and A. Cescatti. 2008. Spatial variabilty and optimal sampling strategy of soil respiration. *Forest Ecology and Management* 255:106-112.

Rosenbloom, N.A., S.C. Doney and D.S. Schimel. 2001. Geomorphic evolution of soil texture and organic matter in eroding landscapes. *Global Biogeochemical Cycles* 15:365-381.

Ruysschaert, G., J. Poesen, G. Verstraeten and G. Govers. 2004. Soil loss due to crop harvesting: significance and determining factors. *Progress in Physical Geography* 4:467-501.

Ruysschaert, G., J. Poesen, G. Verstraeten and G. Govers. 2005. Interannual variation of soil losses due to sugar beet harvesting in West Europe. *Agriculture Ecosystems & Environment* 107:317-329.

Saiz, G., C. Green, K. Butterbach-Bahl, R. Kiese, V. Avitabile and E.P. Farrell. 2006. Seasonal and spatial variability of soil respiration in four Sitka spruce stands. *Plant and Soil* 287:161-176.

Salomé, C., N. Nunan, V. Pouteau, T.Z. Lerch and C. Chenu. 2010. Carbon dynamics in topsoil and in subsoil may be controlled by different regulatory mechanisms. *Global Change Biology* 16:416-426.

Schäuble, H., 2004. HydroTools 1.0 for ArcView 3.x. http://www.terracs.de/Hydrotools_eng.pdf.

Schiettecatte, W., D. Gabriels, W.M. Cornelis and G. Hofman. 2008. Enrichment of organic carbon in sediment transport by interrill and rill erosion processes. *Soil Science Society of America Journal* 72:50-55.

Schimmack, W., K. Auerswald and K. Bunzl. 2001. Can $^{239+240}$Pu replace ^{137}Cs as an erosion tracer in agricultural landscapes contaminated with Chernobyl fallout? *Journal of Environmental Radioactivity* 53:41-57.

Schlesinger, W.H. 1995. Soil respiration and changes in soil carbon stocks. *In* G.M. Woodwell and F.T. Mackenzie (Eds.). *Biotic feedbacks in the global climate system: Will the warming feed the warming?* Oxford University Press, New York. pp. 159-168.

Schlesinger, W.H. 1990. Evidence from chronosequence studies for a low carbon-storage potential of soils. *Nature* 354:232-234.

Schlesinger, W.H. 2005. The global carbon cycle and climate change. *Advances in the Economics of Environmental Resources* 5:31-53.

Schlesinger, W.H. and J.A. Andrews. 2000. Soil respiration and the global carbon cycle. *Biogeochemistry* 48:7-20.

Scholz, G., J.N. Quinton and P. Strauss. 2008. Soil erosion from sugar beet in Central Europe in response to climate change induces seasonal precipitation variations. *Catena* 72:91-105.

Schwendenmann, L., E. Veldkamp, T. Brenes, J.J. O´Brien and J. Mackensen. 2003. Spatial and temporal variation in soil CO_2 efflux in an old-growth neotropical rainforest, La Selva, Costa Rica. *Biogeochemistry* 64:111-128.

Schwertmann, U., W. Vogl and M. Kainz. 1987. *Bodenerosion durch Wasser - Vorhersage des Abtrags und Bewertung von Gegenmaßnahmen*. Ulmer Verlag, Stuttgart.

Scott-Denton, L.E., K.L. Sparks and R.K. Monson. 2003. Spatial and temporal controls of soil respiration rate in a high-elevation, subalpine forest. *Soil Biology & Biochemistry* 35:525-534.

Shirazi, M.A., L. Boersma and J.W. Hart. 1988. A unifying quantitative analysis of soil texture: Improvement of precision and extension of scale. *Soil Science Society of America Journal* 52:190.

Simbahan, G.C., A. Dobermann, P. Goovaerts, J. Ping and M.L. Haddix. 2006. Fine-resolution mapping of soil organic carbon based on multivariate secondary data. *Geoderma* 132:471-489.

Six, J., G. Guggenberger, K. Paustian, L. Haumaier, E.T. Elliot and W. Zech. 2001. Sources and composition of soil organic matter fractions between and within soil aggregates. *European Journal of Soil Science* 52:607-618.

Smith, P., P. Falloon and W.L. Kutsch. 2009. The role of soils in the Kyoto Protocol. *In* W.L. Kutsch, M. Bahn, and A. Heinemeyer (Eds.). *Soil carbon dynamics. An integrated methodology*. Cambridge University Press, Cambridge. pp. 245-256.

Smith, P., D. Martino, Z. Cai, D. Gwary, H.H. Janzen, P. Kumar, B. McCarl, S. Ogle, F. O´Mara, C.W. Rice, B. Scholes and O. Sirotenko. 2007. Agriculture. *In* B. Metz, O.R. Davidson, P.R. Bosch, R. Dave, and L.A. Meyer (Eds.). *Climate Change 2007: Mitigation. Contribution of Working Group III to the Fourth Assessment Report of the Intergovernmental Panel on Climate Change*. Cambridge University Press, Cambridge. pp. 497-540.

Smith, S.V., W.H. Renwick, R.W. Buddemeier and C.J. Crossland. 2001. Budgets of soil erosion and deposition for sediments and sedimentary organic carbon across the conterminous United States. *Global Biogeochemical Cycles* 15:697-707.

Smith, S.V., R.O. Sleezer, W.H. Renwick and R.W. Buddemeier. 2005. Fates of eroded soil organic carbon: Mississippi basin case study. *Ecological Applications* 15:1929-1940.

Soe, A.R.B. and N. Buchmann. 2005. Spatial and temporal variations in soil respiration in relation to stand structure and soil parameters in an unmanaged beech forest. *Tree Physiology* 25:1427-1436.

Souchère, V., D. King, J. Daroussin, F. Papy and A. Capillon. 1998. Effects of tillage on runoff directions: consequences on runoff contributing area within agricultural catchments. *Journal of Hydrology* 206:256-267.

Stallard, R. 1998. Terrestrial sedimentation and the carbon cycle: Coupling weathering and erosion to carbon burial. *Global Biogeochemical Cycles* 12:231-257.

Stevens, A., B. Van Wesemael, H. Bartholomeus, D. Rosillon, B. Tychon and E. Ben-Dor. 2008. Laboratory, field and airborne spectroscopy for monitoring organic carbon content in agricultural soils. *Geoderma* 144:395-404.

Stuiver, M. and H.A. Polach. 1977. Discussion: Reporting of ^{14}C data. *Radiocarbon* 19:355-363.

Stuiver, M., P.J. Reimer and T.F. Braziunas. 1998. High-precision radiocarbon age calibration for terrestrial and marine samples. *Radiocarbon* 40:1127-1151.

Sumfleth, K. and R. Duttmann. 2008. Prediction of soil property distribution in paddy soil landscapes using terrain data and satellite information as indicators. *Ecological Indicators* 8:485-501.

Takata, Y., S. Funakawa, K. Akshalov, N. Ishida and T. Kosaki. 2007. Spatial prediction of soil organic matter in northern Kazakhstan based on topographic and vegetation information. *Soil Science & Plant Nutrition* 53:289-299.

Takken, I., L. Beuselinck, J. Nachtergaele, G. Govers, J. Poesen and G. Degraer. 1999. Spatial evaluation of a physically-based distributed erosion model (LISEM). *Catena* 37:431-477.

Takken, I., G. Govers, A. Steegen, J. Nachtergaele and J. Guerif. 2001. The prediction of runoff flow directions on tilled fields. *Journal of Hydrology* 248:1-13.

Tans, P.P., I.Y. Fung and T. Takahashi. 1990. Observational constraints on the global atmospheric CO_2 budget. *Science* 247:1431-1438.

Terra, J.A., J.N. Shaw, D.W. Reeves, R.L. Raper, E. van Santen and P.L. Mask. 2004. Soil carbon relationships with terrain attributes, electrical conductivity, and a soil survey in a coastal plain landscape. *Soil Science* 169:819-831.

Torn, M.S., S. Trumbore, O.A. Chadwick, P.M. Vitousek and D.M. Hendricks. 1997. Mineral control of soil organic carbon storage and turnover. *Nature* 389:170-173.

Trumbore, S. 1996. Applications of accelerator mass spectrometry to soil science. *In* T.W. Boutton and S. Yamasaki (Eds.). *Mass spectrometry of soils*. Marcel Dekker, Inc., New York. pp. 311-340.

Trumbore, S. 2006. Carbon respired by terrestrial ecosystems - recent progress and challenges. *Global Change Biology* 12:141-153.

Trumbore, S. 2009. Radiocarbon and soil carbon dynamics. *Annual Review of Earth and Planetary Sciences* 37:47-66.

USDA. 1999. *Soil taxonomy. A basic system of soil classification for making and interpreting soil surveys*. USDA-NRCS, Washington DC.

Vahrson, W.-G. and M. Frielinghaus. 1998. Bodenverlagerung durch Ackerbau in einer Jungmoränenlandschaft. *Beiträge für Forstwirtschaft und Landschaftsökologie* 32:109-114.

Van Hemelryck, H., P. Fiener, K. Van Oost and G. Govers. 2010a. The effect of soil redistribution on soil organic carbon: an experimental study. *Biogeosience* 7:3971-3986.

Van Hemelryck, H., G. Govers, K. Van Oost and R. Merckx. 2010b. Evaluating the impact of soil redistribution on the in situ mineralization of soil organic carbon. *Earth Surface Processes and Landforms* DOI: 10.1002/esp.2055.

Van Oost, K. and G. Govers. 2006. Tillage erosion. *In* J. Boardman and J. Poesen (Eds.). *Soil erosion in Europe*. Wiley, Chichester. pp. 599-608.

Van Oost, K., G. Govers and P. Desmet. 2000. Evaluating the effects of changes in landscape structure on soil erosion by water and tillage. *Landscape ecology* 15:577-589.

Van Oost, K., G. Govers, T. Quine, G. Heckarth, J.E. Olesen, S. De Gryze and R. Merckx. 2005a. Landscape-scale modeling of carbon cycling under the impact of soil redistribution: The role of tillage erosion. *Global Biogeochemical Cycles* 19:GB4014.

Van Oost, K., G. Govers and W. Van Muysen. 2003. A process-based conversion model for caesium-137 derived erosion rates on agricultural land: An integrated spatial approach. *Earth Surface Processes and Landforms* 28:187-207.

Van Oost, K., T. Quine, G. Govers and G. Heckrath. 2005b. Modeling soil erosion induced carbon fluxes between soil and atmosphere on agricultural land using SPEROS-C. *In* E.J. Roose, R. Lal, C. Feller, B. Barthes, and B.A. Stewart (Eds.). *Advances in soil science. Soil erosion and carbon dynamics*. CRC Press, Boca Raton. pp. 37-51.

Van Oost, K., T.A. Quine, G. Govers, S. De Gryze, J. Six, J.W. Harden, J.C. Ritchie, G.W. McCarty, G. Heckrath, C. Kosmas, J.V. Giraldez, J.R. Marques da Silva and R. Merckx. 2007. The impact of agricultural soil erosion on the global carbon cycle. *Science* 318:doi:10.1126/science.1145724.

Van Oost, K., H. Van Hemelryck and J.W. Harden. 2009. Erosion of soil organic carbon: Implications for carbon sequestration. *In* B.J. McPherson and E.T. Sundquist (Eds.). *Carbon sequestration and its role in the global carbon cycle*. American Geophysical Union, Washington DC. pp. 189-202.

Van Rompaey, A.J.J., G. Verstraeten, K. Van Oost, G. Govers and J. Poesen. 2001. Modelling mean annual sediment yield using a distributed approach. *Earth Surface Processes and Landforms* 26:1221-1236.

VandenBygaart, A.J. 2001. Erosion and deposition history derived by depth-stratigraphy of ^{137}Cs and soil organic carbon. *Soil & Tillage Research* 61:187-192.

Venterea, R.T., K.A. Spokas and J.A. Baker. 2009. Accuracy and precision of chamber-based nitrous oxide gas flux estimates. *Soil Science Society of America Journal* 73:1087-1093.

Verstraeten, G., J. Poesen, K. Gillijns and G. Govers. 2006. The use of riparian vegetated filter strips to reduce river sediment loads: an overestimated control measure? *Hydrological Processes* 20:4259-4267.

Verstraeten, G., K. Van Oost, A. Van Rompaey, J. Poesen and G. Govers. 2002. Evaluating an integrated approach to catchment management to reduce soil loss and sediment pollution through modelling. *Soil Use and Management* 19:386-394.

von Lützow, M., I. Kögel-Knabner, K. Ekschmitt, H. Flessa, G. Guggenberger, E. Matzner and B. Marschner. 2007. SOM fractionation methods: Relevance to functional pools and to stabilization mechanisms. *Soil Biology & Biochemistry* 39:2183-2207.

Walling, D.E. and Q. He. 1999. Using fallout lead-210 measurements to estimate soil erosion on cultivated land. *Soil Science Society of America Journal* 63:1404-1412.

Walling, D.E., Q. He and P.A. Whelan. 2003. Using ^{137}Cs measurements to validate the application of the AGNPS and ANSWERS erosion and sediment yield models in two small Devon catchments. *Soil & Tillage Research* 69:27-43.

Wang, Z., G. Govers, A. Steegen, W. Clymans, A. Van den Putte, C. Langhans, R. Merckx and K. Van Oost. 2010. Catchment-scale carbon redistribution and delivery by water erosion in an intensively cultivated area. *Geomorphology* 124:65-74.

Webster, R. and M.A. Oliver. 2001. *Geostatistics for environmental scientists*. Wiley, Chichester.

West, T.O. and W.M. Post. 2002. Soil organic carbon sequestration rates by tillage and crop rotation: A global data analysis. *Soil Science Society of America Journal* 66:1930-1946.

Wischmeier, W.H. and D.D. Smith. 1978. *Predicting rainfall erosion losses - a guide to conservation planning*. U.S. Gov. Print Office, Washington, DC.

Xu, M. and Y. Qi. 2001. Soil-surface CO_2 efflux and its spatial and temporal variations in a young ponderosa pine plantation in northern California. *Global Change Biology* 7:667-677.

Yadav, V. and G.P. Malanson. 2009. Modeling impacts of erosion and deposition on soil organic carbon in the Big Creek Basin of southern Illinois. *Geomorphology* 106:304-314.

Yoo, K., R. Amundson, A.M. Heimsath and W.E. Dietrich. 2005. Erosion of upland hillslope soil organic carbon: Coupling field measurements with a sediment transport model. *Global Biogeochemical Cycles* 19:GB 3003.

Zhang, J.N., T.A. Quine, S. Ni and F. Ge. 2006. Stocks and dynamics of SOC in relation to soil redistribution by water and tillage erosion. *Global Change Biology* 12:1834-1841.

Zimmermann, M., J. Leifeld, M.W.I. Schmidt, P. Smith and J. Fuhrer. 2007. Measured soil organic matter fractions can be related to pools in the RothC model. *European Journal of Soil Science* 58:658-667.

LIST OF SYMBOLS AND ABBREVIATIONS

α	Angle between tillage and aspect direction	°
a	Aspect	°
A_i	Input ^{14}C concentration of plant residues	pMC
A_t	^{14}C concentration of soil at time t	pMC
$A_{t/Dpl}$	^{14}C concentration of soil in the plough layer at deposition sites at time t	pMC
$A_{t/Dbur}$	^{14}C concentration of soil in the buried plough layer at deposition sites at time t	pMC
$A_{t/Epl}$	^{14}C concentration of soil in the plough layer at erosion sites at time t	pMC
A_{sub}	^{14}C concentration of subsoil	pMC
balance	Sum of net vertical C flux, exported and oxidised C	g C m^{-2}
BC	Black carbon	-
BD	Bulk density	kg m^{-3}
γ	semivariance	unit of variable
C factor	Crop management factor	-
CA	Catchment area	m^2
C_{ero}	Eroded SOC from the topsoil layer	g C m^{-2} a^{-1}
cl	Clay content	wt %
C-plan	Curvature perpendicular to the direction of maximum slope	0.01 m
C-prof	Curvature in the direction of maximum slope	0.01 m
CV	Coefficient of variation	%
D50	Median grain size diameter	µm
DEM	Digital elevation model	-
depo	Mean vertical C flux at deposition sites	g C m^{-2}
dGPS	Differential global positioning system	-
DOC	Dissolved organic carbon	-
E	Enrichment factor	-
E_{har}	Harvest erosion	m
ero	Mean vertical C flux at erosion sites	g C m^{-2}
E_{til}	Tillage erosion	mm a^{-1} or kg m^{-2} a^{-1}
E_{tot}	Total erosion	mm a^{-1} or kg m^{-2} a^{-1}
E_{wat}	Water erosion	mm a^{-1} or kg m^{-2} a^{-1}
exp	C exported by water erosion	g C m^{-2}
f_D	Fraction of deposited soil of the plough layer	-
f_E	Fraction of eroded soil of the plough layer	-
f_{oxi}	Fraction of C oxidised during transport by water	-
GIS	Geographic information system	-
GPP	Gross primary productivity	-
H	Height at hill slope	m
h	Lag distance	m
$h_{c/m}$	Humification coefficient	-
h_c	Humification coefficient for crop residues and roots	-

h_m	Humification coefficient for organic manure	-
i	C input	g C m^{-2} a^{-1}
i_c	C input from crop residues and roots	g C m^{-2} a^{-1}
ICBM	Introductory Carbon Balance Model	-
i_m	C input from organic manure	g C m^{-2} a^{-1}
K factor	Soil erodibility factor	kg h m^{-2} N^{-1}
KED	Kriging with external drift	-
k	Turnover rate of SOC	a^{-1}
k_O	Turnover rate of old SOC pool	a^{-1}
ktc	Transport capacity coefficient	m
ktil	Tillage transport coefficient	kg m a^{-1}
k_Y	Turnover rate of young SOC pool	a^{-1}
λ	Weights for solving the kriging system	-
λ_{14C}	^{14}C decay constant	a^{-1}
L factor	Slope length factor	-
ME	Mean error	unit of variable
MEF	Model efficiency coefficient	-
M_{ero}	Mass of eroded soil	g
M_{plough}	Mass of soil in the plough layer	g
n	Sample size	-
net	Mean net vertical C flux for the test site	g C m^{-2}
NPP	Net primary productivity	-
O	Old SOC pool	g C m^{-2}
OK	Ordinary kriging	-
oxi	C oxidised during transport by water	g C m^{-2}
P factor	Erosion control practice factor	-
PD	Depth of plough layer	m
pMC	Percent modern carbon	-
Q_{til}	Net sediment flux due to tillage operations	kg m a^{-1}
r	Climate coefficient	-
R factor	Rainfall erosivity factor	N h^{-1} a^{-1}
R_{17}	17.7 x 17.7 m sample raster	-
R_{25}	25 x 25 m sample raster	-
R_{50}	50 x 50 m sample raster	-
RE	Relative elevation	m
RI	Relative improvement	%
RK	Regression kriging	-
RMSE	Root mean square error	unit of variable
R_O	Oriented roughness	cm
RUSLE	Revised Universal Soil Loss Equation	-
s	Slope	° or %
S factor	Slope gradient factor	-
SC	Skewness coefficient	-
SCA	Specific catchment area	m^2 m^{-1}
SD	Standard deviation	unit of variable
SEDEM	Sediment Delivery Model	-
SIC	Soil inorganic carbon	-
SM	Soil moisture	vol%

SOC	Soil organic carbon	-
SPI	Stream power index	-
T	Mean annual air temperature	°C
TC	Transport capacity	kg m^{-1} a^{-1}
u	Exponent for decrease of turnover rate with depth	-
USLE	Universal Soil Loss Equation	-
WaTEM	Water and Tillage Erosion Model	-
WI	Wetness index	-
φ	Lagrange multiplier	-
x	Horizontal distance	m
Y	Young SOC pool	g C m^{-2}
I	Soil layer 0-0.25 m	-
I_a	Soil layer 0-0.1 m	-
I_b	Soil layer 0.1-0.25 m	-
II	Soil layer 0.25-0.5 m	-
III	Soil layer 0.5-0.9 m	-

ERKLÄRUNG

Ich versichere, dass ich die von mir vorgelegte Dissertation selbständig angefertigt, die benutzten Quellen und Hilfsmittel vollständig angegeben und die Stellen der Arbeit – einschließlich Tabellen, Karten und Abbildungen -, die anderen Werken im Wortlaut oder Sinn nach entnommen sind, in jedem Einzelfall als Entlehnung kenntlich gemacht habe; dass diese Dissertation noch keiner anderen Fakultät oder Universität zur Prüfung vorgelegen hat; dass sie - abgesehen von unten angegebenen Teilpublikationen – noch nicht veröffentlicht worden ist sowie, dass ich eine solche Veröffentlichung vor Abschluss des Promotionsverfahrens nicht vornehmen werde. Die Bestimmungen der Promotionsordnung sind mir bekannt. Die von mir vorgelegte Dissertation ist von PD Dr. Peter Fiener betreut worden.

Nachfolgend genannte Teilpublikationen liegen vor:

- Dlugoß, V., P. Fiener and K. Schneider. 2010. Layer-specific analysis and spatial prediction of soil organic carbon using terrain attributes and erosion modelling. Soil Science Society of America Journal 74 (3): 922-935.

Köln, 10. Februar 2011 Verena Dlugoß